This is to certify that the

dissertation entitled

A CONTINUUM-BASED SHELL ELEMENT FOR
LAMINATED COMPOSITES UNDER LARGE DEFORMATION

presented by

Chienhom Lee

has been accepted towards fulfillment
of the requirements for

Ph.D. degree in Mechanics

Dahsin Liu
Major professor

Date 5/29/98

A CONTINUUM-BASED SHELL ELEMENT FOR LAMINATED COMPOSITES UNDER LARGE DEFORMATION

By

Chienhom Lee

A DISSERTATION

Submitted to
Michigan State University
in partial fulfillment of the requirements
for the degree of

DOCTOR OF PHILOSOPHY

Department of Materials Science and Mechanics

1998

ABSTRACT

A CONTINUUM-BASED SHELL ELEMENT FOR LAMINATED COMPOSITES UNDER LARGE DEFORMATION

By

Chienhom Lee

Driving by lack of accuracy of existing finite element programs in analyzing laminated composites under large deformation, a continuum-based shell element is proposed in this study. The objective is to develop an accurate but inexpensive (in terms of computer time) shell element that can solve large scale engineering problems. The new shell element is based on the Generalized Zigzag Theory to better describe transverse shear stresses and kinky in-plane displacements through the laminate thickness. It also uses the rate-of-deformation tensor and the Truesdell rate of Cauchy stress, in an updated Lagrangian sense, to describe kinematic and kinetic relations for a structure under large deformation. The accuracy of the proposed shell element is demonstrated by comparing its numerical results with several well-recognized investigations based on theoretical and experimental approaches.

To

Yufang, Grace and Diane

ACKNOWLEDGMENTS

Dear Heavenly Father, thank You for Your grace, which always amazes me. Without Your help, I would never have been able to finish this dissertation. Thank You for putting all the helping hands around me when I needed them: my most sincere appreciation to my advisor, Dr. Dahsin Liu for his wholehearted support and friendship, also for his persistence in keeping hold of academic excellence with love and kindness; my truthful gratitude to my manager, Mr. Chuan Seng Lee for his patience, encouragements, and constant prayers; my special thanks to my company TRW VSSI for the support of my time and equipment; my deepest appreciation to one of my committee members and colleagues, Dr. Ying-Kuo Lee for his mentoring and his inspiring enthusiasm in finding truths in Continuum Mechanics; my gratitude to my genuine friend, Dr. Chun-Ying Lee and my colleague, Dr. Huai-Yang Chiang for their encouragement and advice; my special thankfulness to my committee members, Drs. Nicholas Altiero, Thomas Pence, and Zhengfang Zhou for their help in reviewing and approving this dissertation; my appreciation to Dr. Joop Nagtegaal and Mr. Lance Hill of HKS Inc. for their help in handling the software; my sincere appreciation to those who pray for me and my family, their names are too many to be listed; finally, gratefulness from my heart to my parents who always reflect Your love on me.

My Lord, please allow me to have one more request: so many of those mentioned above do not know You. Please show Your mercy to them so that they can also enjoy their lives with You eternally. I know You love them much more than I do. In the glorious name of Jesus Christ, Amen.

TABLE OF CONTENTS

LIST OF TABLES

LIST OF FIGURES

Chapter 1

INTRODUCTION

1.1 Motivation

With their superior strength-to-weight ratio, stiffness tailored-ability, formability, and environmental stability, advanced polymer-matrix composite materials have become a key ingredient in the design of future automotive and aircraft components. The complex structural responses and design versatility associated with such materials provide a strong motivation for developing a numerical design tool (besides experimental trial-and-errors).

Many finite element programs have been widely used in the automotive and aerospace industries to investigate structural problems in the context of large deformation. Yet their lack of accuracy in analyzing laminated composite structures has been well recognized. The reason is simply because most programs are designed for isotropic materials. On the other hand, although many laminate theories have been postulated to improve the accuracy of laminated composite analysis, very few of them have been ádopted and introduced to the finite-element community. The primary reason is that they are too sophisticated to implement. Obviously, in the finite element simulation of laminated composites, there exists a gap between what has been developed and advanced and what has been actually used. The motivation behind this thesis, therefore, is to bridge such a gap. In order to achieve this goal, a shell element is to be formulated to fulfill the accuracy requirements for both displacement field and stress state and yet retain computational efficiency. The method of achieving the goal is to first conduct thorough reviews on all existing large deformation theories used in finite element formulation as well as the latest development of laminate theories for composite analysis. Compromises between accuracy and efficiency are then taken in developing a new shell element that has degrees of freedom that are low enough for reasonable efficiency in computation and yet high enough for acceptable accuracy in results.

Figure 1.1 outlines what need to be considered in order to formulate a laminated composite shell element for large deformation analysis. The following sections provide literature reviews of existing laminate theories and nonlinear finite element analysis. Also included are descriptions of the problem-solving methodology and organization of the thesis.

1.2 Laminate Theories

When a laminated composite structure is subjected to out-of-plane loading, accurate transverse stresses are very important in structural design and failure analysis . If a laminated composite structure is moderately thick or thick, or if it consists of a matrix with low shear modulus, the transverse shear deformation may not be negligible. In addition, it should be noted that delamination is a primary damage mode in laminated composites. Both central delamination and edge delamination occur in laminated composite structures quite often. In general, central delamination may occur as a result of impact loading [41] and edge delamination may be attributed to free edge effect [56]. Since the interlaminar stresses are responsible for delamination, a correct prediction of transverse stresses is critical to laminated composite analysis. Various laminate theories for composites analysis have been proposed in the past and are briefly summarized as follows.

(1) First-order Shear Deformation Theory

The First-order Shear Deformation Theory, developed by Reissner [65] and Mindlin [51] independently, is known as the Reissner-Mindlin (RM) Theory. It relaxed the Kirchhoff-Love hypothesis that required normals to the mid-plane to remain normal throughout deformation. By including two additional rotational degrees of freedom, the normals are then free to rotate with respect to the mid-plane during deformation. This type of deformation implies constant transverse shear stresses through the shell thickness. Consequently, shear correction factors are required for the equilibrium process. The RM Theory provides accurate displacements and stresses for thin and moderately thick, isotropic structures. However, as can be seen later, the theory leads to unsatisfactory displacements and stresses for laminated composites. Nevertheless, the finite element formulation based on RM Theory is still the most widely used in commercial software for investigating structures made of conventional metals and composites. The reason is believed to be its high efficiency in computation resulting from using only five degrees of freedom.

(2) High-order Shear Deformation Theories

Many refined shear deformation theories have been presented to improve the prediction of displacements and stresses (especially transverse stresses) for laminated composites. Literature reviews regarding these theories can be found in the book by Palazotto and Dennis [55] and the dissertation by Li [37]. This category of laminate theories is based on an assumed displacement field that is of high-order polynomial functions of the thickness coordinate. Accordingly, both the in-plane and transverse displacements are smooth and continuous through the laminate thickness. In reality, however, the abrupt change of material properties across the laminate interfaces usually results in kinky distributions of the in-plane displacements. Another deficiency of the High-order Shear Deformation Theories is the prediction of double-valued transverse stresses on the laminate interfaces. This results from the single-valued strains on the interface being multiplied by different material properties in different layers. This deficiency originates in the assumption of continuous in-plane displacements, resulting in continuous strain distribution through the laminate thickness. Although this unsatisfactory result can be avoided by a recovering technique based on equilibrium equations, a theory that can give correct displacement field and stress state based on constitutive equations is strongly preferred.

(3) Layerwise Theories

In order to resolve the deficiencies of the High-order Shear Deformation Theories, it may be intuitive to describe each composite laminate as an assembly of individual layers. Some quasi-three-dimensional techniques based on so-called Layerwise Theories were proposed [6, 33, 37, 46]. These theories treated each layer individually and imposed one or more continuity conditions on the laminate interfaces to preserve the kinky displacement distributions and continuous shear stress states through the laminate thickness. As a result, the total number of degrees of freedom were reduced. Li and Liu [38] showed that the aforementioned High-order Shear Deformation Theories were merely simplified cases of the Generalized Layerwise Theory that they proposed. Despite the high accuracy of displacements and stresses obtained from the Layerwise Theories, a large number of degrees-of-freedom proportional to the total number of layers in the laminate was needed. Thus, the theories are computationally inefficient. This disadvantage is especially true when the layer number of composite laminates becomes overwhelmingly large. In view of the advantages and disadvantages of the High-order Shear Deformation Theories and the Layerwise Theories, a theory that would be a compromise between the numerical accuracy and computational efficiency is highly desired.

(4) Zigzag Theories

A group of theories called Zigzag Theories, [17, 37, 72, 73], uses a presumed displacement field for each layer and utilizes interlaminar continuity conditions (displacement, stresses, or both) to assemble individual layers. The name "zigzag" is due to their capability of representing the kinky distributions of in-plane displacements through the laminate thickness when the laminated composite is subjected to bending. Similar to the Layerwise Theory, the Zigzag Theories do not need any shear correction factor; and consequently all the transverse shear strains and stresses can be calculated based on the constitutive equations.

The Generalized Zigzag Theory (ZIGZAG) presented by Li and Liu [38] indicated that all other Zigzag Theories were special cases of theirs. As pointed out by Liu and Li [42], the third-order Generalized Zigzag Theory is a simplified case of the third-order Generalized Layerwise Theory because the layer-dependent variables were only designated to the zeroth-order and the first-order terms (as opposed to all four terms in the Generalized Layerwise Theory). Therefore, the total number of degrees of freedom of the Generalized Zigzag Theory was layer-number dependent. It was then reduced to be layer-number independent after using the continuity conditions of displacement and interlaminar shear stress. Hence, the major advantage of the Generalized Zigzag Theory over the Generalized Layerwise Theory is that the number of degrees of freedom is independent of the number of layers. Thus, it gives higher computational efficiency. However, it is also because there is no layer-dependent variables that the Generalized Zigzag Theory is less accurate than the Generalized Layerwise Theory.

In comparison with the previously mentioned High-order Shear Deformation Theories, the Generalized Zigzag Theory gives correct kinky in-plane displacement fields and transverse stress states. However, due to the fact that the assumed displacement fields for the Generalized Zigzag Theory require transverse deflection to be C^1 continuous in finite element formulation, additional degrees of freedom must be introduced. The same situation also happens to any of the high-order shear deformation theories. The Generalized Zigzag Theory is therefore more complicated in formulation and less efficient than the First-order Shear Deformation Theory.

(5) Quasi-layerwise Theories and Others

Following the same method described in the Generalized Zigzag Theory, Li [37] developed some Quasi-layerwise Theories with the use of only two layer-dependent variables in different orders. Although the accuracy in displacements and stresses can be improved more or less in comparison with the Generalized Zigzag Theory, the Quasi-layerwise Theories suffer numerical deficiency because they are very sensitive to the selection of coordinate systems. Global-local Superposition and Double-superposition Theories are two other ideas presented by Li and Liu [39]. The theories utilize the thickness coordinate of a local layer in combination with the laminate thickness coordinate. As a result, the total number of degrees of freedom of these theories is independent of the total number of layers in the laminate. Although some of these theories can provide higher accuracy, they are less efficient than the Generalized Zigzag Theory because a larger number of degrees of freedom is required. Table 1.1 summarizes the displacement fields for various laminate theories discussed herein. The Generalized Zigzag Theory is chosen to be used in this thesis because it results correct kinky in-plane displacements and continuous transverse stresses. More importantly, the Generalized Zigzag Theory has a constant number of degrees of freedom.

1.3 Nonlinear Analysis

All laminate theories discussed in the previous section can be used for both linear and nonlinear finite element analyses. A linear analysis is used when deformation is small, material response is linear, and boundary conditions remain unchanged during the course of deformation. In general, nonlinear analysis would be otherwise considered. There are two categories of nonlinearity: material nonlinearity and geometric nonlinearity [8]. Material nonlinearity is associated with nonlinear elastic or plastic deformations. Geometric nonlinearity occurs when a structure is subjected to large strains and/or large rotations. In this thesis, the main focus is on geometrically nonlinear problems under static loading conditions.

The essential feature of geometric nonlinearity is that equilibrium equations must be written with respect to an instantaneous state [14]. A large deformation problem can be analyzed using either Lagrangian (material) description or Eulerian (spatial) description. The Lagrangian description is also called total Lagrangian. When this approach is used, movements of material particles are described with respect to the original or undeformed configuration. In other words, regardless how large the strain and rotation are, all displacement differentiations and integrations are performed with respect to the original frame. As deformation becomes larger and larger, more and more terms (usually nonlinear) must be added to the strain-displacement relations in order to account for the nonlinearity.

When the Eulerian description is used, movements of material particles are described with respect to the current or deformed configuration. In actual implementation, the Eulerian approach takes a form that is usually called updated Lagrangian. In this approach, differentiations and integrations are performed with respect to the deformed configuration. The current deformed configuration is also used as the reference state prior to the next increment of the solution. After the incremental solution is obtained, the reference state is updated and then the solution proceeds to the next increment.

It is noted that although different formulations may exist when using different approaches (one may be more complicated than another), final solutions to a problem should be identical. In the total Lagrangian approach, the kinematic relations are always nonlinear because the deformation is usually given by a displacement field. In the updated Lagrangian approach, deformation can be described either by a displacement field or by a velocity field (see Section 2.2 for details) [48]. When a velocity field (such as the rate-of-deformation tensor) is utilized to describe the deformation, the kinematic relations become linear. When dealing with laminated composites, displacement fields are in general very complex. Therefore, it is preferred to use linear kinematic relations.

1.4 Formulation for Large Deformation

Although the advancement in the computational techniques for structural analysis is very significant in the last two decades, the development of finite element formulations for laminated composites subjected to large deformation is very limited. Many commercial programs such as ABAQUS, LS-DYNA3D, PAM-CRASH, and RADIOSS CRASH, and publications [2, 11, 24, 68, 78] use the Reissner-Mindlin Theory with various updated Lagrangian approaches. Most of them imply that their large deformation finite element formulations are valid not only for isotropic materials but also for laminated composites. However, although its prediction on overall behavior of structures, such as transverse deflections may be acceptable, the Reissner-Mindlin Theory gives incorrect in-plane displacement and transverse shear stresses for laminated composites.

As mentioned before, numerous studies have been presented using different laminate theories to improve the accuracy of simulating laminated composites in linear analysis. However, when their techniques were extended to large deformation analysis of symmetric or unsymmetric laminated plates and beams subjected to bending, most of them used a total Lagrangian approach and the von Kármán nonlinear strains [7, 12, 26, 34, 35, 63, 66, 69, 73, 74]. The von Kármán nonlinear strains are a simplification of the Green (Lagrangian) strain tensors with some nonlinear terms eliminated. Most researchers used them for small rotation and small strain nonlinear problems, although the theory can be used for moderately large rotations. Liao and Reddy [40] used a three-dimensional degenerated shell element along with the Green strain tensor and the second Piola-Kirchhoff stress tensor, which is a total Lagrangian approach, to study post-buckling behaviors of stiffened composite shells. Kweon, et al. [30, 31] also used the Green strain tensor and the second Piola-Kirchhoff stress tensor along with the First-order Shear Deformation Theory to study the postbuckling compressive strength of graphite/epoxy laminated cylindrical panels. In their book, Palazotto and Dennis [55] used a forth-order shear deformation theory, in addition to the Green strain tensor and the second Piola-Kirchhoff stress tensor, to formulate a shell element.

1.5 Problem-Solving Methodology

As seen in the previous section, there has been lack of a shell element with computational efficiency that would accurately describe behaviors of laminated composites under large deformation (large rotation and large strain). Therefore, a continuum-based shell element based on the Generalized Zigzag Theory is proposed in this thesis. To avoid the complexity of involving nonlinear strain-displacement relations, the formulation for large deformation adopts an updated Lagrangian approach based on the rate-of-deformation tensor and the Truesdell rate of Cauchy stress. The rate-of-deformation tensor is a linear formulation.

When it is used with the Truesdell rate of Cauchy stress, a symmetric stiffness matrix can be achieved. More importantly, the rate-of-deformation tensor is not a simplification of any strain-displacement relations. Hence, it can be used for investigations involving large strain and/or large rotation. The finite element formulation in this thesis leads to a four-node shell element, which has seven degrees of freedom at each node.

The finite element formulation was programmed as a subroutine called LACOS (LAminated COmposite Shells) using FORTRAN and was then linked to ABAQUS/Standard as a new addition to its element library. The user defined element is called U101 in the element library. It follows the naming convention required by ABAQUS/Standard. The elements of each finite element model are then assembled in global coordinates and solved iteratively by the ABAQUS/Standard solver. ABAQUS/Standard is a general nonlinear finite element package that has been developed and maintained by Hibbitt, Karlsson and Sorensen(HKS), Inc. for more than two decades. The concept of employing user subroutines is to make the most use of the commercial package's existing functions, i.e. solver, post-processing, etc., while the user is still able to tailor the program for specific applications. The subroutine developed in this thesis can also be used in other similar finite element packages with slight modifications.

1.6 Organization of the Thesis

A flow chart of the thesis organization is illustrated in Figure 1.1. We begin in Chapter 2 by establishing some basic knowledge about objective stress rates and the rate-of-deformation tensor before we start deriving governing equations. The rate form of static equilibrium equations is also discussed to show its essential differences from equilibrium equations. In Chapter 3, derivations of the governing equations for a structure undergoing large deformation (both large strain and large rotation) are described. In Chapter 4, incremental displacement fields using the Generalized Zigzag Theory are presented. In Chapter 5, descriptions of finite element formulation for the U101 element are given. In Chapter 6, various numerical studies are presented to evaluate the performance of U101. Finally, conclusions and recommendations are given in Chapter 7.

Table 1.1 Summary of various laminate theories

Theory	Displacement Fields	D.O.F.	Remarks
1. Classic Plate Theory	$u(x,y,z) = u_0(x,y) - zw_{,x}$ $v(x,y,z) = v_0(x,y) - zw_{,y}$ $w(x,y,z) = w_0(x,y)$	3	Global
2. Reissner-Mindlin Theory	$u(x,y,z) = u_0(x,y) + z\psi_x(x,y)$ $v(x,y,z) = v_0(x,y) + z\psi_y(x,y)$ $w(x,y,z) = w_0(x,y)$	5	Global
3. Generalized High-order Shear Deformation Theory (third order)	$u(x,y,z) = u_0(x,y) + z\psi_x(x,y) + z^2\zeta_x(x,y) + z^3\phi_x(x,y)$ $v(x,y,z) = v_0(x,y) + z\psi_y(x,y) + z^2\zeta_y(x,y) + z^3\phi_y(x,y)$ $w(x,y,z) = w_0(x,y)$	7	Global
4. Generalized Higher-order Shear Deformation Theory (4th order and higher) (2)	$u(x,y,z) = \sum_{i=0}^{M} z^i u_i(x,y)$ $v(x,y,z) = \sum_{i=0}^{M} z^i v_i(x,y)$ $w(x,y,z) = w_0(x,y)$	[2(m+1)+1]-4	Global
5. Generalized Layerwise Theory (third order) (1)	$u^k(x,y,z) = u_0^k(x,y) + zu_1^k + z^2u_2^k(x,y) + z^3u_3^k(x,y)$ $v^k(x,y,z) = v_0^k(x,y) + zv_1^k + z^2v_2^k(x,y) + z^3v_3^k(x,y)$ $w(x,y,z) = w_0(x,y)$	4(k+1)+1	Local
6. Generalized Zigzag Theory (third order) (1)	$u^k(x,y,z) = u_0^k(x,y) + zu_1^k + z^2u_2(x,y) + z^3u_3(x,y)$ $v^k(x,y,z) = v_0^k(x,y) + zv_1^k + z^2v_2(x,y) + z^3v_3(x,y)$ $w(x,y,z) = w_0(x,y)$	7	Global-Local
7. Generalized Higher-order Zigzag Theory (4th order and higher) (1),(2)	$u^k(x,y,z) = u_0^k(x,y) + zu_1^k(x,y) + \sum_{i=2}^{M} z^i u_i(x,y)$ $v^k(x,y,z) = v_0^k(x,y) + zv_1^k(x,y) + \sum_{i=2}^{M} z^i v_i(x,y)$ $w(x,y,z) = w_0(x,y)$	[2(M+1)-4]+1	Global-Local
8. Quasi-layerwise Theory (third order) (1),(3)	$u^k(x,y,z) = \sum_{i=0}^{3} z^i u_i^k(x,y)$ $v^k(x,y,z) = \sum_{i=0}^{3} z^i v_i^k(x,y)$ $w(x,y,z) = w_0(x,y)$	7	Global-Local
9. Global-local Superposition Theory (third order) (1),(4)	$u^k(x,y,z) = (\xi_k)^m u_m^k(x,y) + (\xi_k)^n u_n^k(x,y) + \sum_{i=0}^{3} z^i u_i(x,y)$ $v^k(x,y,z) = (\xi_k)^m v_m^k(x,y) + (\xi_k)^n v_n^k(x,y) + \sum_{i=0}^{3} z^i v_i(x,y)$ $w(x,y,z) = w_0(x,y)$	11	Global-Local
10. Double Superposition Theory (third order) (1),(5)	$u^k(x,y,z) = (\xi_k)^m u_m^k(x,y) + (\xi_k)^n u_n^k(x,y) + (\xi_k)^p u_p^k(x,y) + \sum_{i=0}^{3} z^i u_i(x,y)$ $v^k(x,y,z) = (\xi_k)^m v_m^k(x,y) + (\xi_k)^n v_n^k(x,y) + (\xi_k)^p v_p^k(x,y) + \sum_{i=0}^{3} z^i v_i(x,y)$ $w(x,y,z) = w_0(x,y)$	13	Global-Local
(1) k=number of layers (2)M = number of terms in the polynominal (3) k=0 in any two out of four terms (4) m,n=1,1,2, or 3; m≠n (5)m,n,p=1,2, or 3; m≠n≠p			

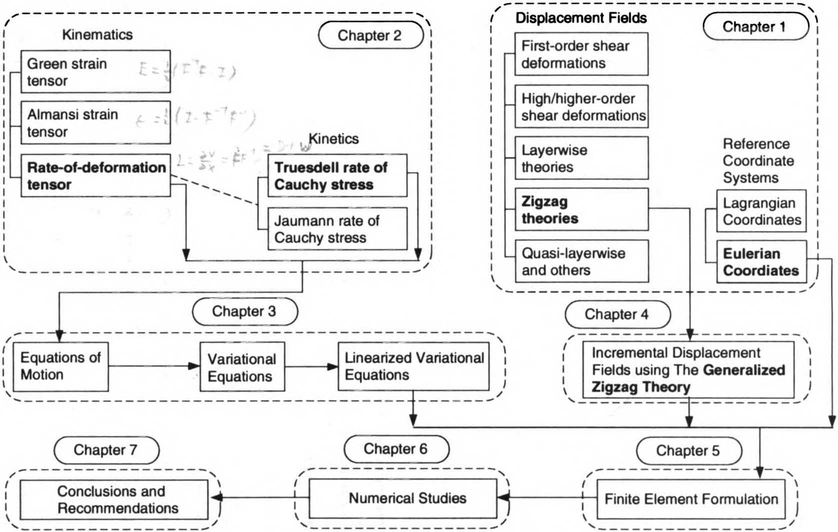

Figure 1.1 List of considerations and flow chart of thesis organization

Chapter 2

LARGE DEFORMATION ANALYSIS

2.1 Introduction

Once the Generalized Zigzag Theory is chosen as the displacement field, there are many different ways of establishing kinematic and kinetic relations for large deformation analysis. Careful considerations must be given and choices must be made before we start the development of governing equations and the subsequent formulation of a shell element that deals with laminated composites. In this chapter, we introduce the principle of objectivity (or material frame indifference) for stress rate and the rate-of-deformation tensor. This will enable us to describe the motion of a particle in a continuum at any instant of time during the process of a large deformation. Numerous studies have been done on this topic, for example, Fung [19] and Malvern [48]. Here, we only outline some of the important concepts needed for future use. Since the rate form of static equilibrium equations is quite different from the equilibrium equations themselves, one section is devoted to present different ways of obtaining the rate form of static equilibrium equations.

2.2 Descriptions of Kinematic Relations

When dealing with geometrically nonlinear problems, numerous measures of strain are available. However, most theoretical works and computer programs utilize the following three kinematic relations:

1. The Green strain tensor (also called the Lagrangian strain tensor)

Non linear terms

$$\epsilon_{ij} = \frac{1}{2}\left(\frac{\partial u_i}{\partial X_j} + \frac{\partial u_j}{\partial X_i} + \frac{\partial u_k}{\partial X_i}\frac{\partial u_k}{\partial X_j}\right) = \frac{1}{2}\left(F^T F - I\right) \tag{2.1}$$

2. The Almansi strain tensor (also called the Eulerian strain tensor)

$$\epsilon^*_{ij} = \frac{1}{2}\left(\frac{\partial u_i}{\partial x_j} + \frac{\partial u_j}{\partial x_i} - \frac{\partial u_k}{\partial x_i}\frac{\partial u_k}{\partial x_j}\right) = \frac{1}{2}\left(I - F^{-T} F^{-1}\right) \tag{2.2}$$

3. The rate-of-deformation tensor (also called the stretching tensor or the velocity strain tensor)

$L = D + W$

$$D_{ij} = \frac{1}{2}\left(\frac{\partial \dot{u}_i}{\partial x_j} + \frac{\partial \dot{u}_j}{\partial x_i}\right) \tag{2.3}$$

In Eq.(2.1), X_i are components of Lagrangian coordinates. They are also called material coordinates because they describe the material particles with respect to the original or undeformed configuration. An approach is called total Lagrangian when the Lagrangian coordinate system is used to describe the motion of a particle. In Eqs.(2.2) and (2.3), x_i are components of Eulerian coordinates. They are also called spatial coordinates because they describe the material particles with respect to the current or deformed configuration. An approach is called updated Lagrangian when the Eulerian coordinate system is used to describe the motion of a particle. The two sets of coordinates are related by

$$x_i = X_i + u_i \tag{2.4}$$

where u_i are components of a displacement vector.

It is noted that both the Green and Almansi strain tensors have nonlinear, coupling terms. The rate-of-deformation tensor is linear, but it is not derived by removing nonlinear terms from the Green or Almansi strain tensors. It is also noted that the rate-of-deformation tensor is calculated from velocity fields while the Green and Almansi strain tensors are calculated from displacement fields. The rate-of-deformation tensor expresses a change of the displacement vector from the current state to the next state along the loading history.

Remark 2.1

The von Kármán nonlinear strains used in many large deformation finite element formulations is a simplified, special case derived by removing some nonlinear terms from the Green strain tensor. It is mostly used for small rotation and small strain nonlinear problems.

2.3 Rate of Deformation

In this thesis, we choose the rate-of-deformation tensor in Eq.(2.3) as the kinematic relations for large deformation analysis. When dealing with complex displacement fields for laminated composites such as the Generalized Zigzag Theory, it is preferred to use linear kinematic relations. More importantly, the rate-of-deformation tensor is not a simplification of any strain-displacement relations and, hence, can be used for problems involving large strains and/or large rotations.

The following is a brief introduction of the rate-of-deformation tensor. Since our focus in the current study is on the instantaneous motion of a continuum, we describe the motion of a typical particle P inside the continuum by choosing the spatial description and use velocity of the particle as functions of its instantaneous position (x_1, x_2, x_3) in space.

As shown in Figure 2.1, we consider two infinitesimal neighborhood particles P_1 and P_2

with instantaneous coordinates $\mathbf{x}$ and $\mathbf{x} + d\mathbf{x}$ respectively. The relative motion of the two particles from one time instant t to another time instant $t + \Delta t$ can be completely described by a tensor quantity called velocity gradient (L_{ij}) defined as follows.

$$L_{ij} = \frac{\partial v_i}{\partial x_j} \equiv v_{i,j} \tag{2.5}$$

L_{ij} in Eq.(2.5) can be additively decomposed into two tensors

$$L_{ij} = D_{ij} + W_{ij} \tag{2.6}$$

where

$$D_{ij} = \frac{1}{2}(L_{ij} + L_{ij}^T) = \frac{1}{2}(v_{i,j} + v_{j,i}) \equiv v_{(i,j)} \tag{2.7}$$

$$W_{ij} = \frac{1}{2}(L_{ij} - L_{ij}^T) = \frac{1}{2}(v_{i,j} - v_{j,i}) \equiv v_{[i,j]} \tag{2.8}$$

$$D_{ij} = D_{ji} \quad \mathit{and} \quad W_{ij} = -W_{ji} \tag{2.9}$$

The symmetric tensor D_{ij} is called the rate-of-deformation tensor, and the skew-symmetric tensor W_{ij} is called the spin tensor.

The rate-of-deformation tensor D_{ij} is a well defined quantity; it vanishes when the continuum performs a rigid-body motion. Therefore, it is an objective quantity. On the other hand, when there is no rigid body motion, the spin tensor W_{ij} becomes zero.

2.4 Descriptions of Kinetic Relations

In describing the kinetic relations, a frame indifference (also called objectivity) condition must be satisfied. When using a stress or strain tensor to describe the response of a material, it must be frame indifferent; otherwise, no constitutive relation measured from physical material tests can be established to accomplish the calculation of material response. In addition, a condition called energy conjugate must also be fulfilled. A stress is "energy conjugate" to the strain if its scalar product with that strain gives equivalent work (energy) to that in a reference frame [15].

Although the Cauchy stress is the energy conjugate to the time integration of the rate-of-deformation tensor, neither its material nor time derivative is frame indifferent [19]. The Cauchy stress $\sigma_{ij}(x_1, x_2, x_3, t)$ is a time-dependent stress field in a continuum and is referred to a fixed reference coordinate system. It is a true measure of the stress state inside the deformed continuum. The material derivative of the Cauchy stress

$$\frac{d\sigma_{ij}}{dt} = \frac{\partial\sigma_{ij}}{\partial t} + \frac{\partial\sigma_{ij}}{\partial x_k} v_k \tag{2.10}$$

indicates the time rate change of a typical stress component at a particle of the continuum. For a stressed continuum performing rigid body rotation, neither the time derivative ($\partial\sigma_{ij}/\partial t$) nor the material derivative ($d\sigma_{ij}/dt$) of the Cauchy stress vanishes identically. This can be seen in an example illustrated in Figure 2.2 [19]. A bar is subjected to simple tension and rigid body rotation about the z axis. At one instant, when the bar is parallel to y-axis, $\sigma_x = 0$ and $\sigma_y \neq 0$. At another instant, when the bar is parallel to x-axis, $\sigma_x \neq 0$ and $\sigma_y = 0$. Accordingly, a rigid body rotation changes the stress tensor while the stress state is unchanged inside the bar. Thus, neither $\partial\sigma_{ij}/\partial t$ nor $d\sigma_{ij}/dt$ can serve as an appropriate stress rate measure to be related simply to the rate-of-deformation D_{ij}. In other words, it is impossible to establish a constitutive relation between D_{ij} and $d\sigma_{ij}/dt$ (or $\partial\sigma_{ij}/\partial t$). This is why an objective stress rate must be introduced.

2.5 Measure of Objective Stress Rate

As described by Prager [57], the objective stress rate must vanish when a stressed continuum performs a rigid body motion. Apparently, this restriction is not severe enough to lead to a unique definition of objective stress rate. A variety of definitions of stress rate have been proposed in the literature on mechanics of continua. Among the many frame-indifferent stress rates of the Cauchy stress, the Jaumann (also called Zaremba-Jaumann-Noll) rate and Truesdell rate of Cauchy stress are commonly used. Although many lecturers have contributed their efforts in discussing the superiority of one stress rate to the others, [16, 18, 20, 23, 50, 57, 58], the results were inconclusive. Theoretically, the result of using any one of them should be identical from a continuum mechanics point of view. However, depending on formulations and applications, one stress rate may be more suitable than the other. In this thesis, the Truesdell rate of Cauchy stress is used. When it is used with the rate-of-deformation tensor in an updated Lagrangian approach, a symmetric stiffness matrix can result in the finite element formulation.

In the following, the Truesdell rate and Jaumann rate of Cauchy stress are briefly introduced.

(1) Truesdell Rate of Cauchy Stress

The relationship between the symmetric second Piola-Kirchoff (2nd PK) stress tensor and the Cauchy stress tensor is given by [49]

$$S_{ij} = JF_{ik}^{-1}\sigma_{kl}F_{jl}^{-1} \tag{2.11}$$

where S_{ij} is the second Piola-Kirchoff stress defined with respect to the material coordinates (X_1, X_2, X_3), F_{ij} is the deformation gradient, and $J = det\ (F_{ij})$. Using the method of consistent linearization shown in Appendix A, we have

$$\begin{aligned} \mathcal{L}[S_{ij}] &= \mathcal{L}[J](F_{ik}^{-1})\sigma_{kl}(F_{jl}^{-1}) + J\mathcal{L}[F_{ik}^{-1}]\sigma_{kl}(F_{jl}^{-1}) \\ &+ J(F_{ik}^{-1})\mathcal{L}[\sigma_{kl}](F_{jl}^{-1}) + J(F_{ik}^{-1})\sigma_{kl}\mathcal{L}[F_{jl}^{-1}] \end{aligned} \tag{2.12}$$

Now choose the frame of reference $\mathbf{X}$ to be the instantaneous motion $\mathbf{x}$, then

$$J = 1 \qquad \text{and} \qquad (F_{ij}^{-1}) = \delta_{ij} \tag{2.13}$$

and from Eqs.(A.9) and (A.11)

$$\mathcal{L}[J] = \Delta u_{k,k} \qquad \text{and} \qquad \mathcal{L}[F_{ij}^{-1}] = -\Delta u_{i,j} \tag{2.14}$$

Hence

$$\mathcal{L}[S_{ij}] \stackrel{def}{=} \nabla\sigma_{ij}^{t} = \Delta\sigma_{ij} + \sigma_{ij}\Delta u_{k,k} - \sigma_{il}\Delta u_{j,l} - \Delta u_{i,l}\sigma_{lj} \tag{2.15}$$

or

$$\Delta\sigma_{ij} = \nabla\sigma_{ij}^{t} - \sigma_{ij}\Delta u_{k,k} + \sigma_{il}\Delta u_{j,l} + \Delta u_{i,l}\sigma_{lj} \tag{2.16}$$

where $\nabla\sigma_{ij}^{t}$ is the Truesdell rate of Cauchy stress and $\Delta\sigma_{ij}$ is the Cauchy stress rate.

(2) Jaumann Rate of Cauchy Stress

Let us consider a field of flow with velocity components v_i attached to a rectangular Cartesian frame of reference (x_1, x_2, x_3). For convenience of discussion, we follow Fung's work [19] and take the origin of the coordinate system at a generic point P in the flow field. Let (x'_1, x'_2, x'_3) be another rectangular Cartesian frame of reference that has the same origin at P and rotates with the continuum at an incremental rotation (spin tensor) $\mathbf{W}$, where the components of W_{ij} are

$$W_{23} = \frac{1}{2}\left(\frac{\partial v_2}{\partial x_3} - \frac{\partial v_3}{\partial x_2}\right), W_{31} = \frac{1}{2}\left(\frac{\partial v_3}{\partial x_1} - \frac{\partial v_1}{\partial x_3}\right), W_{12} = \frac{1}{2}\left(\frac{\partial v_1}{\partial x_2} - \frac{\partial v_2}{\partial x_1}\right) \tag{2.17}$$

Let x'_i coincide with x_i at any instant of time t. Then the stress tensor at P is $\sigma'_{ij}(t) = \sigma_{ij}(t)$. Referring to the rotating axes x'_i at a later instant of time $t+dt$, let the stress at the particle P be denoted by $\sigma'_{ij}(t+dt)$. Then the Jaumann rate of Cauchy stress is defined as

$$\sigma_{ij}^{\nabla} = \lim_{dt\to 0}\frac{1}{dt}[\sigma'_{ij}(t+dt) - \sigma'_{ij}(t)] \tag{2.18}$$

Now, the coordinates x'_i and x_i are related by

$$x'_i = x_i + \frac{\partial v_i}{\partial x_k} x_k dt = \left(\delta_{ik} + \frac{\partial v_i}{\partial x_k} dt\right) x_k \tag{2.19}$$

Decomposing the velocity gradient tensor $\partial v_i / \partial x_k$ in the equation above into the rate-of-deformation tensor(D_{ij}) and the spin tensor (W_{ij}) using Eq.(2.6), we obtain

$$x'_i = (\delta_{ik} + W_{ik} dt) x_k \tag{2.20}$$

where $D_{ij} = 0$ for rigid body rotation. The stress tensor at particle P at the instant $t + dt$, with reference to the fixed coordinates x_j, is

$$\sigma_{ij}(t + dt) = \sigma_{ij}(t) + \frac{d\sigma_{ij}}{dt} dt \tag{2.21}$$

Transforming the stress tensor of Eq.(2.21) through the coordinate transformation Eq.(2.20) into the x'_j axes, we obtain

$$\begin{aligned} \sigma'_{ij}(t + dt) &= (\delta_{ip} + W_{ip} dt)(\delta_{jq} + W_{jq} dt)\left[\sigma_{pq}(t) + \frac{d\sigma_{pq}}{dt} dt\right] \\ &= \sigma_{ij}(t) + \left\{\frac{d\sigma_{ij}}{dt} + W_{ip}\sigma_{pj} + W_{jq}\sigma_{iq}\right\} dt + O(dt^2) \end{aligned} \tag{2.22}$$

Accordingly, from Eq.(2.18), we obtain

$$\begin{aligned} \sigma^{\nabla}_{ij} &= \frac{d\sigma_{ij}}{dt} + W_{ip}\sigma_{pj} + W_{jq}\sigma_{iq} \\ &= \Delta\sigma_{ij} + W_{ip}\sigma_{pj} + W_{jq}\sigma_{iq} \end{aligned} \tag{2.23}$$

Remark 2.2

The use of the Jaumann rate is to view the stress-strain relation from the standpoint of an observer in a moving material frame relative to which the local rotation vanishes. In other words, the Jaumann stress rate provides an objective measure of the change in stress viewed from a frame rotating with the material.

Remark 2.3

The generalized Hooke's law can be applied as the stress-strain relation between the Jaumann stress rate and the rate of deformation in the coordinates aligned with the material principal directions, assuming the material is linear elastic. The engineering constants are Young's moduli, Poisson's ratios, and shear moduli that are measured from simple tests such as uniaxial tension or pure shear tests.

2.6 Rate Form of Static Equilibrium Equations

$\sigma_{ij,j} + \rho b_i = 0$

At any instant of time, without considering the body force and acceleration of a continuum, equilibrium requires that the total force acting on the body must vanish, that is

$$\int_S t_i dS = \int_S \sigma_{ij} n_j dS = 0 \tag{2.24}$$

where S is surface of the body and the traction $t_i = \sigma_{ij} n_j$ with n_j being a unit normal to the surface. The divergence theorem allows Eq.(2.24) to be written as

$$\int_V \frac{\partial \sigma_{ij}}{\partial x_j} dV = 0 \tag{2.25}$$

$\sigma_{ij,j}$

This equation must be valid for an arbitrary volume V (every portion of the body is in equilibrium), thus, we obtain the familiar stress equations of equilibrium

$$\frac{\partial \sigma_{ij}}{\partial x_j} = 0 \tag{2.26}$$

As given in Lee [36] and Osias and Swedlow [52], to maintain the deforming body in equilibrium during a loading history, it is required that the time rate of the net applied force be zero. Thus, we have the material derivative of Eq.(2.24) as

$$\frac{d}{dt}\left(\int_S t_i dS\right) = \int_S (\dot{t}_i dS + t_i d\dot{S}) = 0 \tag{2.27}$$

Applying the divergence theorem to Eq.(2.27) again will lead to the stress rate equations of equilibrium. Alternatively, we can take the material derivative of Eq.(2.26) directly (also use Eq.(2.10)), that is

$v_k(\sigma_{ij,j})_{,k}$

$$\frac{d}{dt}\left(\frac{\partial \sigma_{ij}}{\partial x_j}\right) = \frac{\partial^2 \sigma_{ij}}{\partial t \partial x_j} + \frac{\partial^2 \sigma_{ij}}{\partial x_k \partial x_j} v_k = 0 \tag{2.28}$$

Eq.(2.28) leads to the following equation provided that $\sigma_{ij,kj}$ is continuous because $\sigma_{ij,kj}$ becomes zero when total stress equilibrium $\sigma_{ij,j} = 0$, i.e.

$$\frac{d}{dt}\left(\frac{\partial \sigma_{ij}}{\partial x_j}\right) = \left(\frac{\partial \sigma_{ij}}{\partial t}\right)_{,j} = 0 \tag{2.29}$$

Using Eq.(2.10) again, we have $\frac{\partial \sigma_{ij}}{\partial t} = \frac{d\sigma_{ij}}{dt} - \frac{\partial \sigma_{ij}}{\partial x_k} v_k = \dot{\sigma}_{ij} - \frac{\partial \sigma_{ij}}{\partial x_k} v_k$

$$\left(\frac{\partial \sigma_{ij}}{\partial t}\right)_{,j} = \frac{\partial \dot{\sigma}_{ij}}{\partial x_j} - \frac{\partial^2 \sigma_{ij}}{\partial x_k \partial x_j} v_k - \frac{\partial \sigma_{ij}}{\partial x_k}\frac{\partial v_k}{\partial x_j} = 0 \tag{2.30}$$

$v_k(\sigma_{ij,j})_{,k}$

Finally, we have $\dot{\sigma}_{ij,j} - \sigma_{ij,k} v_{k,j} = 0$

$$\frac{\partial \dot{\sigma}_{ij}}{\partial x_j} - \frac{\partial \sigma_{ij}}{\partial x_k}\frac{\partial v_k}{\partial x_j} = 0 \qquad \nabla\dot{\sigma} - \nabla\sigma L = 0 \tag{2.31}$$

This equation is in a rate form, and, thus, it governs the stress field irrespective of deformation magnitude and material structure. Satisfaction of Eq.(2.31) not only implies total stress equilibrium $\sigma_{ij,j} = 0$ but also assures that, given an equilibrated stress field, equilibrium is maintained in the presence of time varying loading [36].

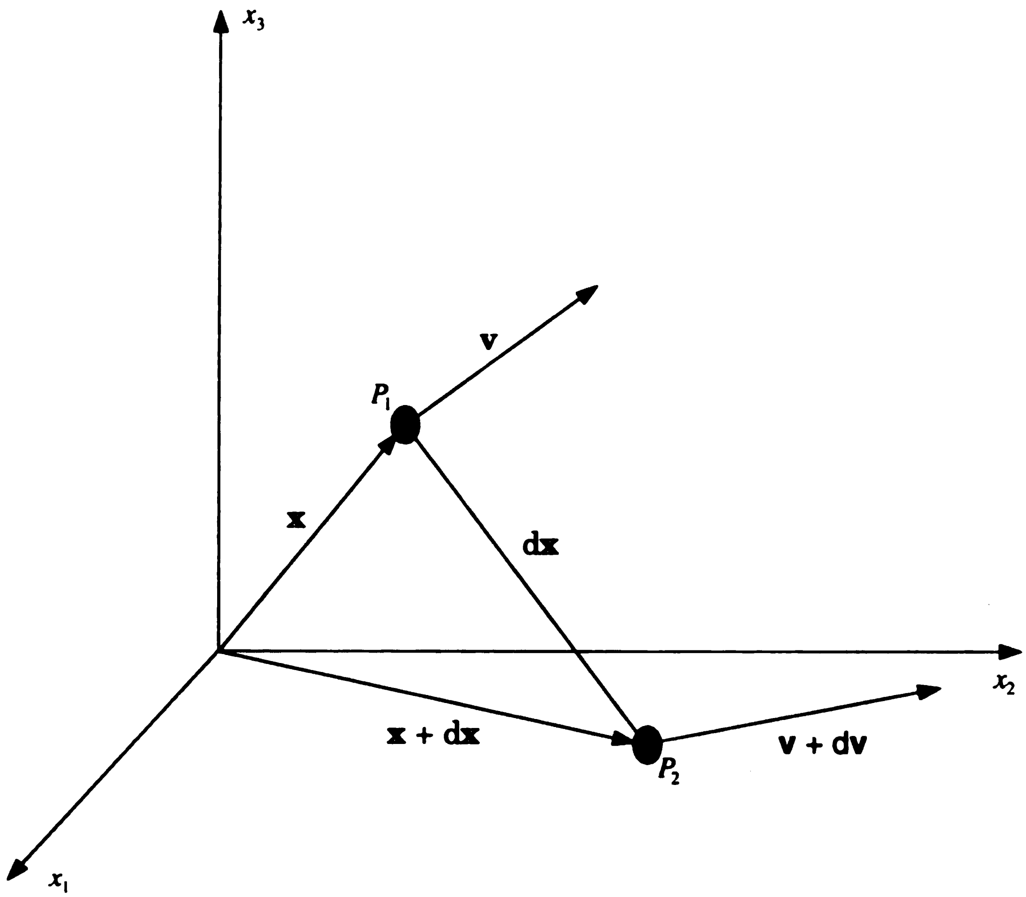

Figure 2.1 Illustration of relative motion between two particles in space

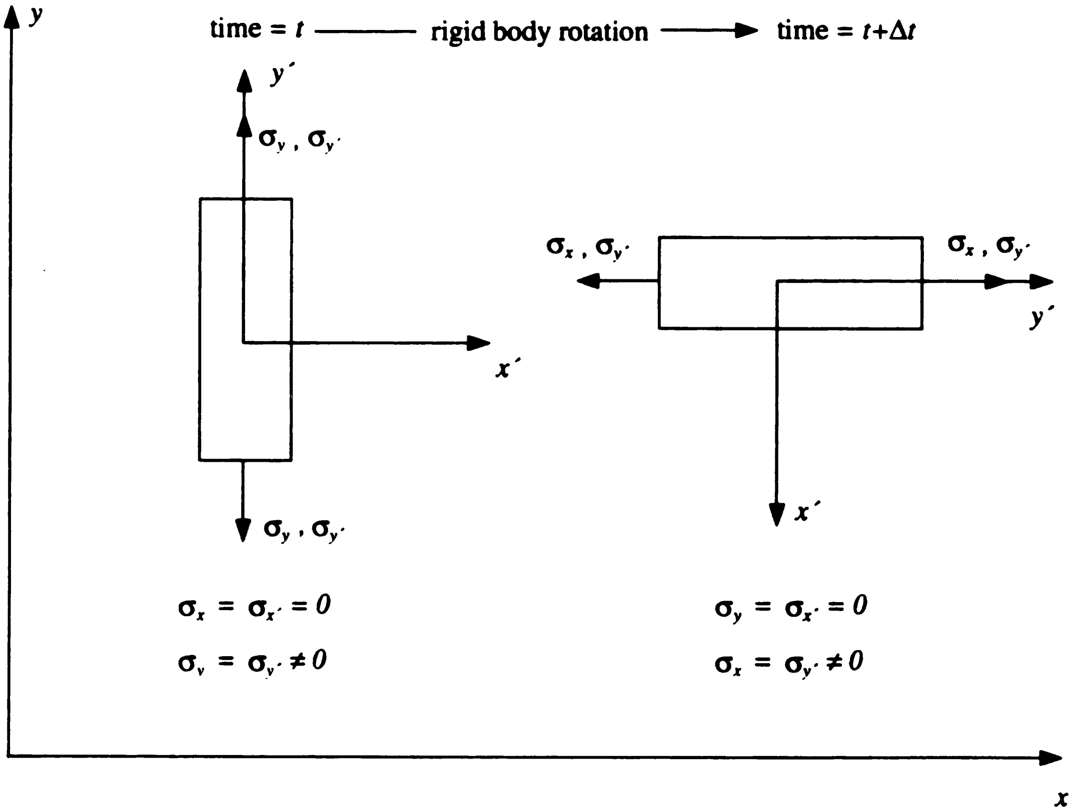

Figure 2.2 Illustration of time and material derivatives of Cauchy stress under a rigid body rotation

Chapter 3

GOVERNING EQUATIONS

3.1 Introduction

Starting from equations of motion, a variational approach is performed to convert the governing equations into variational equations. Since the variational equations are nonlinear, linearization based on Tayler's expansion is required to simplify the nonlinear equations, resulting in linear approximation of the variational equations. Subsequently, the Truesdell rate of Cauchy stress and the rate-of-deformation tensor are introduced into the formulation to form the final linearized variational equations. Once the linearization formulation is completed, a finite element method can be used to convert the linearized variational equations into finite element formulation, which will lead to a symmetric stiffness matrix. The stiffness matrix can be used in a Newton-Raphson iteration scheme. Therefore, nonlinear solutions can be obtained systematically by using many small linear increments. This procedure is consistent with an updated Lagrangian scheme [8]. It is noted that the procedure presented herein is general and not restricted to any type of deformation (finite or infinitesimal) or structure (bulky or thin-walled).

3.2 Differential Equations

Consider components of a displacement vector $u_i(x_1, x_2, x_3, t)$ that satisfies the equations of motion

$$\frac{\partial \sigma_{ij}}{\partial x_j} + b_i = \rho \ddot{u}_i \tag{3.1}$$

throughout the interior of the body which has a current volume V over the time interval $t \in (0, T)$, and is subjected to the following conditions:

displacement (essential) boundary condition

$$u_i = g_i(x_1, x_2, x_3, t) \qquad \text{on } \Gamma_{g_i}, \tag{3.2}$$

traction (natural) boundary condition

$$h_i(x_1, x_2, x_3, t) = \sigma_{ij} n_j \qquad \text{on } \Gamma_{h_i}, \tag{3.3}$$

and initial conditions

$$u_i(X_1, X_2, X_3, 0) = u_i^0(X_1, X_2, X_3)$$

$$\dot{u}_i(X_1, X_2, X_3, 0) = v_i^0(X_1, X_2, X_3) \tag{3.4}$$

where

$$\Gamma_{g_i} \cup \Gamma_{h_i} = S$$

$$\Gamma_{g_i} \cap \Gamma_{h_i} = 0$$

$$\tag{3.5}$$

and S is the surface of the continuum.

Some variables appeared in Eqs.(3.1) through (3.5) are defined as follows:

X_i are components of the material coordinates,

x_i are components of the spatial coordinates and $x_i = X_i + u_i(x_1, x_2, x_3, t)$,

$\sigma_{ij}(x_1, x_2, x_3, t)$ are components of the Cauchy (true) stress tensor,

$b_i(x_1, x_2, x_3, t)$ are components of the body-force vector per unit volume,

$\rho(x_1, x_2, x_3, t)$ is the mass density, and

n_i are components of the unit normal vector relative to the boundary Γ_{h_i}.

Since the dot over a variable represents time differentiation, $\dot{u}_i$ indicates velocity of a material point and $\ddot{u}_i$ acceleration of the same point. Furthermore, the indices i and j denote Cartesian coordinates relative to a fixed reference frame and they range from 1 to 3. Repeated indices imply a summation over the range.

3.3 Variational Formulation

The variational form of the equations of motion, Eqs.(3.1), can be written as follows

$$\int_V \delta u_i \left(\frac{\partial \sigma_{ij}}{\partial x_j} + b_i - \rho \ddot{u}_i \right) dV = 0 \tag{3.6}$$

where δu_i is an arbitrary weight function and must satisfy the homogeneous form of the essential boundary conditions, i.e.,

$$\delta u_i = 0 \qquad \text{on } \Gamma_{g_i} \tag{3.7}$$

Integrating by parts of Eqs.(3.6) leads to

$$\int_V \delta u_i b_i dV + \int_\Gamma \delta u_i h_i d\Gamma - \int_V \frac{\partial \delta u_i}{\partial x_j} \sigma_{ij} dV = \int_V \delta u_i \rho \ddot{u}_i dV \tag{3.8}$$

It is noted that Eq.(3.8) is a result of transferring differentiation of u_i to δu_i, thus equalizing the continuity requirement on u_i and δu_i and weakening the requirement on u_i [5]. Now, instead of obtaining an analytical solution to Eq.(3.1), we try to find a numerically approximated solution by using Eq.(3.8) and its associated boundary conditions.

3.4 Variational Equations

In this stage, it is to find $u_i(x_1, x_2, x_3, t)$ that satisfies the variational equation

$$F^{ext}(u_i) - F^{int}(u_i) = M(\ddot{u}_i) \tag{3.9}$$

where, by referring to Eq.(3.8) in the previous section,

$$F^{ext}(u_i) = \int_V \delta u_i b_i dV + \int_\Gamma \delta u_i \hat{h}_i d\Gamma \tag{3.10}$$

$$F^{int}(u_i) = \int_V \frac{\partial \delta u_i}{\partial x_j} \sigma_{ij} dV \tag{3.11}$$

$$M(\ddot{u}_i) = \int_V \delta u_i \rho \ddot{u}_i dV \tag{3.12}$$

Some remarks regarding the above equations are listed below.

1. Components of the variational displacement vector δu_i should satisfy appropriate continuity conditions and

$$\delta u_i = 0 \qquad \text{on } \Gamma_{g_i} \tag{3.13}$$

2. Eq.(3.9) is subjected to the following initial conditions

$$u_i(X_1, X_2, X_3, 0) = u_i^0(X_1, X_2, X_3)$$

$$\dot{u}_i(X_1, X_2, X_3, 0) = v_i^0(X_1, X_2, X_3), \tag{3.14}$$

3. The traction boundary conditions have been absorbed in the variational process as the surface contribution ($\int_\Gamma$) in Eq.(3.10).

3.5 Linearization of Variational Equations

The governing equation, Eq.(3.9), of a continuum undergoing large deformation (both large strain and large rotation) is generally nonlinear. The consistent linearization procedure described in Appendix A can be used to find the linear approximation of the equation.

Taking the function $\mathcal{F}$ in Appendix A and recalling Eq.(3.9) yields

$$\mathcal{F}(x_i^{v+1}) = F^{ext}(x_i^{v+1}) - F^{int}(x_i^{v+1}) - M(\ddot{x}_i^{v+1}) = 0 \tag{3.15}$$

The linearized variational equations can be written as

$$\begin{aligned} & - \mathcal{L}[F^{ext}] + \mathcal{L}[F^{int}] + \mathcal{L}[M] \\ & = F^{ext}(x_i^v) - F^{int}(x_i^v) - M(\ddot{x}_i^v) \end{aligned} \tag{3.16}$$

Now, if we restrict the derivation to a static case and ignore the contribution of the body-force, we let

$$\begin{aligned} & \mathcal{L}[F^{ext}] = 0, \\ & b_i = 0, \\ & \mathcal{L}[M] = 0, \text{ and} \\ & M(\ddot{x}_i^v) = 0 \end{aligned} \tag{3.17}$$

Eq.(3.16) is then reduced to

$$\mathcal{L}[F^{int}] = F^{ext}(x_i^v) - F^{int}(x_i^v) \tag{3.18}$$

Therefore, only $\mathcal{L}[F^{int}]$ in Eq.(3.18) needs to be further discussed.

By using Eq.(3.11), Eq.(3.18) becomes

$$\begin{aligned} \mathcal{L}[F^{int}] &= \mathcal{L}\left[\int_V \frac{\partial \delta u_i}{\partial x_j} \sigma_{ij} dV\right] \\ &= \mathcal{L}\left[\int_{V_0} \frac{\partial \delta u_i}{\partial X_k} \frac{\partial X_k}{\partial x_j} \sigma_{ij} J dV_0\right] \\ &= \int_{V_0} \frac{\partial \delta u_i}{\partial X_k} \left\{ \mathcal{L}[F_{kj}^{-1}] \sigma_{ij}^v J^v + F_{kj}^{-1} \mathcal{L}[\sigma_{ij}] J^v + F_{kj}^{-1} \sigma_{ij}^v \mathcal{L}[J] \right\} dV_0 \end{aligned} \tag{3.19}$$

In Eq.(3.19), we introduce $dV = JdV_0$, where V_0 is the original (initial) volume of the continuum. By defining

$$\mathcal{L}[\sigma_{ij}] \stackrel{def}{=} \Delta\sigma_{ij} \tag{3.20}$$

and using Eqs.(A.9) and (A.11), we obtain

$$\mathcal{L}[F^{int}] = \int_V \frac{\partial \delta u_i}{\partial X_k}\left\{-F^{-1}_{km}\frac{\partial \Delta u_m}{\partial X_l}F^{-1}_{lj}\sigma^v_{ij} + F^{-1}_{kj}\Delta\sigma_{ij} + F^{-1}_{kj}\sigma^v_{ij}\Delta u_{l,l}\right\}dV \tag{3.21}$$

Using

$$\begin{aligned} \frac{\partial \delta u_i}{\partial X_k}F^{-1}_{km} &= \frac{\partial \delta u_i}{\partial x_m} \\ \frac{\partial \Delta u_m}{\partial X_l}F^{-1}_{lj} &= \frac{\partial \Delta u_m}{\partial x_j} \end{aligned} \tag{3.22}$$

we obtain

$$\mathcal{L}[F^{int}] = \int_V \frac{\partial \delta u_i}{\partial x_j}\{\Delta\sigma_{ij} + \sigma^v_{ij}\Delta u_{k,k} - \sigma^v_{ik}\Delta u_{j,k}\}dV \tag{3.23}$$

As explained in Chapter 2, the Cauchy stress rate $\Delta\sigma_{ij}$ is not an objective measure of stress; it cannot be involved in any constitutive equation directly. Therefore, Eq.(3.23) is not useful unless the Cauchy stress rate is further specified. Later in this section, we will revisit the definition of the Truesdell rate of Cauchy stress defined in Eq.(2.16).

Recall Eq.(2.5)

$$L_{ij} = \frac{\partial v_i}{\partial x_j} \equiv v_{i,j} \tag{3.24}$$

In a static loading condition, the terms "time increment" and "velocity" really indicate, respectively, an increment along the loading path and the corresponding increment of displacement (Δu_i). Therefore, we rewrite the velocity gradient, rate-of-deformation tensor and spin tensor in Eqs.(2.5), (2.7) and (2.8), respectively, as follows

$$L_{ij} = \frac{\partial \Delta u_i}{\partial x_j} \equiv u_{i,j} \tag{3.25}$$

$$D_{ij} = \frac{1}{2}(L_{ij} + L^T_{ij}) = \frac{1}{2}(\Delta u_{i,j} + \Delta u_{j,i}) \equiv \Delta u_{(i,j)} \tag{3.26}$$

$$W_{ij} = \frac{1}{2}(L_{ij} - L^T_{ij}) = \frac{1}{2}(\Delta u_{i,j} - \Delta u_{j,i}) \equiv \Delta u_{[i,j]} \tag{3.27}$$

Let's define the Truesdell kinetic relations as

$$\nabla\sigma^t_{ij} = C^t_{ijkl}\Delta u_{(k.l)} \tag{3.28}$$

where C^t_{ijkl} is determined experimentally or transformed accordingly. Here we transform the constitutive equation C^t_{ijkl} from the generalized Hookie's law C_{ijkl} by using the following formula

$$C^t_{ijkl} = C_{ijkl} + \sigma^v_{ij}\delta_{kl} - \frac{1}{2}(\sigma^v_{ik}\delta_{jl} + \sigma^v_{il}\delta_{jk} + \sigma^v_{jk}\delta_{il} + \sigma^v_{jl}\delta_{ik}) \tag{3.29}$$

The detailed derivation of the above formula is given in Appendix C. From Eqs.(2.16) and (3.28), we have

$$\Delta\sigma_{ij} = C^t_{ijkl}\Delta u_{(k,l)} - \sigma^v_{ij}\Delta u_{k,k} + \sigma^v_{il}\Delta u_{j,l} + \Delta u_{i,l}\sigma^v_{lj} \tag{3.30}$$

Now let's recall the final form of $\mathcal{L}[F^{int}]$ from Eq.(3.23) and denote

$$\Delta\sigma^*_{ij} = \Delta\sigma_{ij} + \sigma^v_{ij}\Delta u_{k,k} - \sigma^v_{ik}\Delta u_{j,k} \tag{3.31}$$

Then Eq.(3.23) becomes

$$\mathcal{L}[F^{int}] = \int_V \frac{\partial \delta u_i}{\partial x_j}\Delta\sigma^*_{ij}dV \tag{3.32}$$

By substituting Eq.(3.30) into Eq.(3.31)

$$\begin{aligned}\Delta\sigma^*_{ij} &= C^t_{ijkl}\Delta u_{(k,l)} + \Delta u_{i,l}\sigma^v_{lj} + \sigma^v_{il}\Delta u_{j,l} - \sigma^v_{ik}\Delta u_{j,k} \\ &= C^t_{ijkl}\Delta u_{(k,l)} + \sigma^v_{lj}\Delta u_{i,l}\end{aligned} \tag{3.33}$$

Therefore,

$$\mathcal{L}[F^{int}] = \int_V \delta u_{i,j}C^t_{ijkl}\Delta u_{(k,l)}dV + \int_V \delta u_{i,j}\sigma^v_{jl}\Delta u_{i,l}dV \tag{3.34}$$

Later in the finite element formulation, the first term of Eq.(3.34) will lead to the material stiffness matrix K^{matl}. For most of engineering materials we are going to discuss later, C^t_{ijkl} possesses both minor and major symmetries, i.e.,

$$\begin{aligned}&C^t_{ijkl} = C^t_{jikl} = C^t_{ijlk} = C^t_{jilk} \text{ and} \\ &C^t_{ijkl} = C^t_{klij}\end{aligned} \tag{3.35}$$

Therefore, only symmetric part of $\delta u_{i,j}$ is required, i.e.,

$$\delta u_{(i,j)} = \frac{1}{2}(\delta u_{i,j} + \delta u_{j,i}) \tag{3.36}$$

Hence, the computation of K^{matl} is quite similar to those of small deformation analysis.

The second term of Eq.(3.34) will lead to the geometrical stiffness matrix K^{geom}. Since the components of the σ^v_{ij} possess major symmetry, a symmetric K^{geom} will be obtained from finite element formulation. From Eqs.(3.10), (3.11), (3.18) and (3.34), the final linearized variational equation becomes

$$\begin{aligned} &\int_V \delta u_{(i,j)} C^t_{ijkl} \Delta u_{(k,l)} dV + \int_V \delta u_{i,j} \sigma^v_{jl} \Delta u_{i,l} dV = \\ &\int_\Gamma \delta u_i h_i d\Gamma - \int_V \frac{\partial \delta u_i}{\partial x^v_j} \sigma^v_{ij} dV \end{aligned} \tag{3.37}$$

3.6 Cauchy Stress Update

In the previous sections, both displacement and stress components are expressed as incremental forms when a consistent linearization approach is taken to approximate the variational equations. As discussed in Chapter 2, the Cauchy stress rate cannot be calculated directly because it is not objective. On the contrary, the Truesdell rate of Cauchy stress can be evaluated via a suitable constitutive equation. Certainly, this cannot be accomplished until the displacement increment is identified. Once the Truesdell rate is obtained, Eq.(2.16) can be used to calculate the Cauchy stress rate. It is noted that both Cauchy stress and Cauchy stress rate are referred to a fixed reference frame during deformation. Therefore, once the Cauchy stress rate is obtained, it is to be added to the Cauchy stress that has been accumulated over previous increments to become the current Cauchy stress.

3.7 Newton-Raphson Iteration

The Newton-Raphson iteration scheme is used for incremental solutions. A step-by-step solution procedure using the equations presented in the previous sections is described below.

1. In the beginning of current increment, a set of trial displacement increments Δu_i is assumed.

2. The Truesdell constitutive equation is calculated using Eq.(3.29).

3. The rate-of-deformation and velocity gradient tensors are identified using Eqs.(3.26) and (3.25), respectively.

4. The Cauchy stress rate is evaluated using Eq.(3.30).

5. Every term in Eq.(3.37) is then calculated.

6. If the residual (right-hand side of Eq.(3.37)) satisfies the convergency criterion (see Appendix D), update the Cauchy stress by using $\sigma_{ij}^{v+1} = \sigma_{ij}^{v} + \Delta\sigma_{ij}$, and start the next increment.

7. If the convergency criterion is not satisfied, solve the system of simultaneous equations, Eq.(3.37), for a displacement correction vector Δu_i^c

8. Let $\Delta u_i^u = \Delta u_i + \Delta u_i^c$.

9. Repeat the steps starting from Step 3 by using Δu_i^u as the new displacement increment, instead of Δu_i.

Chapter 4

INCREMENTAL DISPLACEMENT FIELD

4.1 Introduction

An incremental displacement field based on the Generalized Zigzag Theory is presented in this chapter. It needs to be established before the rate-of-deformation and velocity gradient tensors can be evaluated. The major advantage of the Generalized Zigzag theory as described in Chapter 1 is that its variables are independent of the total number of layers for a composite laminate. The theory was originally proposed by Li & Liu [38] in studying infinitesimal deformation of a composite laminate. In order to be used for large deformation analysis, the linear displacement field must be written in an incremental form. The major difference between the infinitesimal deformation and the large deformation analyses is due to the fact that, in discussing infinitesimal deformation, the spatial coordinate system always coincides with the material coordinate system in a continuum. However, in dealing with large deformation, the two coordinate systems must be described separately.

4.2 Displacement Field

Shown in Figure 4.1 for a continuum, when a particle at position P at time t is deformed to a new position P' at time $t + \Delta t$, components of the displacement increment of the particle at time t can be expressed as follows.

$$\Delta u^k(x,y,z) = \Delta u_0^k(x,y) + \Delta u_1^k(x,y)z + \Delta u_2(x,y)z^2 + \Delta u_3(x,y)z^3 \tag{4.1}$$

$$\Delta v^k(x,y,z) = \Delta v_0^k(x,y) + \Delta v_1^k(x,y)z + \Delta v_2(x,y)z^2 + \Delta v_3(x,y)z^3 \tag{4.2}$$

$$\Delta w^k(x,y,z) = \Delta w_0(x,y) \tag{4.3}$$

where x, y, z are spatial Cartesian coordinates of the particle P at the instant of time t,

k is a layer-number index, where the bottom layer corresponds to $k = 1$,

Δu_0^k, Δv_0^k and Δw_0 are translational displacement components in x, y, and z directions, respectively,

Δu_1^k and Δv_1^k are first-order rotational displacement components about y and x axes, respectively, and

Δu_i and Δv_i ($i = 2, 3$) are higher-order rotational displacement components about y and x axes, respectively.

4.3 Displacement Continuity Conditions

Imposing displacement continuity condition at each laminate interface, we have, for k^{th} layer where $k = 2, \ldots\ldots, n$ with n being the total number of layers,

$$\begin{aligned}
\Delta u^{k-1}\Big|_{z=z_k} &= \Delta u^k\Big|_{z=z_k} \\
\Delta v^{k-1}\Big|_{z=z_k} &= \Delta v^k\Big|_{z=z_k} \\
\Delta w^{k-1}\Big|_{z=z_k} &= \Delta w^k\Big|_{z=z_k} = \Delta w_0
\end{aligned} \tag{4.4}$$

By using Eqs.(4.1),(4.2) and (4.3), Eqs.(4.4) can be written as

$$\Delta u_0^k - \Delta u_0^{k-1} = (\Delta u_1^{k-1} - \Delta u_1^k) z_k$$

$$\Delta v_0^k - \Delta v_0^{k-1} = (\Delta v_1^{k-1} - \Delta v_1^k) z_k \tag{4.5}$$

If we let

$$\Delta u_0^1 = \Delta u_0 \quad \text{and} \quad \Delta v_0^1 = \Delta v_0 \tag{4.6}$$

Eqs.(4.5) become, for k=2,3,....., n,

$$\Delta u_0^k = \Delta u_0 + \sum_{j=2}^{k} (\Delta u_1^{j-1} - \Delta u_1^j) z_j$$

$$\Delta v_0^k = \Delta v_0 + \sum_{j=2}^{k} (\Delta v_1^{j-1} - \Delta v_1^j) z_j \tag{4.7}$$

Now let's introduce the kinetic relations for the k^{th} layer of the laminate,

$$\{\sigma^{(k)}\} = [C^k]\{D\} \tag{4.8}$$

where

$$\left\{\sigma^{(k)}\right\} = \left\{\sigma_x^{(k)}, \sigma_y^{(k)}, \sigma_z^{(k)}, \tau_{yz}^{(k)}, \tau_{xz}^{(k)}, \tau_{xy}^{(k)}\right\}^T, \tag{4.9}$$

$[C^k]$ is the constitutive equation, i.e.

$$[C^k] = \begin{bmatrix} C_{11}^k & C_{12}^k & C_{13}^k & 0 & 0 & C_{16}^k \\ C_{12}^k & C_{22}^k & C_{23}^k & 0 & 0 & C_{26}^k \\ C_{13}^k & C_{23}^k & C_{33}^k & 0 & 0 & C_{36}^k \\ 0 & 0 & 0 & C_{44}^k & 0 & 0 \\ 0 & 0 & 0 & 0 & C_{55}^k & 0 \\ C_{16}^k & C_{26}^k & C_{36}^k & 0 & 0 & C_{66}^k \end{bmatrix} \tag{4.10}$$

and $\{D\}$ it the rate-of-deformation tensor,

$$\{D\} = \begin{Bmatrix} \partial \Delta u^k/\partial x \\ \partial \Delta v^k/\partial y \\ \partial \Delta w^k/\partial z \\ \partial \Delta v^k/\partial z + \partial \Delta w^k/\partial y \\ \partial \Delta u^k/\partial z + \partial \Delta w^k/\partial x \\ \partial \Delta u^k/\partial y + \partial \Delta v^k/\partial x \end{Bmatrix} \tag{4.11}$$

Remark 4.1

Later in the development of a finite element, the (x,y,z) coordinate system will be so chosen that it coincides with the coordinate system of each element. The coordinates (x,y,z) in general do not coincide with the material principal directions for each lamina.

Remark 4.2

In Eq.(4.10), $C_{45}^k = 0$ implies that the out-of-plane shear moduli, G_{13}^k and G_{23}^k, are equal. As can be seen in the following derivation, when interlaminar shear stress continuity conditions are imposed, it will cause strong coupling between in plane displacement components if $C_{45}^k \neq 0$.

4.4 Interlaminar Shear Stress Continuity Conditions

Impose the following interlaminar shear stress continuity conditions:

$$\begin{aligned} \tau_{yz}^{(k-1)}\Big|_{z=z_k} &= \tau_{yz}^{(k)}\Big|_{z=z_k} \\ \tau_{xz}^{(k-1)}\Big|_{z=z_k} &= \tau_{xz}^{(k)}\Big|_{z=z_k} \end{aligned} \tag{4.12}$$

By using Eqs.(4.8), (4.9), (4.10), and (4.11), Eqs.(4.12) become

$$\begin{bmatrix} C_{44}^{k-1} & 0 \\ 0 & C_{55}^{k-1} \end{bmatrix} \begin{Bmatrix} \partial\Delta v^{k-1}/\partial z + \partial\Delta w^{k-1}/\partial y \\ \partial\Delta u^{k-1}/\partial z + \partial\Delta w^{k-1}/\partial x \end{Bmatrix}_{z=z_k} =$$

$$\begin{bmatrix} C_{44}^{k} & 0 \\ 0 & C_{55}^{k} \end{bmatrix} \begin{Bmatrix} \partial\Delta v^{k}/\partial z + \partial\Delta w^{k}/\partial y \\ \partial\Delta u^{k}/\partial z + \partial\Delta w^{k}/\partial x \end{Bmatrix}_{z=z_k} \tag{4.13}$$

By expanding Eq.(4.13), we obtain, for $k = 2, 3, ..., n$,

$$\begin{aligned} C_{44}^{k}\Delta v_1^k - C_{44}^{k-1}\Delta v_1^{k-1} &= 2\Theta_k z_k \Delta v_2 + 3\Theta_k z_k^2 \Delta v_3 + \Theta_k \Delta w_{0,y} \\ C_{55}^{k}\Delta u_1^k - C_{55}^{k-1}\Delta u_1^{k-1} &= 2\Omega_k z_k \Delta u_2 + 3\Omega_k z_k^2 \Delta u_3 + \Omega_k \Delta w_{0,x} \end{aligned} \tag{4.14}$$

where

$$\Omega_k = C_{55}^{k-1} - C_{55}^{k} \quad \text{and} \quad \Theta_k = C_{44}^{k-1} - C_{44}^{k} \tag{4.15}$$

Giving the following new definition,

$$\Delta u_1^1 = \Delta u_1 \quad \text{and} \quad \Delta v_1^1 = \Delta v_1 \tag{4.16}$$

Eq.(4.14) can be rewritten as Δu^k ($\Delta u_{1,2,3}$)

$$\begin{aligned} \Delta u_1^k &= F_1^k \Delta u_1 + F_2^k \Delta u_2 + F_3^k \Delta u_3 + F_4^k \Delta w_{0,x} \\ \Delta v_1^k &= L_1^k \Delta v_1 + L_2^k \Delta v_2 + L_3^k \Delta v_3 + L_4^k \Delta w_{0,y} \end{aligned} \tag{4.17}$$

where, for $k = 1$,

$$\begin{aligned} F_1^1 = 1, \quad F_2^1 = 0, \quad F_3^1 = 0, \quad F_4^1 = 0 \\ L_1^1 = 1, \quad L_2^1 = 0, \quad L_3^1 = 0, \quad L_4^1 = 0 \end{aligned} \tag{4.18}$$

and, for $k = 2, 3, \ldots\ldots, n$,

$$\begin{aligned}
F_1^k &= a_k F_1^{k-1} & L_1^k &= b_k L_1^{k-1} \\
F_2^k &= a_k F_2^{k-1} + 2(\Omega_k / C_{55}^k) z_k & L_2^k &= b_k L_2^{k-1} + 2(\Theta_k / C_{44}^k) z_k \\
F_3^k &= a_k F_3^{k-1} + 3(\Omega_k / C_{55}^k) z_k^2 & L_3^k &= b_k L_3^{k-1} + 3(\Theta_k / C_{44}^k) z_k^2 \\
F_4^k &= a_k F_4^{k-1} + (\Omega_k / C_{55}^k) & L_4^k &= b_k L_4^{k-1} + (\Theta_k / C_{44}^k) \\
a_k &= C_{55}^{k-1} / C_{55}^k & b_k &= C_{44}^{k-1} / C_{44}^k
\end{aligned} \tag{4.19}$$

4.5 Free Surface Shear Stress Conditions

In most laminated composite studies, surface shear stresses are set free. By imposing the free shear stress conditions on the top and bottom surfaces of the composite laminate, we have

$$\begin{aligned}
\tau_{yz}^{(1)}\Big|_{z=z_1} &= \tau_{yz}^{(n)}\Big|_{z=z_{n+1}} = 0 \\
\tau_{xz}^{(1)}\Big|_{z=z_1} &= \tau_{xz}^{(n)}\Big|_{z=z_{n+1}} = 0
\end{aligned} \tag{4.20}$$

By using Eqs.(4.8) and (4.16), Eqs.(4.20) can be expressed as

$$\begin{bmatrix} D_{11} & D_{12} \\ D_{21} & D_{22} \end{bmatrix} \begin{Bmatrix} \Delta u_2 \\ \Delta u_3 \end{Bmatrix} = \begin{bmatrix} E_{11} & E_{12} \\ E_{21} & E_{22} \end{bmatrix} \begin{Bmatrix} \Delta u_1 \\ \Delta w_{0,x} \end{Bmatrix} \tag{4.21}$$

$$\begin{bmatrix} F_{11} & F_{12} \\ F_{21} & F_{22} \end{bmatrix} \begin{Bmatrix} \Delta v_2 \\ \Delta v_3 \end{Bmatrix} = \begin{bmatrix} H_{11} & H_{12} \\ H_{21} & H_{22} \end{bmatrix} \begin{Bmatrix} \Delta v_1 \\ \Delta w_{0,y} \end{Bmatrix} \tag{4.22}$$

where

$$\begin{aligned}
D_{11} &= 2z_{n+1} + F_2^n & D_{12} &= 3z_{n+1}^2 + F_3^n & D_{21} &= 2z_1 & D_{22} &= 3z_1^2 \\
E_{11} &= -F_1^n & E_{12} &= -\left(F_4^n + 1\right) & E_{21} &= -1 & E_{22} &= -1 \\
F_{11} &= 2z_{n+1} + L_2^n & F_{12} &= 3z_{n+1}^2 + L_3^n & F_{21} &= 2z_1 & F_{22} &= 3z_1^2 \\
H_{11} &= -L_1^n & H_{12} &= -\left(L_4^n + 1\right) & H_{21} &= -1 & H_{22} &= -1
\end{aligned} \tag{4.23}$$

Solving Eq.(4.21) and (4.22) for Δu_2, Δu_3, Δv_2, and Δv_3, we obtain

$$\Delta u_2 = A_1 \Delta u_1 + A_2 \Delta w_{0,x}, \quad \Delta u_3 = B_1 \Delta u_1 + B_2 \Delta w_{0,x}$$

$$\Delta v_2 = C_1 \Delta v_1 + C_2 \Delta w_{0,y}, \quad \Delta v_3 = D_1 \Delta v_1 + D_2 \Delta w_{0,y} \tag{4.24}$$

where

$$\begin{aligned}
A_1 &= \tfrac{1}{(det)_1}(E_{11}D_{22} - E_{21}D_{12}) \quad A_2 = \tfrac{1}{(det)_1}(E_{12}D_{22} - E_{22}D_{12}) \\
B_1 &= \tfrac{1}{(det)_1}(E_{21}D_{11} - E_{11}D_{21}) \quad B_2 = \tfrac{1}{(det)_1}(E_{22}D_{11} - E_{12}D_{21}) \\
(det)_1 &= D_{11}D_{22} - D_{21}D_{12} \neq 0 \\
C_1 &= \tfrac{1}{(det)_2}(H_{11}F_{22} - H_{21}F_{12}) \quad C_2 = \tfrac{1}{(det)_2}(H_{12}F_{22} - H_{22}F_{12}) \\
D_1 &= \tfrac{1}{(det)_2}(H_{21}F_{11} - H_{11}F_{21}) \quad D_2 = \tfrac{1}{(det)_2}(H_{22}F_{11} - H_{12}F_{21}) \\
(det)_2 &= F_{11}F_{22} - F_{21}F_{12} \neq 0
\end{aligned} \tag{4.25}$$

Substituting Eqs.(4.24) into Eqs.(4.17), we have

$$\begin{aligned}
\Delta u_1^k &= R_1^k \Delta u_1 + R_2^k \Delta w_{0,x} \\
\Delta v_1^k &= O_1^k \Delta v_1 + O_2^k \Delta w_{0,y}
\end{aligned} \tag{4.26}$$

Substituting Eqs.(4.26) into Eqs.(4.7), we have

$$\begin{aligned}
\Delta u_0^k &= \Delta u_0 + S_1^k \Delta u_1 + S_2^k \Delta w_{0,x} \\
\Delta v_0^k &= \Delta v_0 + P_1^k \Delta v_1 + P_2^k \Delta w_{0,y}
\end{aligned} \tag{4.27}$$

where, for k=1,

$$\begin{aligned}
&R_1^1 = 1, \quad R_2^1 = 0, \quad O_1^1 = 0, \quad O_2^1 = 0 \\
&S_1^1 = 0, \quad S_2^1 = 0, \quad P_1^1 = 0, \quad P_2^1 = 0
\end{aligned} \tag{4.28}$$

and, for k=2,3......,n,

$$R_1^k = F_1^k + A_1 F_2^k + B_1 F_3^k, \quad R_2^k = F_4^k + A_2 F_2^k + B_2 F_3^k$$

$$O_1^k = L_1^k + C_1 L_2^k + D_1 L_3^k, \quad O_2^k = L_4^k + C_2 L_2^k + D_2 L_3^k$$

$$S_1^k = \sum_{l=2}^{k}\left(R_1^{l-1} - R_1^l\right)z_l, \qquad S_2^k = \sum_{l=2}^{k}\left(R_2^{l-1} - R_2^l\right)z_l$$

$$P_1^k = \sum_{l=2}^{k}\left(O_1^{l-1} - O_1^l\right)z_l, \qquad P_2^k = \sum_{l=2}^{k}\left(O_2^{l-1} - O_2^l\right)z_l \tag{4.29}$$

Finally, substituting Eqs.(4.24), (4.26) and (4.27) into Eqs.(4.1), (4.2) and (4.3), we have the final incremental displacement field

$$\begin{aligned}\Delta u^k(x,y,z) = \Delta u_0(x,y) \quad &+ \quad (S_1^k + R_1^k z + A_1 z^2 + B_1 z^3)\Delta u_1(x,y) \\ &+ \quad (S_2^k + R_2^k z + A_2 z^2 + B_2 z^3)\left[\frac{\partial \Delta w_0(x,y)}{\partial x}\right]\end{aligned} \tag{4.30}$$

$$\begin{aligned}\Delta v^k(x,y,z) = \Delta v_0(x,y) \quad &+ \quad (P_1^k + O_1^k z + C_1 z^2 + D_1 z^3)\Delta v_1(x,y) \\ &+ \quad (P_2^k + O_2^k z + C_2 z^2 + D_2 z^3)\left[\frac{\partial \Delta w_0(x,y)}{\partial y}\right]\end{aligned} \tag{4.31}$$

$$\Delta w^k(x,y,z) = \Delta w_0(x,y) \tag{4.32}$$

It is noted from Eqs.(4.1), (4.2), (4.3), (4.30), (4.31) and (4.32) that the total number of variables in the incremental displacement field have been reduced from layer-number dependent to layer-number independent (seven variables in the final form).

Remark 4.3

When we use the free surface shear stress conditions, some errors will be introduced. The error may come from the following two aspects:

1. *The applied load may not necessarily perpendicular to the laminate's top and bottom surfaces in the beginning of the loading history.*

2. *During deformation, the applied load may not be always perpendicular to the laminate's top and bottom surfaces.*

However, if free surface shear stress conditions are not imposed, the total number of independent variables in the incremental displacement field will increase from seven to nine.

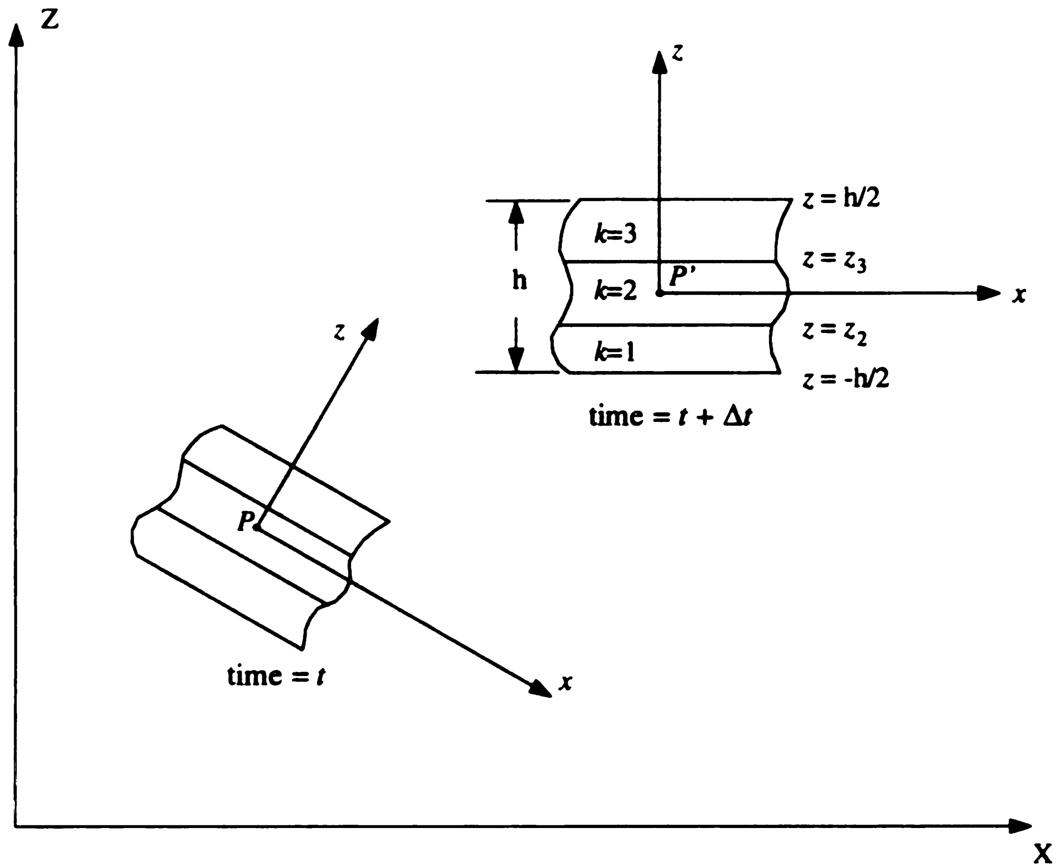

Figure 4.1 Coordinate systems for a laminate shell

Chapter 5

FINITE ELEMENT FORMULATION

5.1 Introduction

The purpose of this chapter is to establish a solution procedure for general three-dimensional shell problems by spatially discretizing the governing equations derived in Chapter 3 via a finite element method. It is to transform the linearized variational equations into a system of linear algebraic equations by using the assembly of construction-identical element contributions.

Once a linearization formulation is completed, the introduction of finite elements into the governing equations is merely a matter of selecting appropriate interpolation functions to approximate the unknown variables element by element. While the choice of appropriate interpolation functions and associated integration schemes, eg. full, reduced, or selectively reduced integrations, are still topics of many ongoing research endeavors, we do not attempt to settle the matter here. Instead, we start with a four-node, quadrilateral shell element using a four-point integration scheme, and each node has seven degrees of freedom. In fact, the linearized governing equations we have formulated can be used with any new shell elements once they become available.

Due to the dissimilarity between laminated composites and isotropic materials, a method called Zigzag Jacobian is proposed. The purpose of this technique is to emphasize the fact that the in-plane displacements of laminated shells are in a zigzag fashion through the laminate thickness. It is different from the Reissner-Mindlin theory, which assumes linear displacements through laminate thickness. Through the calculation of the Zigzag Jacobian matrix, kinematics of laminated shells can be expressed more precisely. Although the Zigzag Jacobian matrix requires nodal displacements at each element on the interfaces, it can be done in a postprocessing procedure. Hence, the total number of degrees of freedom for each element will not change.

5.2 Incremental Strains

Recall Eqs.(4.30), (4.31), and (4.32) in the previous chapter, the incremental displacement equations can be rearranged as

$$
\begin{aligned}
\Delta u^k &= \left(\Delta u_0 + S_1^k \Delta u_1 + S_2^k \frac{\partial \Delta w_0}{\partial x}\right) + \left(R_1^k \Delta u_1 + R_2^k \frac{\partial \Delta w_0}{\partial x}\right) z \\
&+ \left(A_1 \Delta u_1 + A_2 \frac{\partial \Delta w_0}{\partial x}\right) z^2 + \left(B_1 \Delta u_1 + B_2 \frac{\partial \Delta w_0}{\partial x}\right) z^3 \qquad (5.1) \\
\Delta v^k &= \left(\Delta v_0 + P_1^k \Delta v_1 + P_2^k \frac{\partial \Delta w_0}{\partial y}\right) + \left(O_1^k \Delta v_1 + O_2^k \frac{\partial \Delta w_0}{\partial y}\right) z \\
&+ \left(C_1 \Delta v_1 + C_2 \frac{\partial \Delta w_0}{\partial y}\right) z^2 + \left(D_1 \Delta v_1 + D_2 \frac{\partial \Delta w_0}{\partial y}\right) z^3 \qquad (5.2) \\
\Delta w^k &= \Delta w_0 \qquad (5.3)
\end{aligned}
$$

Define a new vector $\{\Delta\epsilon^k\}$ by rearranging the entries of the rate-of-deformation tensor in Eqs.(4.11) as

$$\{\Delta\epsilon^k\} = \left\{ \begin{array}{c} \partial\Delta u^k/\partial x \\ \partial\Delta v^k/\partial y \\ \partial\Delta u^k/\partial y + \partial\Delta v^k/\partial x \\ \partial\Delta v^k/\partial z + \partial\Delta w^k/\partial y \\ \partial\Delta u^k/\partial z + \partial\Delta w^k/\partial x \end{array} \right\} \tag{5.4}$$

Combining Eqs.(5.1), (5.2), (5.3), and (5.4), it yields

$$\{\Delta\epsilon^k\} = \{\Delta\epsilon^0\} + \{\Delta\gamma^0\} + \{\Delta\kappa^1\}z + \{\Delta\kappa^2\}z^2 + \{\Delta\kappa^3\}z^3 \tag{5.5}$$

where

$$\{\Delta\epsilon^0\} = \left\{ \begin{array}{c} \frac{\partial\Delta u_0}{\partial x} + S_1^k\frac{\partial\Delta u_1}{\partial x} + S_2^k\frac{\partial^2\Delta w_0}{\partial x^2} \\ \frac{\partial\Delta v_0}{\partial y} + P_1^k\frac{\partial\Delta v_1}{\partial y} + P_2^k\frac{\partial^2\Delta w_0}{\partial y^2} \\ \frac{\partial\Delta u_0}{\partial y} + S_1^k\frac{\partial\Delta u_1}{\partial y} + S_2^k\frac{\partial^2\Delta w_0}{\partial x\partial y} + \frac{\partial\Delta v_0}{\partial x} + P_1^k\frac{\partial\Delta v_1}{\partial x} + P_2^k\frac{\partial^2\Delta w_0}{\partial x\partial y} \\ 0 \\ 0 \end{array} \right\} \tag{5.6}$$

$$\{\Delta\gamma^0\} = \left\{ \begin{array}{c} 0 \\ 0 \\ 0 \\ O_1^k\Delta v_1 + \left(O_2^k + 1\right)\frac{\partial\Delta w_0}{\partial y} \\ R_1^k\Delta u_1 + \left(R_2^k + 1\right)\frac{\partial\Delta w_0}{\partial x} \end{array} \right\} \tag{5.7}$$

$$\{\Delta\kappa^1\} = \left\{\begin{array}{c} R_1^k \frac{\partial \Delta u_1}{\partial x} + R_2^k \frac{\partial^2 \Delta w_0}{\partial x^2} \\ O_1^k \frac{\partial \Delta v_1}{\partial y} + O_2^k \frac{\partial^2 \Delta w_0}{\partial y^2} \\ R_1^k \frac{\partial \Delta u_1}{\partial y} + O_1^k \frac{\partial \Delta v_1}{\partial x} + \left(R_2^k + O_2^k\right) \frac{\partial^2 \Delta w_0}{\partial x \partial y} \\ 2C_1 \Delta v_1 + 2C_2 \frac{\partial \Delta w_0}{\partial y} \\ 2A_1 \Delta u_1 + 2A_2 \frac{\partial \Delta w_0}{\partial x} \end{array}\right\} \tag{5.8}$$

$$\{\Delta\kappa^2\} = \left\{\begin{array}{c} A_1 \frac{\partial \Delta u_1}{\partial x} + A_2 \frac{\partial^2 \Delta w_0}{\partial x^2} \\ C_1 \frac{\partial \Delta v_1}{\partial y} + C_2 \frac{\partial^2 \Delta w_0}{\partial y^2} \\ A_1 \frac{\partial \Delta u_1}{\partial y} + C_1 \frac{\partial \Delta v_1}{\partial x} + (A_2 + C_2) \frac{\partial^2 \Delta w_0}{\partial x \partial y} \\ 3D_1 \Delta v_1 + 3D_2 \frac{\partial \Delta w_0}{\partial y} \\ 3B_1 \Delta u_1 + 3B_2 \frac{\partial \Delta w_0}{\partial x} \end{array}\right\} \tag{5.9}$$

$$\{\Delta\kappa^3\} = \left\{\begin{array}{c} B_1 \frac{\partial \Delta u_1}{\partial x} + B_2 \frac{\partial^2 \Delta w_0}{\partial x^2} \\ D_1 \frac{\partial \Delta v_1}{\partial y} + D_2 \frac{\partial^2 \Delta w_0}{\partial y^2} \\ B_1 \frac{\partial \Delta u_1}{\partial y} + D_1 \frac{\partial \Delta v_1}{\partial x} + (B_2 + D_2) \frac{\partial^2 \Delta w_0}{\partial x \partial y} \\ 0 \\ 0 \end{array}\right\} \tag{5.10}$$

5.3 Incremental Displacement Gradients

Incremental displacement gradients can be expressed as follows:

$$\nabla\left(\Delta u_i^k\right) = \left\{\begin{array}{c} \partial \Delta u_i^k / \partial x \\ \partial \Delta u_i^k / \partial y \\ \partial \Delta u_i^k / \partial z \end{array}\right\}_{i=1,2,3} \tag{5.11}$$

where

$$\left\{\begin{array}{c}\Delta u_1^k\\ \Delta u_2^k\\ \Delta u_3^k\end{array}\right\}=\left\{\begin{array}{c}\Delta u^k\\ \Delta v^k\\ \Delta w^k\end{array}\right\} \tag{5.12}$$

Let

$$\begin{aligned}\nabla\left(\Delta u^k\right) &= \left\{\begin{array}{c}\partial\Delta u^k/\partial x\\ \partial\Delta u^k/\partial y\\ \partial\Delta u^k/\partial z\end{array}\right\}\\ &= \{\Delta\varpi^0\}+\{\Delta\varpi^1\}z+\{\Delta\varpi^2\}z^2+\{\Delta\varpi^3\}z^3\end{aligned} \tag{5.13}$$

where

$$\{\Delta\varpi^0\} = \left\{\begin{array}{c}\frac{\partial\Delta u_0}{\partial x}+S_1^k\frac{\partial\Delta u_1}{\partial x}+S_2^k\frac{\partial^2\Delta w_0}{\partial x^2}\\ \frac{\partial\Delta u_0}{\partial y}+S_1^k\frac{\partial\Delta u_1}{\partial y}+S_2^k\frac{\partial^2\Delta w_0}{\partial x\partial y}\\ R_1^k\Delta u_1+R_2^k\frac{\partial\Delta w_0}{\partial x}\end{array}\right\} \tag{5.14}$$

$$\{\Delta\varpi^1\} = \left\{\begin{array}{c}R_1^k\frac{\partial\Delta u_1}{\partial x}+R_2^k\frac{\partial^2\Delta w_0}{\partial x^2}\\ R_1^k\frac{\partial\Delta u_1}{\partial y}+R_2^k\frac{\partial^2\Delta w_0}{\partial x\partial y}\\ 2A_1\Delta u_1+2A_2\frac{\partial\Delta w_0}{\partial x}\end{array}\right\} \tag{5.15}$$

$$\{\Delta\varpi^2\} = \left\{\begin{array}{c}A_1\frac{\partial\Delta u_1}{\partial x}+A_2\frac{\partial^2\Delta w_0}{\partial x^2}\\ A_1\frac{\partial\Delta u_1}{\partial y}+A_2\frac{\partial^2\Delta w_0}{\partial x\partial y}\\ 3B_1\Delta u_1+3B_2\frac{\partial\Delta w_0}{\partial x}\end{array}\right\} \tag{5.16}$$

$$\{\Delta\varpi^3\} = \left\{\begin{array}{c}B_1\frac{\partial\Delta u_1}{\partial x}+B_2\frac{\partial^2\Delta w_0}{\partial x^2}\\ B_1\frac{\partial\Delta u_1}{\partial y}+B_2\frac{\partial^2\Delta w_0}{\partial x\partial y}\\ 0\end{array}\right\} \tag{5.17}$$

Similarly,

$$\nabla\left(\Delta v^k\right) = \begin{Bmatrix} \partial\Delta v^k/\partial x \\ \partial\Delta v^k/\partial y \\ \partial\Delta v^k/\partial z \end{Bmatrix}$$
$$= \{\Delta\varphi^0\} + \{\Delta\varphi^1\}z + \{\Delta\varphi^2\}z^2 + \{\Delta\varphi^3\}z^3 \quad (5.18)$$

where

$$\{\Delta\varphi^0\} = \begin{Bmatrix} \frac{\partial\Delta v_0}{\partial x} + P_1^k\frac{\partial\Delta v_1}{\partial x} + P_2^k\frac{\partial^2\Delta w_0}{\partial x\partial y} \\ \frac{\partial\Delta v_0}{\partial y} + P_1^k\frac{\partial\Delta v_1}{\partial y} + P_2^k\frac{\partial^2\Delta w_0}{\partial y^2} \\ O_1^k\Delta v_1 + O_2^k\frac{\partial\Delta w_0}{\partial y} \end{Bmatrix} \quad (5.19)$$

$$\{\Delta\varphi^1\} = \begin{Bmatrix} O_1^k\frac{\partial\Delta v_1}{\partial x} + O_2^k\frac{\partial^2\Delta w_0}{\partial x\partial y} \\ O_1^k\frac{\partial\Delta v_1}{\partial y} + O_2^k\frac{\partial^2\Delta w_0}{\partial y^2} \\ 2C_1\Delta v_1 + 2C_2\frac{\partial\Delta w_0}{\partial y} \end{Bmatrix} \quad (5.20)$$

$$\{\Delta\varphi^2\} = \begin{Bmatrix} C_1\frac{\partial\Delta v_1}{\partial x} + C_2\frac{\partial^2\Delta w_0}{\partial x\partial y} \\ C_1\frac{\partial\Delta v_1}{\partial y} + C_2\frac{\partial^2\Delta w_0}{\partial y^2} \\ 3D_1\Delta v_1 + 3D_2\frac{\partial\Delta w_0}{\partial y} \end{Bmatrix} \quad (5.21)$$

$$\{\Delta\varphi^3\} = \begin{Bmatrix} D_1\frac{\partial\Delta v_1}{\partial x} + D_2\frac{\partial^2\Delta w_0}{\partial x\partial y} \\ D_1\frac{\partial\Delta v_1}{\partial y} + D_2\frac{\partial^2\Delta w_0}{\partial y^2} \\ 0 \end{Bmatrix} \quad (5.22)$$

and

$$\nabla\left(\Delta w^k\right) = \begin{Bmatrix} \partial\Delta w^k/\partial x \\ \partial\Delta w^k/\partial y \\ \partial\Delta w^k/\partial z \end{Bmatrix} = \{\Delta\vartheta^0\} \quad (5.23)$$

where

$$\{\Delta\vartheta^0\} = \left\{ \begin{array}{c} \frac{\partial \Delta w_0}{\partial x} \\ \frac{\partial \Delta w_0}{\partial y} \\ 0 \end{array} \right\} \tag{5.24}$$

5.4 Finite Element Description of Displacements

Here, we introduce a two-dimensional quadrilateral element and use bilinear shape functions to describe the unknown displacements within each element [28], i.e.

$$\begin{aligned} \Delta u_0 &= \sum_{a=1}^{4} N_a(\xi,\eta)\,(\Delta u_0)_a \\ \Delta u_1 &= \sum_{a=1}^{4} N_a(\xi,\eta)\,(\Delta u_1)_a \\ \Delta v_0 &= \sum_{a=1}^{4} N_a(\xi,\eta)\,(\Delta v_0)_a \\ \Delta v_1 &= \sum_{a=1}^{4} N_a(\xi,\eta)\,(\Delta v_1)_a \end{aligned} \tag{5.25}$$

where the bilinear shape function N_a is for the a^{th} node in the element. Figure 5.1 delineates a typical element and shape functions for corresponding nodes. The natural coordinates ξ and η have values between -1 and 1. The nodal unknowns $(\Delta u_0)_a$, $(\Delta u_1)_a$, $(\Delta v_0)_a$, and $(\Delta v_1)_a$ are for the a^{th} node.

Since Δw_0, $\partial\Delta w_0/\partial x$, and $\partial\Delta w_0/\partial y$ are involved in Eqs.(5.1), (5.2), and (5.3) as degrees of freedom, shape functions with C^1 continuity are required for Δw_0. The so-called Hermite cubic shape functions [55] are required for describing Δw_0, i.e.

$$\Delta w_0 = \sum_{a=1}^{4} H_a(\xi,\eta) q_a \tag{5.26}$$

where

$$H_a(\xi,\eta) = \left\{ \begin{array}{c} \mathcal{H}_{a1}(\xi,\eta) \\ \mathcal{H}_{a2}(\xi,\eta) \\ \mathcal{H}_{a3}(\xi,\eta) \end{array} \right\} \tag{5.27}$$

$$q_a^T = \left\{ (\Delta w_0)_a, \left(\frac{\partial \Delta w_0}{\partial x}\right)_a, \left(\frac{\partial \Delta w_0}{\partial y}\right)_a \right\} \tag{5.28}$$

Descriptions of H_a are outlined in Figure 5.1. By substituting Eqs.(5.25) and (5.26) into Eqs.(5.1) through (5.3), we have

$$\Delta u^k = \left(\{XU_0\} + \{XU_1\}z + \{XU_2\}z^2 + \{XU_3\}z^3\right)_{(1\times 28)} \{\Delta u\}_{(28\times 1)} \tag{5.29}$$

$$\Delta v^k = \left(\{XV_0\} + \{XV_1\}z + \{XV_2\}z^2 + \{XV_3\}z^3\right)_{(1\times 28)} \{\Delta u\}_{(28\times 1)} \tag{5.30}$$

$$\Delta w^k = \{XW_0\}_{(1\times 28)} \{\Delta u\}_{(28\times 1)} \tag{5.31}$$

Similarly, we can rewrite other equations with use of Eqs.(5.25) and (5.26). From Eqs.(5.6) through (5.10), we have

$$\left\{\Delta\epsilon^0\right\}_{(5\times 1)} = [MA]_{(5\times 28)}\{\Delta u\}_{(28\times 1)} \tag{5.32}$$

$$\left\{\Delta\gamma^0\right\}_{(5\times 1)} = [MB]_{(5\times 28)}\{\Delta u\}_{(28\times 1)} \tag{5.33}$$

$$\left\{\Delta\kappa^1\right\}_{(5\times 1)} = [MD_1]_{(5\times 28)}\{\Delta u\}_{(28\times 1)} \tag{5.34}$$

$$\left\{\Delta\kappa^2\right\}_{(5\times 1)} = [MD_2]_{(5\times 28)}\{\Delta u\}_{(28\times 1)} \tag{5.35}$$

$$\left\{\Delta\kappa^3\right\}_{(5\times 1)} = [MD_3]_{(5\times 28)}\{\Delta u\}_{(28\times 1)} \tag{5.36}$$

From Eqs.(5.14) through (5.17), we have

$$\left\{\Delta\varpi^0\right\}_{(3\times 1)} = [GU_0]_{(3\times 28)}\{\Delta u\}_{(28\times 1)} \tag{5.37}$$

$$\left\{\Delta\varpi^1\right\}_{(3\times 1)} = [GU_1]_{(3\times 28)}\{\Delta u\}_{(28\times 1)} \tag{5.38}$$

$$\left\{\Delta\varpi^2\right\}_{(3\times 1)} = [GU_2]_{(3\times 28)}\{\Delta u\}_{(28\times 1)} \tag{5.39}$$

$$\left\{\Delta\varpi^3\right\}_{(3\times 1)} = [GU_3]_{(3\times 28)}\{\Delta u\}_{(28\times 1)} \tag{5.40}$$

From Eqs.(5.19) through (5.22), we have

$$\left\{\Delta\varphi^0\right\}_{(3\times 1)} = [GV_0]_{(3\times 28)}\{\Delta u\}_{(28\times 1)} \tag{5.41}$$

$$\left\{\Delta\varphi^1\right\}_{(3\times 1)} = [GV_1]_{(3\times 28)}\{\Delta u\}_{(28\times 1)} \tag{5.42}$$

$$\left\{\Delta\varphi^2\right\}_{(3\times 1)} = [GV_2]_{(3\times 28)}\{\Delta u\}_{(28\times 1)} \tag{5.43}$$

$$\left\{\Delta\varphi^3\right\}_{(3\times 1)} = [GV_3]_{(3\times 28)}\{\Delta u\}_{(28\times 1)} \tag{5.44}$$

Finally, from Eq.(5.24), we have

$$\left\{\Delta\vartheta^0\right\}_{(3\times 1)} = [GW_0]_{(3\times 28)}\{\Delta u\}_{(28\times 1)} \tag{5.45}$$

where

$$\begin{aligned}\{\Delta u\}^T = \Big\{&(\Delta u_0)_1,\ (\Delta v_0)_1,\ (\Delta w_0)_1,\ (\Delta u_1)_1,\ (\Delta v_1)_1,\ \left(\tfrac{\partial\Delta w_0}{\partial x}\right)_1,\ \left(\tfrac{\partial\Delta w_0}{\partial y}\right)_1, \\ &(\Delta u_0)_2,\ (\Delta v_0)_2,\ (\Delta w_0)_2,\ (\Delta u_1)_2,\ (\Delta v_1)_2,\ \left(\tfrac{\partial\Delta w_0}{\partial x}\right)_2,\ \left(\tfrac{\partial\Delta w_0}{\partial y}\right)_2, \\ &(\Delta u_0)_3,\ (\Delta v_0)_3,\ (\Delta w_0)_3,\ (\Delta u_1)_3,\ (\Delta v_1)_3,\ \left(\tfrac{\partial\Delta w_0}{\partial x}\right)_3,\ \left(\tfrac{\partial\Delta w_0}{\partial y}\right)_3, \\ &(\Delta u_0)_4,\ (\Delta v_0)_4,\ (\Delta w_0)_4,\ (\Delta u_1)_4,\ (\Delta v_1)_4,\ \left(\tfrac{\partial\Delta w_0}{\partial x}\right)_4,\ \left(\tfrac{\partial\Delta w_0}{\partial y}\right)_4\Big\}\end{aligned} \tag{5.46}$$

Detailed components of $\{XU_0\}$, $\{XU_1\}$, $\{XU_2\}$, $\{XU_3\}$, $\{XV_0\}$, $\{XV_1\}$, $\{XV_2\}$, $\{XV_3\}$, $\{XW_0\}$, $[MA]$, $[MB]$, $[MD_1]$, $[MD_2]$, $[MD_3]$, $[GU_0]$, $[GU_1]$, $[GU_2]$, $[GU_3]$, $[GV_0]$, $[GV_1]$, $[GV_2]$, $[GV_3]$, and $[GW_3]$ are shown in Appendix B. It should be noted that the subscript numbers outside the parenthesis in the above equations indicate the dimension of the array. Hence, the incremental strains and increment displacement gradients in Eqs.(5.5), (5.13), (5.18), and (5.23) can be rewritten, respectively, as

$$\{\Delta\epsilon^k\} = \left([MA] + [MB] + [MD_1]z + [MD_2]z^2 + [MD_3]z^3\right)\{\Delta u\} \tag{5.47}$$

$$\nabla(\Delta u^k) = \left([GU_0] + [GU_1]z + [GU_2]z^2 + [GU_3]z^3\right)\{\Delta u\} \tag{5.48}$$

$$\nabla(\Delta v^k) = \left([GV_0] + [GV_1]z + [GV_2]z^2 + [GV_3]z^3\right)\{\Delta u\} \tag{5.49}$$

$$\nabla(\Delta w^k) = [GW_0]\{\Delta u\} \tag{5.50}$$

5.5 Description of Geometry

Under the Reissner-Mindlin theory, a straight line normal to the mid-plane of a shell is straight but not necessarily normal to the mid-plane after deformation. However, as shown at the bottom of Figure 5.2, a straight line normal to the mid-plane of a composite laminate before deformation is neither normal to the mid-plane nor a straight line after deformation. Instead, it becomes a zigzag line. As explained previously, this phenomenon is due to the difference of material properties across the laminate interfaces. It is also noted that each segment of the zigzag line is generally not straight inside each layer.

By combining the nodal displacements and shape functions presented in the previous section, it is possible to describe the displacements anywhere within an element. Similarly, it requires a method to mathematically delineate the geometry of an element so that the coordinates of any point within the element can be characterized. Intuitively, one will think of using a consistent way for both the kinematics and the geometry. This is how isoparametric elements are utilized. Apparently, for laminated shells, the isoparametric concept needs some modifications. The following description for the geometry of a laminate shell element is proposed. The method is called Zigzag Jacobian. It is different from the traditional Reissner-Mindlin way of constructing a Jacobian matrix and is specifically designed for laminated shells with a zigzag displacement field.

First of all, segments of the zigzag line through the laminate thickness are assumed linear for individual layers. Although in reality, each line segment is of a high-order curve, it is not too far away from a linear line assumption because the thickness of each layer is usually very thin. The coordinates (x, y, z) of a point anywhere within an element is expressed below.

$$\begin{Bmatrix} x \\ y \\ z \end{Bmatrix} = \sum_{a=1}^{4} N_a(\xi,\eta)\frac{1+\zeta}{2}\begin{Bmatrix} x_a^{k+1} \\ y_a^{k+1} \\ z_a^{k+1} \end{Bmatrix} + \sum_{a=1}^{4} N_a(\xi,\eta)\frac{1-\zeta}{2}\begin{Bmatrix} x_a^{k} \\ y_a^{k} \\ z_a^{k} \end{Bmatrix} \tag{5.51}$$

As shown in Figure 5.2, $a = 1, 2, 3, 4$ are the local nodal numbers for a typical element. The interface number k is counted from the bottom free surface, and (ξ, η, ζ) are coordinates of a natural coordinate systems. In addition, $N_a(\xi, \eta)$ is the same bilinear shape functions as used in the previous section, and (x_a^k, y_a^k, z_a^k) is the nodal coordinates for the a^{th} node at the k^{th} interface. The nodal coordinates are to be found after solving the assembled finite element equations for unknown displacements.

By definition, the Jacobian matrix can be expressed in the following form:

$$[J] = \begin{bmatrix} \frac{\partial x}{\partial \xi} & \frac{\partial y}{\partial \xi} & \frac{\partial z}{\partial \xi} \\ \frac{\partial x}{\partial \eta} & \frac{\partial y}{\partial \eta} & \frac{\partial z}{\partial \eta} \\ \frac{\partial x}{\partial \zeta} & \frac{\partial y}{\partial \zeta} & \frac{\partial z}{\partial \zeta} \end{bmatrix} \tag{5.52}$$

From Eqn.(5.51), we have

$$\begin{Bmatrix} \frac{\partial x}{\partial \xi} \\ \frac{\partial y}{\partial \xi} \\ \frac{\partial z}{\partial \xi} \end{Bmatrix} = \sum_{a=1}^{4} \frac{\partial N_a}{\partial \xi}\frac{1+\zeta}{2}\begin{Bmatrix} x_a^{k+1} \\ y_a^{k+1} \\ z_a^{k+1} \end{Bmatrix} + \sum_{a=1}^{4} \frac{\partial N_a}{\partial \xi}\frac{1-\zeta}{2}\begin{Bmatrix} x_a^{k} \\ y_a^{k} \\ z_a^{k} \end{Bmatrix} \tag{5.53}$$

$$\begin{Bmatrix} \frac{\partial x}{\partial \eta} \\ \frac{\partial y}{\partial \eta} \\ \frac{\partial z}{\partial \eta} \end{Bmatrix} = \sum_{a=1}^{4} \frac{\partial N_a}{\partial \eta}\frac{1+\zeta}{2}\begin{Bmatrix} x_a^{k+1} \\ y_a^{k+1} \\ z_a^{k+1} \end{Bmatrix} + \sum_{a=1}^{4} \frac{\partial N_a}{\partial \eta}\frac{1-\zeta}{2}\begin{Bmatrix} x_a^{k} \\ y_a^{k} \\ z_a^{k} \end{Bmatrix} \tag{5.54}$$

$$\begin{Bmatrix} \frac{\partial x}{\partial \zeta} \\ \frac{\partial y}{\partial \zeta} \\ \frac{\partial z}{\partial \zeta} \end{Bmatrix} = \sum_{a=1}^{4} N_a\left(\frac{1}{2}\right)\begin{Bmatrix} x_a^{k+1} \\ y_a^{k+1} \\ z_a^{k+1} \end{Bmatrix} + \sum_{a=1}^{4} N_a\left(\frac{-1}{2}\right)\begin{Bmatrix} x_a^{k} \\ y_a^{k} \\ z_a^{k} \end{Bmatrix} \tag{5.55}$$

Therefore, the Jacobian matrix can be rewritten as follows. The summation notation is omitted in the following matrices with an understanding that repeated indices indicate summation over the range.

$$
\begin{aligned}
[J] &= \begin{bmatrix} \frac{\partial N_a}{\partial \xi}\frac{1+\zeta}{2}x_a^{k+1} & \frac{\partial N_a}{\partial \xi}\frac{1+\zeta}{2}y_a^{k+1} & \frac{\partial N_a}{\partial \xi}\frac{1+\zeta}{2}z_a^{k+1} \\ \frac{\partial N_a}{\partial \eta}\frac{1+\zeta}{2}x_a^{k+1} & \frac{\partial N_a}{\partial \eta}\frac{1+\zeta}{2}y_a^{k+1} & \frac{\partial N_a}{\partial \eta}\frac{1+\zeta}{2}z_a^{k+1} \\ 0 & 0 & 0 \end{bmatrix} \\
&+ \begin{bmatrix} \frac{\partial N_a}{\partial \xi}\frac{1-\zeta}{2}x_a^{k+1} & \frac{\partial N_a}{\partial \xi}\frac{1-\zeta}{2}y_a^{k+1} & \frac{\partial N_a}{\partial \xi}\frac{1-\zeta}{2}z_a^{k+1} \\ \frac{\partial N_a}{\partial \eta}\frac{1-\zeta}{2}x_a^{k+1} & \frac{\partial N_a}{\partial \eta}\frac{1-\zeta}{2}y_a^{k+1} & \frac{\partial N_a}{\partial \eta}\frac{1-\zeta}{2}z_a^{k+1} \\ 0 & 0 & 0 \end{bmatrix} \\
&+ \begin{bmatrix} 0 & 0 & 0 \\ 0 & 0 & 0 \\ N_a\left(\frac{1}{2}\right)x_a^{k+1} & N_a\left(\frac{1}{2}\right)y_a^{k+1} & N_a\left(\frac{1}{2}\right)z_a^{k+1} \end{bmatrix} \\
&+ \begin{bmatrix} 0 & 0 & 0 \\ 0 & 0 & 0 \\ N_a\left(\frac{-1}{2}\right)x_a^{k+1} & N_a\left(\frac{-1}{2}\right)y_a^{k+1} & N_a\left(\frac{-1}{2}\right)z_a^{k+1} \end{bmatrix} \\
&= \begin{bmatrix} \frac{\partial N_a}{\partial \xi}\frac{1}{2}\left(x_a^{k+1}+x_a^k\right) & \frac{\partial N_a}{\partial \xi}\frac{1}{2}\left(y_a^{k+1}+y_a^k\right) & \frac{\partial N_a}{\partial \xi}\frac{1}{2}\left(z_a^{k+1}+z_a^k\right) \\ \frac{\partial N_a}{\partial \eta}\frac{1}{2}\left(x_a^{k+1}+x_a^k\right) & \frac{\partial N_a}{\partial \eta}\frac{1}{2}\left(y_a^{k+1}+y_a^k\right) & \frac{\partial N_a}{\partial \eta}\frac{1}{2}\left(z_a^{k+1}+z_a^k\right) \\ 0 & 0 & 0 \end{bmatrix} \\
&+ \begin{bmatrix} \frac{\partial N_a}{\partial \xi}\frac{\zeta}{2}\left(x_a^{k+1}-x_a^k\right) & \frac{\partial N_a}{\partial \xi}\frac{\zeta}{2}\left(y_a^{k+1}-y_a^k\right) & \frac{\partial N_a}{\partial \xi}\frac{\zeta}{2}\left(z_a^{k+1}-z_a^k\right) \\ \frac{\partial N_a}{\partial \eta}\frac{\zeta}{2}\left(x_a^{k+1}-x_a^k\right) & \frac{\partial N_a}{\partial \eta}\frac{\zeta}{2}\left(y_a^{k+1}-y_a^k\right) & \frac{\partial N_a}{\partial \eta}\frac{\zeta}{2}\left(z_a^{k+1}-z_a^k\right) \\ \frac{1}{2}N_a\left(x_a^{k+1}-x_a^k\right) & \frac{1}{2}N_a\left(y_a^{k+1}-y_a^k\right) & \frac{1}{2}N_a\left(z_a^{k+1}-z_a^k\right) \end{bmatrix}
\end{aligned}
\tag{5.56}
$$

Finally, we have

$$[J] = \begin{bmatrix} \frac{\partial N_1}{\partial \xi} & \frac{\partial N_2}{\partial \xi} & \frac{\partial N_3}{\partial \xi} & \frac{\partial N_4}{\partial \xi} \\ \frac{\partial N_1}{\partial \eta} & \frac{\partial N_2}{\partial \eta} & \frac{\partial N_3}{\partial \eta} & \frac{\partial N_4}{\partial \eta} \\ 0 & 0 & 0 & 0 \end{bmatrix} \begin{bmatrix} \frac{1}{2}\left(x_1^{k+1}+x_1^k\right) & \frac{1}{2}\left(y_1^{k+1}+y_1^k\right) & \frac{1}{2}\left(z_1^{k+1}+z_1^k\right) \\ \frac{1}{2}\left(x_2^{k+1}+x_2^k\right) & \frac{1}{2}\left(y_2^{k+1}+y_2^k\right) & \frac{1}{2}\left(z_2^{k+1}+z_2^k\right) \\ \frac{1}{2}\left(x_3^{k+1}+x_3^k\right) & \frac{1}{2}\left(y_3^{k+1}+y_3^k\right) & \frac{1}{2}\left(z_3^{k+1}+z_3^k\right) \\ \frac{1}{2}\left(x_4^{k+1}+x_4^k\right) & \frac{1}{2}\left(y_4^{k+1}+y_4^k\right) & \frac{1}{2}\left(z_4^{k+1}+z_4^k\right) \end{bmatrix} +$$

$$\begin{bmatrix} \frac{\partial N_1}{\partial \xi}\zeta & \frac{\partial N_2}{\partial \xi}\zeta & \frac{\partial N_3}{\partial \xi}\zeta & \frac{\partial N_4}{\partial \xi} \\ \frac{\partial N_1}{\partial \eta}\zeta & \frac{\partial N_2}{\partial \eta}\zeta & \frac{\partial N_3}{\partial \eta}\zeta & \frac{\partial N_4}{\partial \eta} \\ N_1 & N_2 & N_3 & N_4 \end{bmatrix} \begin{bmatrix} \frac{1}{2}\left(x_1^{k+1}-x_1^k\right) & \frac{1}{2}\left(y_1^{k+1}-y_1^k\right) & \frac{1}{2}\left(z_1^{k+1}-z_1^k\right) \\ \frac{1}{2}\left(x_2^{k+1}-x_2^k\right) & \frac{1}{2}\left(y_2^{k+1}-y_2^k\right) & \frac{1}{2}\left(z_2^{k+1}-z_2^k\right) \\ \frac{1}{2}\left(x_3^{k+1}-x_3^k\right) & \frac{1}{2}\left(y_3^{k+1}-y_3^k\right) & \frac{1}{2}\left(z_3^{k+1}-z_3^k\right) \\ \frac{1}{2}\left(x_4^{k+1}-x_4^k\right) & \frac{1}{2}\left(y_4^{k+1}-y_4^k\right) & \frac{1}{2}\left(z_4^{k+1}-z_4^k\right) \end{bmatrix} \tag{5.57}$$

It should be noted that

$$\begin{Bmatrix} \frac{\partial}{\partial x} \\ \frac{\partial}{\partial y} \\ \frac{\partial}{\partial z} \end{Bmatrix} = \begin{bmatrix} \frac{\partial \xi}{\partial x} & \frac{\partial \eta}{\partial x} & \frac{\partial \zeta}{\partial x} \\ \frac{\partial \xi}{\partial y} & \frac{\partial \eta}{\partial y} & \frac{\partial \zeta}{\partial y} \\ \frac{\partial \xi}{\partial z} & \frac{\partial \eta}{\partial z} & \frac{\partial \zeta}{\partial z} \end{bmatrix} \begin{Bmatrix} \frac{\partial}{\partial \xi} \\ \frac{\partial}{\partial \eta} \\ \frac{\partial}{\partial \zeta} \end{Bmatrix}$$

$$= [J]^{-1} \begin{Bmatrix} \frac{\partial}{\partial \xi} \\ \frac{\partial}{\partial \eta} \\ \frac{\partial}{\partial \zeta} \end{Bmatrix} \tag{5.58}$$

5.6 Stiffness Matrices and Force Vectors

Recall the linearized variational equation, Eq.(3.37). For each element, the governing equation can be expressed as

$$\int_V \{\delta\epsilon^k\}^T [C^{t(k)}] \{\Delta\epsilon^k\} dV + \int_V \nabla(\delta u^k)^T [\sigma] \nabla(\Delta u^k) dV +$$
$$\int_V \nabla(\delta v^k)^T [\sigma] \nabla(\Delta v^k) dV + \int_V \nabla(\delta w^k)^T [\sigma] \nabla(\Delta w^k) dV =$$
$$\int_\Gamma \left\{\delta u_i^k\right\} \{h\} d\Gamma + \int_V \{\delta\epsilon^k\}^T \{\sigma\} dV \tag{5.59}$$

In the above equation, $\{\sigma\}$ is the Cauchy stress vector, i.e.

$$\{\sigma\} = \{\sigma_x, \sigma_y, \tau_{xy}, \tau_{yz}, \tau_{zx}\}^T, \tag{5.60}$$

$[\sigma]$ is the Cauchy stress matrix, i.e.

$$[\sigma] = \begin{bmatrix} \sigma_x & \tau_{xy} & \tau_{zx} \\ \tau_{xy} & \sigma_y & \tau_{yz} \\ \tau_{zx} & \tau_{yz} & 0 \end{bmatrix}, \tag{5.61}$$

and $[C^{t(k)}]$ is the Truesdell constitutive equation (recall Eq.(3.29)) for the k^{th} layer.

(1) Internal Force Vector

Substituting Eq.(5.47) into the second term on the right-hand side of Eq.(5.59), components of the internal force vector can be expressed as

$$\{F^{int}\} = \int_V \left([MA]^T + [MB]^T + [MD_1]^T z + [MD_2]^T z^2 + [MD_3]^T z^3\right) \{\sigma\} dV \tag{5.62}$$

(2) Materaial Stiffness Matrix

Substituting Eq.(5.47) into the first term of the left-hand side of Eq.(5.59), components of the material stiffness matrix can be expressed as

$$\begin{aligned}
\left[K^{matl}\right] &= \int_V \left([MA]^T + [MB]^T + [MD_1]^T z + [MD_2]^T z^2 + [MD_3]^T z^3\right) [C^{t(k)}] \\
& \quad \left([MA] + [MB] + [MD_1]z + [MD_2]z^2 + [MD_3]z^3\right) dV \\
&= \int_V [MA]^T [C^{t(k)}][MA] dV + \int_V [MA]^T [C^{t(k)}][MB] dV \\
&+ \int_V [MB]^T [C^{t(k)}][MA] dV + \int_V [MB]^T [C^{t(k)}][MB] dV \\
&+ \int_V [MD_1]^T [C^{t(k)}] z [MA] dV + \int_V [MD_1]^T [C^{t(k)}] z [MB] dV \\
&+ \int_V [MA]^T [C^{t(k)}] z [MD_1] dV + \int_V [MB]^T [C^{t(k)}] z [MD_1] dV \\
&+ \int_V [MD_1]^T [C^{t(k)}] z^2 [MD_1] dV + \int_V [MD_2]^T [C^{t(k)}] z^2 [MA] dV
\end{aligned}$$

$$
\begin{aligned}
&+ \int_V [MD_2]^T[C^{t(k)}]z^2[MB]dV + \int_V [MA]^T[C^{t(k)}]z^2[MD_2]dV \\
&+ \int_V [MB]^T[C^{t(k)}]z^2[MD_2]dV + \int_V [MD_1]^T[C^{t(k)}]z^3[MD_2]dV \\
&+ \int_V [MD_2]^T[C^{t(k)}]z^3[MD_1]dV + \int_V [MD_3]^T[C^{t(k)}]z^3[MA]dV \\
&+ \int_V [MD_3]^T[C^{t(k)}]z^3[MB]dV + \int_V [MA]^T[C^{t(k)}]z^3[MD_3]dV \\
&+ \int_V [MB]^T[C^{t(k)}]z^3[MD_3]dV + \int_V [MD_1]^T[C^{t(k)}]z^4[MD_3]dV \\
&+ \int_V [MD_3]^T[C^{t(k)}]z^4[MD_1]dV + \int_V [MD_2]^T[C^{t(k)}]z^4[MD_2]dV \\
&+ \int_V [MD_2]^T[C^{t(k)}]z^5[MD_3]dV + \int_V [MD_3]^T[C^{t(k)}]z^5[MD_2]dV \\
&+ \int_V [MD_3]^T[C^{t(k)}]z^6[MD_3]dV \qquad (5.63)
\end{aligned}
$$

(3) Geometric Stiffness Matrix

Substituting Eqs.(5.48), (5.49), and (5.50) into the last three terms on the left-hand side of Eq.(5.59), components of the geometric stiffness matrix can be expressed as

$$
\begin{aligned}
[K^{geom}] &= \int_V \left([GU_0]^T + [GU_1]^T z + [GU_2]^T z^2 + [GU_3]^T z^3\right)[\sigma] \\
&\quad \left([GU_0] + [GU_1]z + [GU_2]z^2 + [GU_3]z^3\right) dV \\
&+ \int_V \left([GV_0]^T + [GV_1]^T z + [GV_2]^T z^2 + [GV_3]^T z^3\right)[\sigma] \\
&\quad \left([GV_0] + [GV_1]z + [GV_2]z^2 + [GV_3]z^3\right) dV \\
&+ \int_V [GW_0]^T[\sigma]dV \\
&= \int_V [GU_0]^T[\sigma][GU_0]dV + \int_V [GU_0]^T[\sigma]z[GU_1]dV \\
&+ \int_V [GU_1]^T[\sigma]z[GU_0]dV + \int_V [GU_1]^T[\sigma]z^2[GU_1]dV \\
&+ \int_V [GU_0]^T[\sigma]z^2[GU_2]dV + \int_V [GU_2]^T[\sigma]z^2[GU_0]dV \\
&+ \int_V [GU_0]^T[\sigma]z^3[GU_3]dV + \int_V [GU_3]^T[\sigma]z^3[GU_0]dV \\
&+ \int_V [GU_1]^T[\sigma]z^3[GU_2]dV + \int_V [GU_2]^T[\sigma]z^3[GU_1]dV \\
&+ \int_V [GU_2]^T[\sigma]z^4[GU_2]dV + \int_V [GU_1]^T[\sigma]z^4[GU_3]dV
\end{aligned}
$$

$$
\begin{aligned}
&+ \int_V [GU_3]^T[\sigma]z^4[GU_1]dV + \int_V [GU_2]^T[\sigma]z^5[GU_3]dV \\
&+ \int_V [GU_3]^T[\sigma]z^5[GU_2]dV + \int_V [GU_3]^T[\sigma]z^6[GU_3]dV \\
&+ \int_V [GV_0]^T[\sigma][GV_0]dV + \int_V [GV_0]^T[\sigma]z[GV_1]dV \\
&+ \int_V [GV_1]^T[\sigma]z[GV_0]dV + \int_V [GV_0]^T[\sigma]z^2[GV_2]dV \\
&+ \int_V [GV_2]^T[\sigma]z^2[GV_0]dV + \int_V [GV_1]^T[\sigma]z^2[GV_1]dV \\
&+ \int_V [GV_0]^T[\sigma]z^3[GV_3]dV + \int_V [GV_3]^T[\sigma]z^3[GV_0]dV \\
&+ \int_V [GV_1]^T[\sigma]z^3[GV_2]dV + \int_V [GV_2]^T[\sigma]z^3[GV_1]dV \\
&+ \int_V [GV_1]^T[\sigma]z^4[GV_3]dV + \int_V [GV_3]^T[\sigma]z^4[GV_1]dV \\
&+ \int_V [GV_2]^T[\sigma]z^4[GV_2]dV + \int_V [GV_2]^T[\sigma]z^5[GV_3]dV \\
&+ \int_V [GV_3]^T[\sigma]z^5[GV_2]dV + \int_V [GV_3]^T[\sigma]z^6[GV_3]dV \\
&+ \int_V [GW_0]^T[\sigma][GW_0]dV \qquad (5.64)
\end{aligned}
$$

(4) External Force Vector

The first term on the right-hand side of Eq.(5.59) can be written in the following form:

$$\int_\Gamma \left\{\delta u_i^k\right\}\{h\}d\Gamma = \int_{S^*} \left(\delta u^k h_x + \delta v^k h_y + \delta w^k h_z\right) dS^* \qquad (5.65)$$

where h_x, h_y, and h_z are tractions in the element x, y, and z directions, respectively, and S^* is current top and bottom surface areas. By using Eqs.(5.29), (5.30), and (5.31), components of the external force vector become

$$
\begin{aligned}
\{F^{ext}\} &= \int_{S^*} \Big(\left(\{XU_0\}^T + \{XU_1\}^T z + \{XU_2\}^T z^2 + \{XU_3\}^T z^3\right) h_x \\
&+ \left(\{XV_0\}^T + \{XV_1\}^T z + \{XV_2\}^T z^2 + \{XV_3\}^T z^3\right) h_y \\
&+ \{XW_0\}^T h_z \Big) dS^* \qquad (5.66)
\end{aligned}
$$

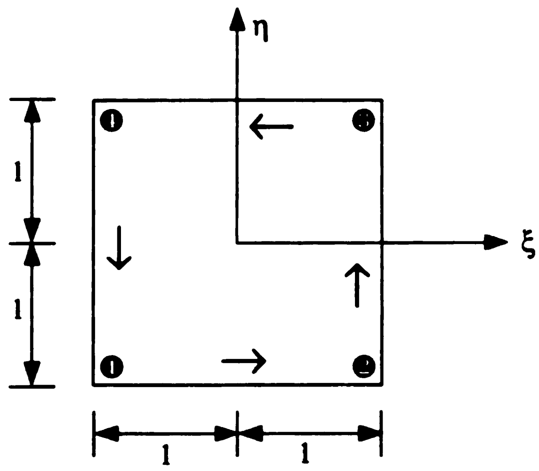

Bilinear Shape Functions

$$N_a = \frac{1}{4}(1 + \xi_a \xi)(1 + \eta_a \eta)$$

Hermite Cubic Shape Functions

$$\begin{Bmatrix} \mathcal{H}_{a1} \\ \mathcal{H}_{a2} \\ \mathcal{H}_{a3} \end{Bmatrix} = \begin{Bmatrix} \frac{1}{8}(1 + \xi_a \xi)(1 + \eta_a \eta)(2 + \xi_a \xi + \eta_a \eta - \xi^2 - \eta^2) \\ \frac{1}{8}\xi_a(1 + \xi_a \xi)^2(1 + \eta_a \eta)(\xi_a \xi - 1) \\ \frac{1}{8}\eta_a(1 + \xi_a \xi)(1 + \eta_a \eta)^2(\eta_a \eta - 1) \end{Bmatrix}$$

Figure 5.1 Shape functions

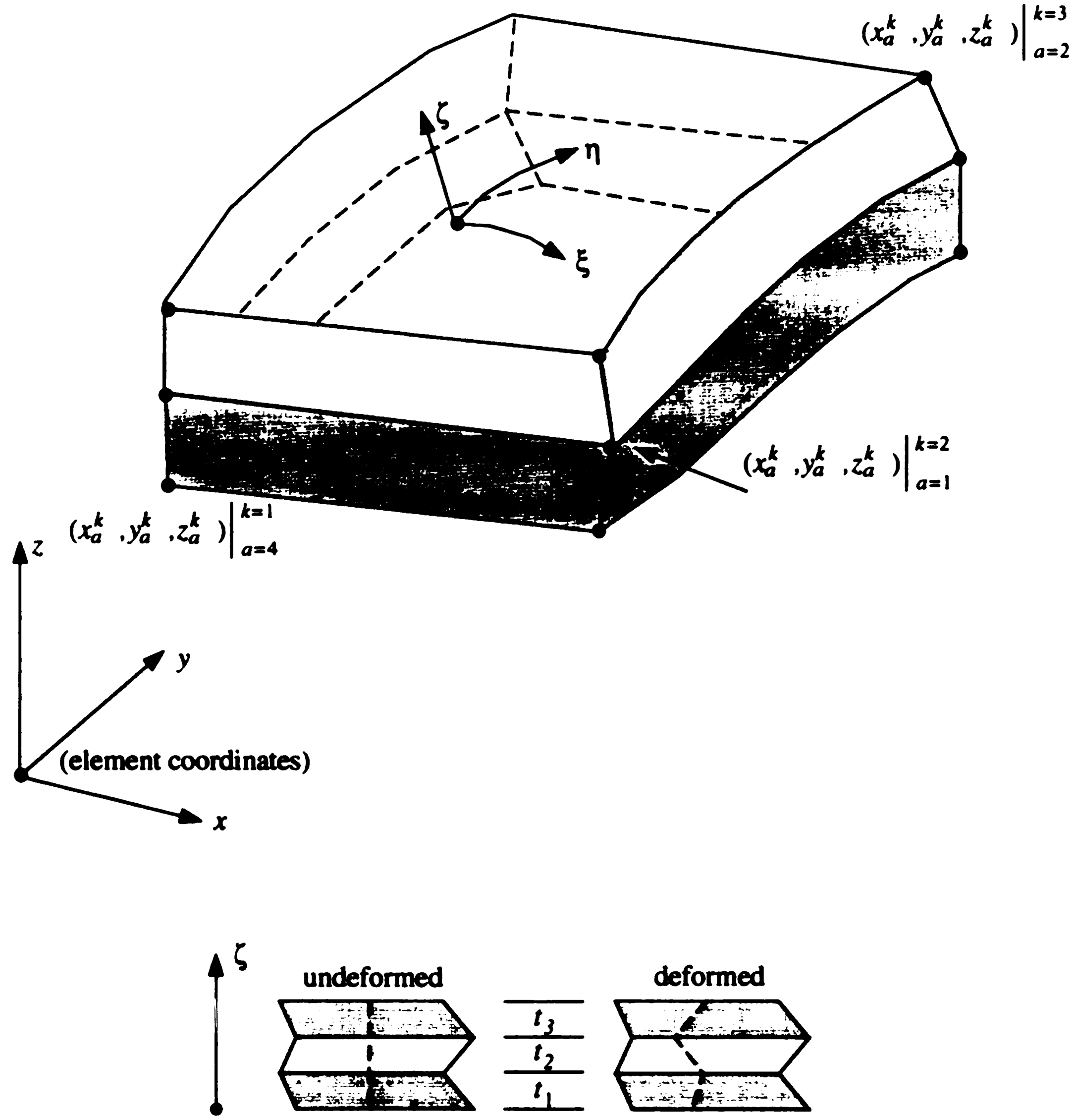

Figure 5.2 Illustration of element and natural coordinate systems for a typical element

Chapter 6

NUMERICAL STUDIES

6.1 Introduction

Following the formulation of using the Generalized Zigzag Theory for large deformation analysis in the previous chapter, a finite element program named LACOS (LAminated COmposite Shells) was programmed using FORTRAN. It was then linked to the commercial software ABAQUS/Standard as a new addition to its element library. This particularly user-defined element was called "U101", which followed the naming convention required by ABAQUS/Standard. Several case studies are performed in this chapter. The case studies are conducted not only to validate the U101 element but also to evaluate the new element in various applications. The entire chapter is divided into two major parts: linear solutions and nonlinear solutions.

Linear solutions are acceptable in many structural mechanics problems. Linear problems that have analytical solutions play a primary role in the validation of a finite element formulation based on a new theory. These linear problems not only help identify programming errors but also help filter numerical problems such as shear locking.

Nonlinear solutions in laminated composite analysis occur when structures are either subjected to large deformation or made of special, laminate stacking-sequences such as unsymmetric and angle-ply laminates. In the second part of this chapter, both experimental and analytical cases resulting in nonlinear solutions are examined. All the calculations of study cases were performed on a HP/C200 workstation with double-precision arithmetic.

6.2 Cross-Ply Laminate Under Cylindrical Bending

As discussed in Chapter 4, the present work is based on the Generalized Zigzag Theory (ZIGZAG). Since there exists an exact solution for a simply supported, cross-ply laminate subjected to sinusoidal transverse-pressure, it is the first objective of this study to compare the theoretical solutions from ZIGZAG with those from other laminate theories. The linear solutions were presented by Pagano [53] by solving the problem based on a plane strain assumption. The results are expressed in terms of displacements and stresses through the laminate thickness.

Among the various laminate theories available, the Interlaminar Shear Stress Continuity Theory (ISSCT) [32] represents a class of layerwise theories with the total number of unknown variables dependent on the number of layers. It therefore requires very high computational time in solving the variables by finite element or other numerical methods.

A third-order shear deformation theory presented by Lo, Christensen and Wu [44, 45] represents a family of "global" (instead of layerwise) theories that use high-order polynomials to describe the displacement fields through the laminate thickness, namely High-order Shear Deformation Theories (HSDT). Like ZIGZAG and HSDT, the First-order Shear Deformation Theory (FSDT) also has five unknown variables and has been now commonly used in commercial software such as ABAQUS, LS-DYNA3D, PAM-CRASH, and RADIOSS

CRASH. The theoretical solutions to the Pagano's problem based on the ZIGZAG, ISSCT, HSDT, and FSDT can be obtained by following the Navier solution procedure using double-Fourier series.

A simply supported, [0/90/0] laminate under cylindrical bending is taken as a case study. The distributions of in-plane displacement is shown in Figure 6.1 for various laminate theories. The composite laminate of the length-to-thickness ratio equal to 4 is used in this study. As shown in the figure, the in-plane displacement distributions are measured at the end of the laminate. The values are normalized by a factor involving elastic constants, thickness of laminate, and the intensity of applied pressure. The kinky patterns from ZIGZAG and ISSCT are clearly illustrated and match with the elasticity solution closely. The solution from HSDT is a smooth cubic polynomial curve deviating from the elastic solution. Also shown in the figure is the result from FSDT, which is only a straight line of a constant slope.

The distribution of the in-plane normal stress through the laminate thickness is depicted in Figure 6.2. Again, solutions from ZIGZAG and ISSCT follow the elasticity solution closely, while HSDT gives much smaller values near the interfaces and FSDT detours to the opposite side of the elasticity solution. It is noted that due to dissimilar material properties (in the sense of different fiber orientations) between adjacent layers, the in-plane normal stress distribution is not continuous through the thickness.

The distributions of the transverse shear stress at the laminate end is shown in Figure 6.3. In this case, ISSCT still matches the elasticity solution very well, while ZIGZAG gives a continuous distribution with certain inaccuracy. However, the distributions of the transverse shear stresses from both HSDT and FSDT are discontinuous through the laminate thickness.

It is clear from the above examples that ISSCT and ZIGZAG present reasonably accurate results when compared to the linear elastic solutions. However, the results from HSDT and FSDT are inaccurate, especially in the transverse shear stresses. Although ZIGZAG is less accurate than ISSCT, it becomes clear that ZIGZAG is a better choice when considering both numerical accuracy and computational efficiencies.

Remark 6.1

As the ratio of length-to-thickness of a laminate increases, e.g. a thin laminate, the difference of transverse shear stress between ZIGZAG and elasticity becomes insignificant.

As an example for the above statement, the maximum error for ZIGZAG is 5.4% (shown in Figure 6.4) for the ratio of length-to-thickness equal to 10, while 30% for the ratio of length-to-thickness equal to 4.

The above example of cylindrical bending is investigated again by using U101 elements with a 10x1 mesh. The results in displacements and stresses are compared with the theoretical solutions from ZIGZAG. The purpose of this study is to evaluate the U101 element and to estimate its feasibility in solving more complicated structural problems where theoretical solutions can not be obtained.

Shown in Figure 6.5 are the in-plane displacements. Excellent agreements exist between the finite element results at the integration points and the corresponding theoretical solutions of ZIGZAG. The finite element solution and the theoretical solutions are expressed by filled circles and a solid line, respectively. Excellent agreement can also be found in Figures 6.6, 6.7 and 6.8 for comparisons of in-plane normal stress, transverse shear stress and transverse deflection, respectively.

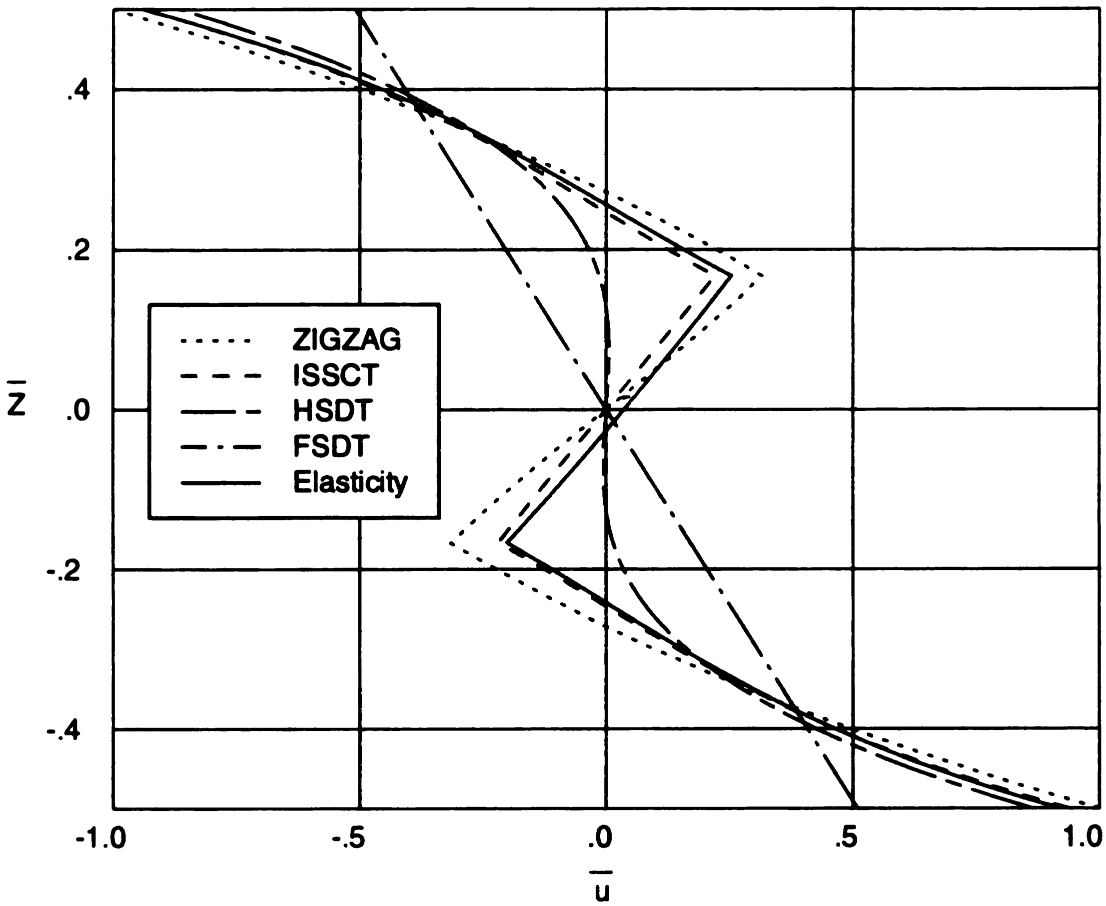

[0/90/0] cross-ply laminate
$S = L / h = 4$
$L = 254.0$ mm $= 10.0$ inch
$E_{11} = 6.9$ GPa $= 1\times10^6$ psi
$E_{22} = 172.5$ GPa $= 25\times10^6$ psi
$G_{12} = 3.45$ GPa $= 0.5\times10^6$ psi
$G_{23} = 1.38$ GPa $= 0.2\times10^6$ psi
$\nu_{12} = \nu_{23} = 0.25$

$\bar{Z} = Z / h$

$$\bar{u} = \frac{E_{22}\, u(0, Z)}{h\, q_o}$$

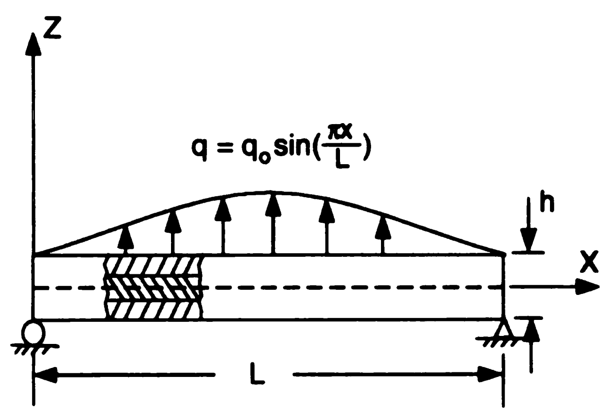

Figure 6.1 In-plane displacement distribution of a S=4, [0/90/0] laminate under cylindrical bending

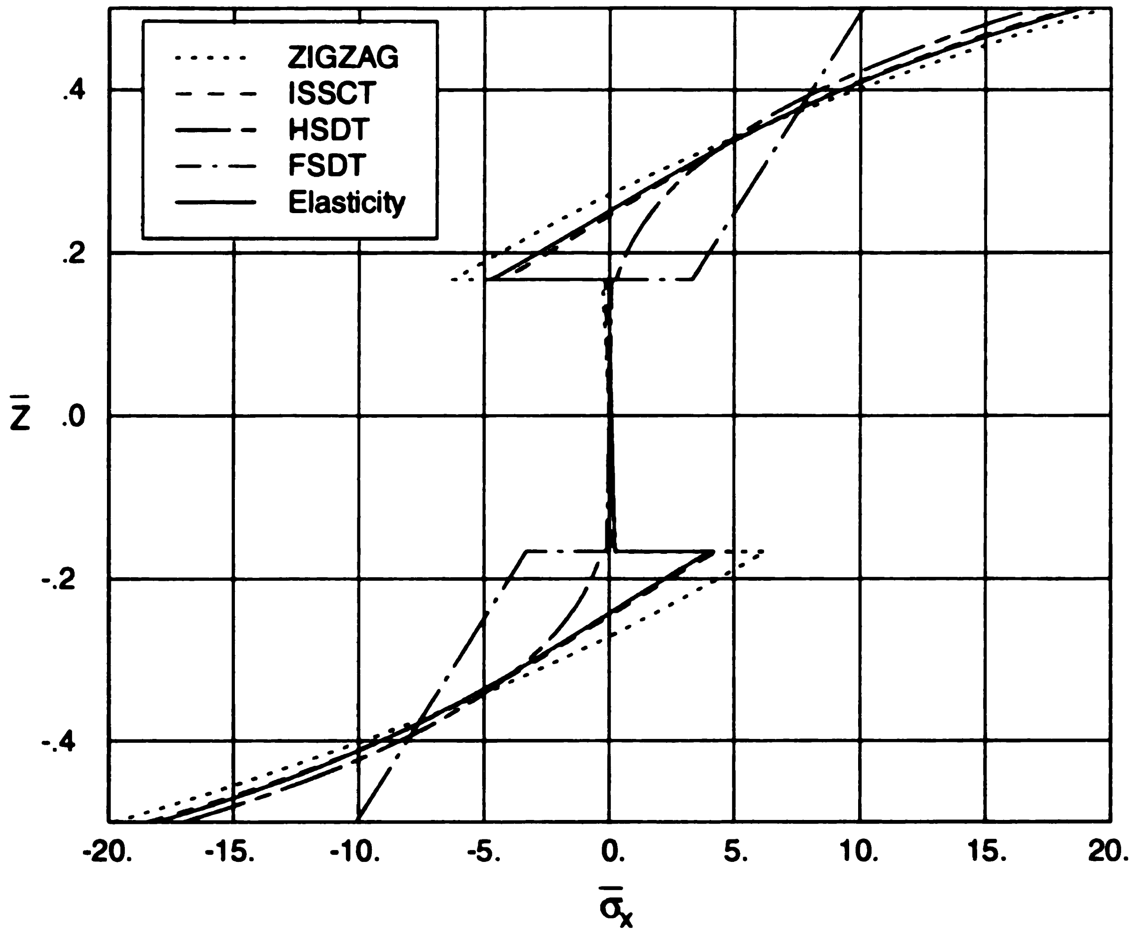

[0/90/0] cross-ply laminate

$S = L/h = 4$

$L = 254.0$ mm $= 10.0$ inch

$E_{11} = 6.9$ GPa $= 1\times10^6$ psi

$E_{22} = 172.5$ GPa $= 25\times10^6$ psi

$G_{12} = 3.45$ GPa $= 0.5\times10^6$ psi

$G_{23} = 1.38$ GPa $= 0.2\times10^6$ psi

$\nu_{12} = \nu_{23} = 0.25$

$\bar{Z} = Z/h$

$$\bar{\sigma}_x = \frac{\sigma_x(L/2, Z)}{q_o}$$

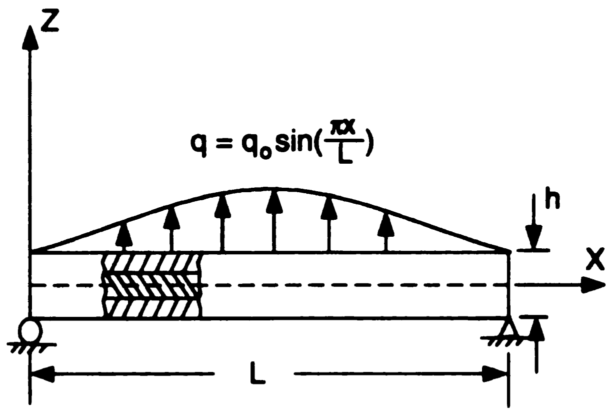

Figure 6.2 In-plane normal stress distribution of a S=4, [0/90/0] laminate under cylindrical bending

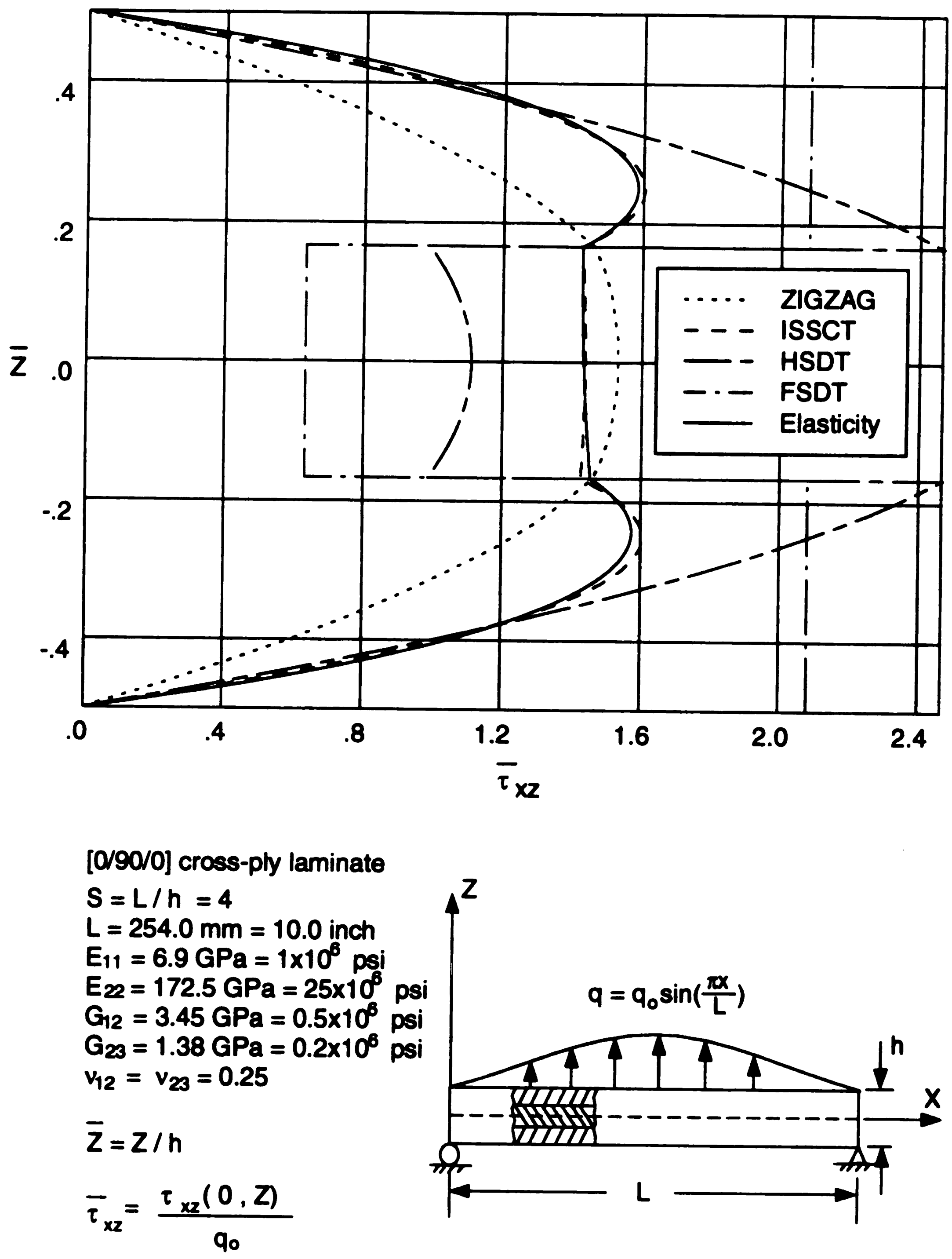

Figure 6.3 Transverse shear stress distribution of a S=4, [0/90/0] laminate under cylindrical bending

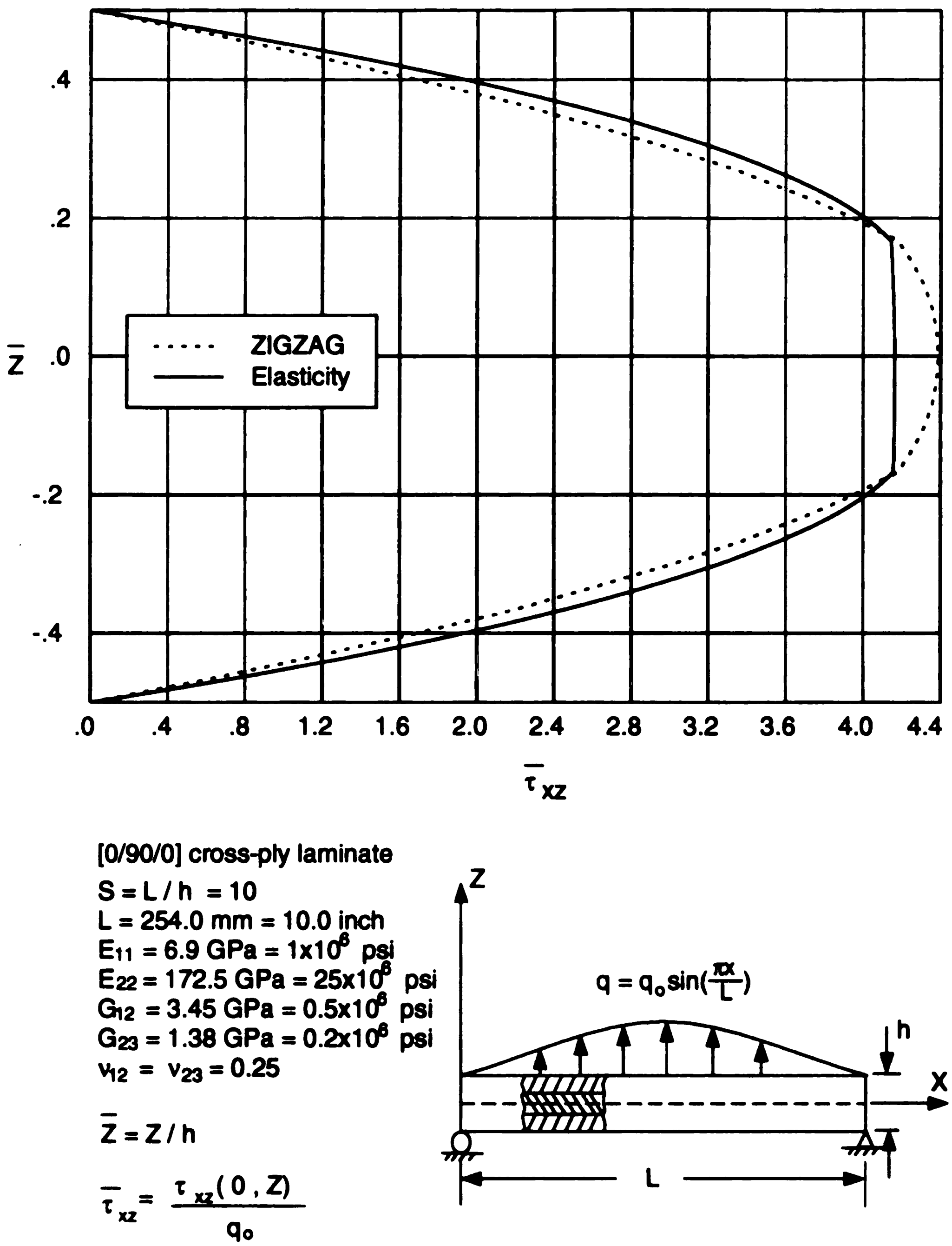

Figure 6.4 Transverse shear stress distribution of a S=10, [0/90/0] laminate under cylindrical bending

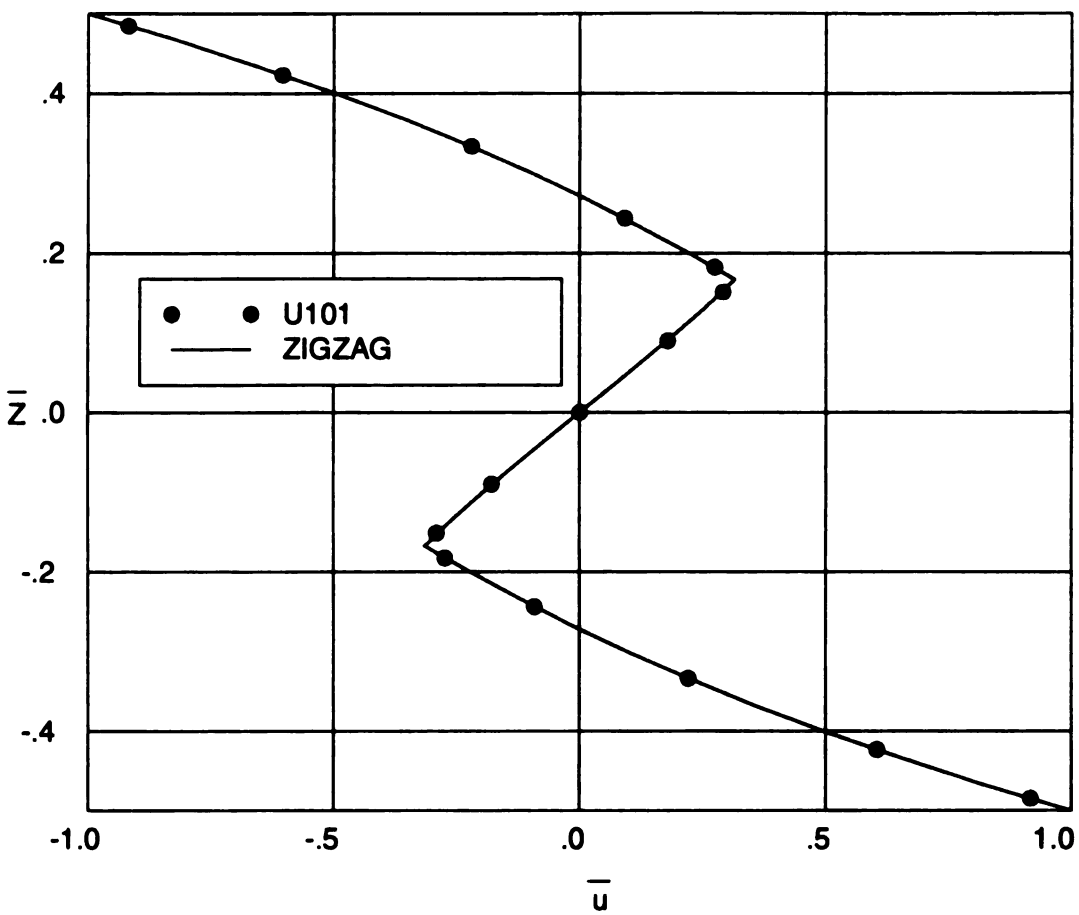

[0/90/0] cross-ply laminate

$S = L / h = 4$

$L = 254.0$ mm = 10.0 inch

$E_{11} = 6.9$ GPa = 1×10^6 psi

$E_{22} = 172.5$ GPa = 25×10^6 psi

$G_{12} = 3.45$ GPa = 0.5×10^6 psi

$G_{23} = 1.38$ GPa = 0.2×10^6 psi

$\nu_{12} = \nu_{23} = 0.25$

$\bar{Z} = Z / h$

$$\bar{u} = \frac{E_{22}\, u(0, Z)}{h\, q_o}$$

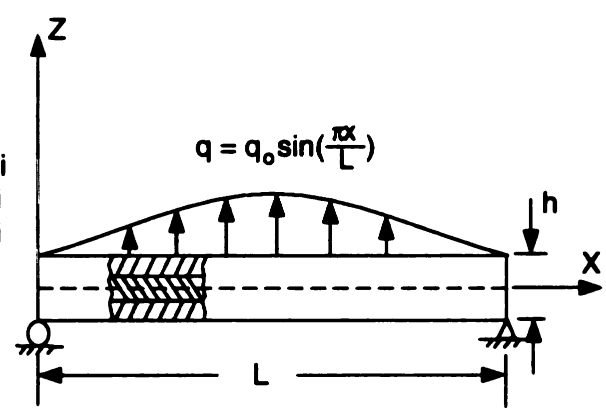

Figure 6.5 Comparison of U101 and the Generalized Zigzag theoretical solutions of in-plane displacement distribution

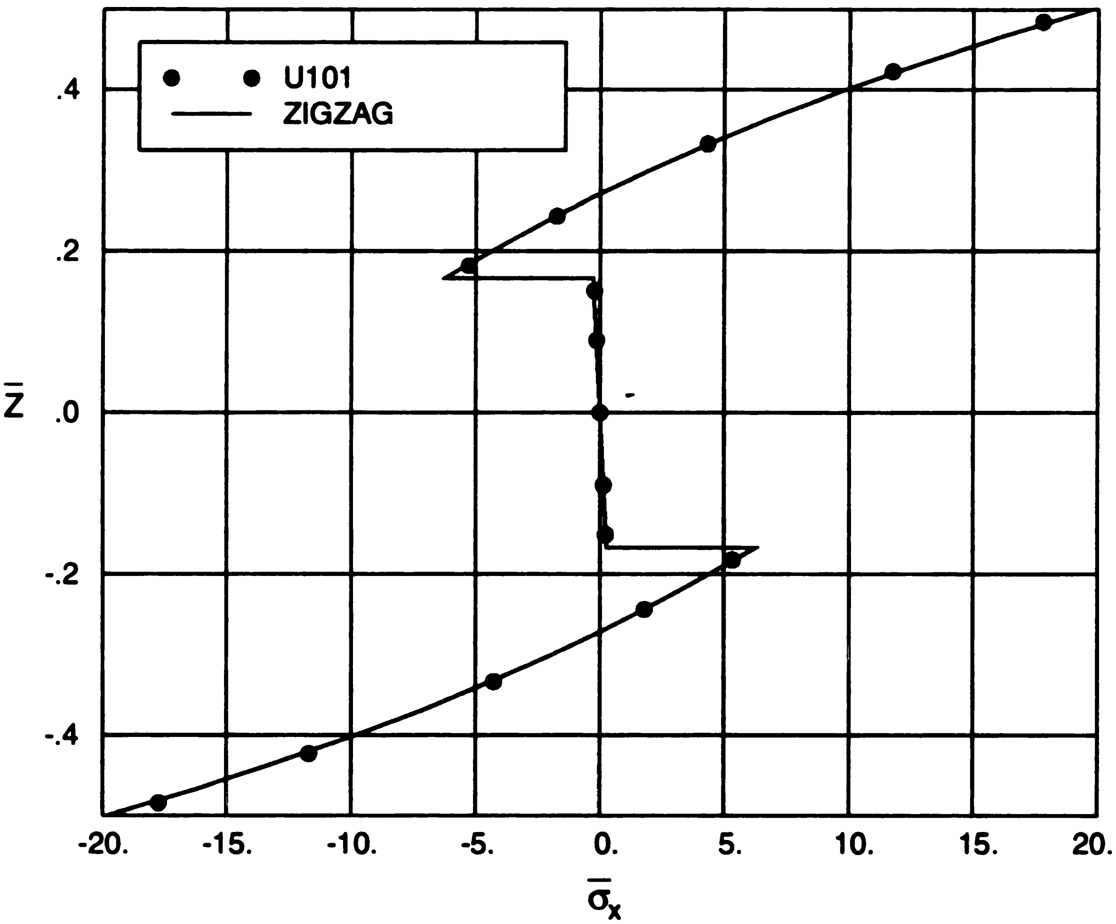

[0/90/0] cross-ply laminate

$S = L / h = 4$

$L = 254.0$ mm = 10.0 inch

$E_{11} = 6.9$ GPa = 1×10^6 psi

$E_{22} = 172.5$ GPa = 25×10^6 psi

$G_{12} = 3.45$ GPa = 0.5×10^6 psi

$G_{23} = 1.38$ GPa = 0.2×10^6 psi

$\nu_{12} = \nu_{23} = 0.25$

$\bar{Z} = Z / h$

$$\bar{\sigma}_x = \frac{\sigma_x(L/2, Z)}{q_o}$$

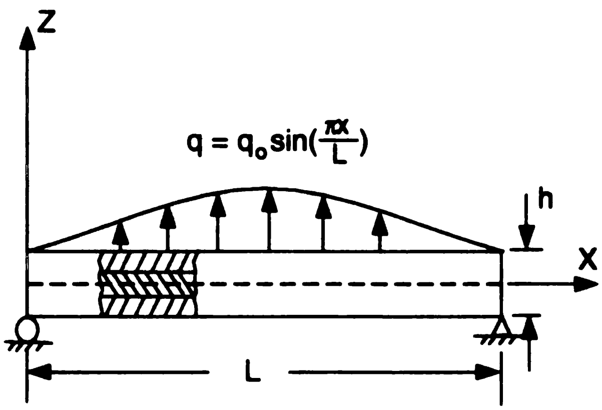

Figure 6.6 Comparison of U101 and the Generalized Zigzag theoretical solutions of in-plane normal stress distribution

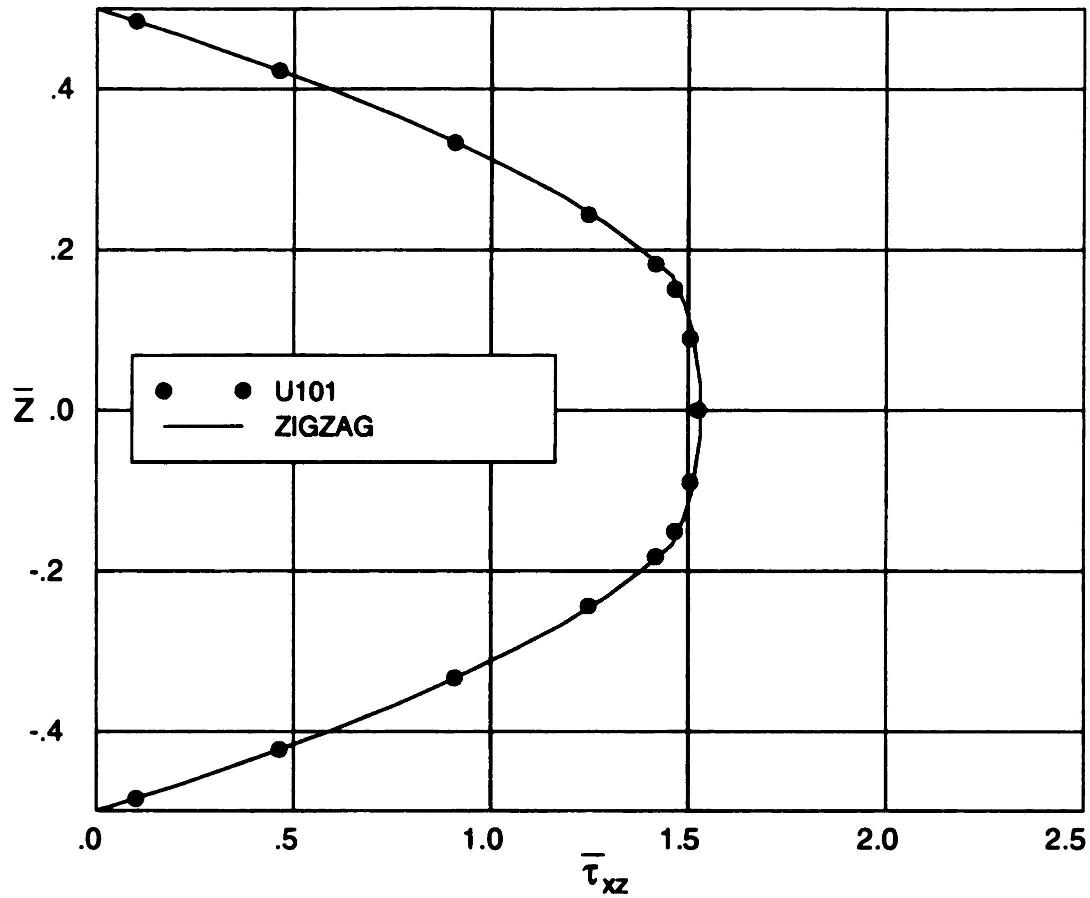

[0/90/0] cross-ply laminate

$S = L/h = 4$

$L = 254.0$ mm $= 10.0$ inch

$E_{11} = 6.9$ GPa $= 1\times10^6$ psi

$E_{22} = 172.5$ GPa $= 25\times10^6$ psi

$G_{12} = 3.45$ GPa $= 0.5\times10^6$ psi

$G_{23} = 1.38$ GPa $= 0.2\times10^6$ psi

$\nu_{12} = \nu_{23} = 0.25$

$\bar{Z} = Z/h$

$$\bar{\tau}_{xz} = \frac{\tau_{xz}(0, Z)}{q_o}$$

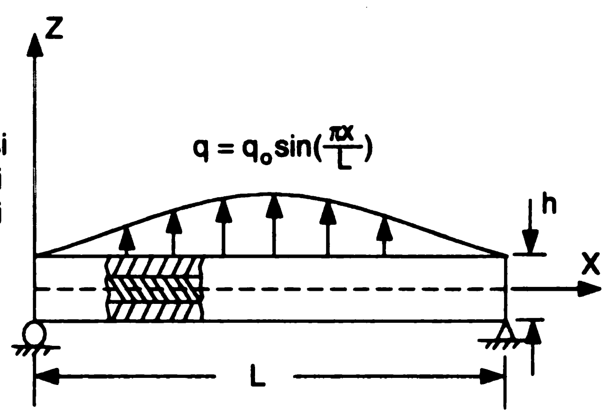

Figure 6.7 Comparison of U101 and the Generalized Zigzag theoretical solutions of transverse shear stress distribution

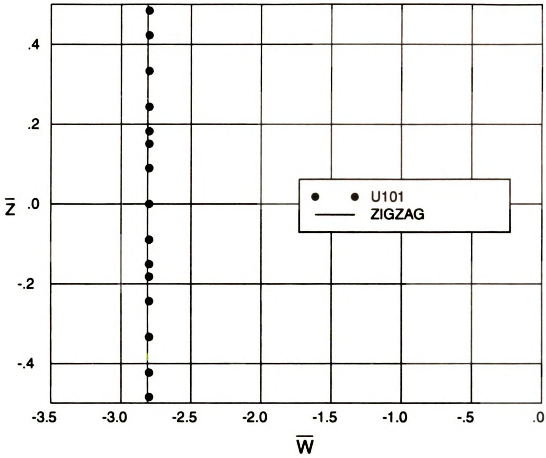

[0/90/0] cross-ply laminate

$S = L / h = 4$

$L = 254.0$ mm = 10.0 inch

$E_{11} = 6.9$ GPa = 1×10^6 psi

$E_{22} = 172.5$ GPa = 25×10^6 psi

$G_{12} = 3.45$ GPa = 0.5×10^6 psi

$G_{23} = 1.38$ GPa = 0.2×10^6 psi

$\nu_{12} = \nu_{23} = 0.25$

$\bar{Z} = Z / h$

$$\overline{W} = \frac{100 \times E_{22} \times h^3 \times W(L/2, Z)}{q_o \times L^4}$$

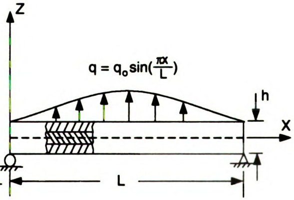

Figure 6.8 Comparison of U101 and the Generalized Zigzag theoretical solutions of transverse deflection

6.3 Bending of Rectangular Laminate

The finite element program is next applied to a square plate made of isotropic material and subjected to uniformly distributed transverse-pressure. Due to the biaxial symmetry of the structure, only one quarter of the plate was modeled and symmetric boundary conditions were imposed. Three different mesh densities (2x2, 4x4, and 8x8) were investigated for convergency. Also, three length-to-thickness ratios ($S = a/h = 5, 10$ and 100) were examined for shear locking. The normalized, central deflection is summarized in Table 6.1. The material properties and the method of normalization are also given in the table.

ABAQUS/S4R [2, 3] is a four-node, doubly curved, reduced integration shell element with hourglass control and is based on the First-order Shear Deformation Theory (FSDT). The element also considers finite membrane strain and thickness change. As shown in the previous study, elements based on FSDT do not have correct displacement and stress calculations through the laminate thickness, especially in-plane displacements and transverse shear stresses. When reasonable transverse stresses are desired, the ABAQUS/S4R element uses in-plane stresses and equilibrium equations to recover them. The four-node, 28 degree-of-freedom element formulated by Palazotto and Dennis [55] is a fully integrated element based on a fourth-order shear deformation theory. Also shown in the table are the closed-form, Navier solutions generated by Reddy [62]. Reddy's results were based on a third-order shear deformation theory. Again, it should be pointed out that recovering techniques for transverse shear stresses through equilibrium equations have been used by Palazotto and Dennis and Reddy. It can be seen from Table 6.1 that the difference of transverse deflection between U101 and Reddy's closed-form solution is within 1% when an 8x8 mesh is used. Based on a study of various length-to-thickness ratios, U101 does not present any shear locking when the thickness of laminate decreases.

As a second example, the same structure is made of a zero-degree, orthotropic laminate. By using an 8x8 mesh, the normalized, central deflection and stresses of three length-to-thickness ratios are shown in Table 6.2. The material properties and normalization factor are also given in the table. The three-dimensional elasticity solutions were given by Srinivas and Rao [67]. Reddy's closed-form solutions [62] were also given for comparison. In general, the solutions from U101 agree very well with the three-dimensional elasticity results.

The difference of the transverse deflection between U101 and three-dimensional elasticity is within 1%. The results from the Classical Laminate Theory (CLT) are also given in the table. It is shown that error increases as the length-to-thickness ratio increases because of the negligence of the shear deformation effect. In other words, CLT is not suitable for thick composite laminates. The in-plane stress σ_y is taken at an integration point near the center of the laminate, while the transverse shear stress σ_{yz} is chosen at an integration point near the laminate boundary. The stresses from U101 do not perform as well as the transverse deflection when compared with the three-dimensional elasticity solutions. It is believed that mesh refinement near the stress sampling locations is required because stress gradients around these regions are very large, especially when the laminate is thin [55]. The difference is also believed to be due to the fact that the stresses from U101 are recorded at integration points, not exactly at the boundary.

The next case deals with a simply-supported [0/90/0], rectangular laminate under sinusoidal transverse-pressure. The normalized transverse-deflections at the center of the laminate are summarized in Table 6.3 for four different length-to-thickness ratios. Also given in the table are material properties, loading conditions, and the normalization factor. The three-dimensional elasticity solutions were given by Pagano [54]. An 8x8 mesh was used in the finite element solutions based on U101, ABAQUS/S4R and Palazotto and Dennis [55]. It is observed from Table 6.3 that U101 outperforms ABAQUS/S4R and Palazotto and Dennis, and even Reddy's closed-form solutions at small length-to-thickness ratios. The superiority diminishes when the laminate becomes thin.

Table 6.1 Normalized, central transverse-deflection of a simply supported, isotropic, square laminate under uniform transverse-pressure

S=a/h	Mesh	U101	ABAQUS/S4R	Palazotto & Dennis	Reddy*
	2 x 2	0.0314	0.0450	0.0240	
100	4 x 4	0.0430	0.0446	0.0425	
	8 x 8	0.0441	0.0444	0.0443	0.0444
	2 x 2	0.0426	0.0476	0.0461	
10	4 x 4	0.0456	0.0468	0.0466	
	8 x 8	0.0464	0.0468	0.0467	0.0467
	2 x 2	0.0500	0.0549	0.0538	
5	4 x 4	0.0525	0.0539	0.0536	
	8 x 8	0.0533	0.0536	0.0536	0.0535

* theoretical solutions

isotropic material
E = 68.9 GPa
= 10.0×10^6 psi
ν = 0.3
a / b = 1.0
uniform pressure = q
normalized deflection =
$W_c h^3 E/qa^4$

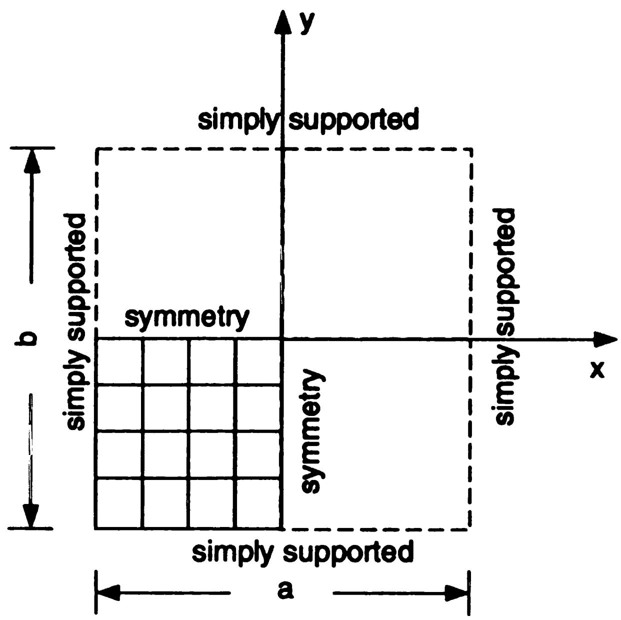

Table 6.2 Normalized deflection and stresses of a simply supported, orthotropic, square laminate under uniform transverse-pressure

		S = a / h		
		20	10	7.143
$\overline{W}$	U101	10394	686.7	190.6
	ABAQUS/S4R	10486	691.4	191.9
	Palazotto & Dennis	10448	689.8	191.7
	Reddy*	10450	689.5	191.6
	3D Elasticity*	10443	688.6	191.1
	CLT*	10250	640.7	166.8
σ	U101	138.9	34.34	17.47
	ABAQUS/S4R	142.8	35.34	17.81
	Palazotto & Dennis	144.6	36.12	18.41
	Reddy*	144.3	36.01	18.34
	3D Elasticity*	144.3	36.02	18.35
τ	U101	10.23	5.11	3.63
	ABAQUS/S4R	10.27	5.12	3.64
	Palazatto & Dennis	8.66	5.07	3.70
	Reddy*	10.85	5.38	3.81
	3D Elasticity*	10.87	5.34	3.73

* theoretical solutions

orthotropic material [0]
E_{11} = 143.62 GPa = 20.83 x 10^6 psi
E_{22} = 75.43 GPa = 10.94 x 10^6 psi
ν_{12} = 0.44
G_{12} = 42.06 GPa = 6.1 x 10^6 psi
G_{13} = 25.58 GPa = 3.71 x 10^6 psi
G_{23} = 25.58 GPa = 3.71 x 10^6 psi
a / b = 1.0
8 x 8 mesh
uniform pressure = q
normalized results:
$\overline{W} = 23.2 \times 10^6 W_c/qh$
$\sigma = \sigma_y (0,0,h/2) / q$
$\tau = \tau_{yz} (0,-b/2, 0) / q$

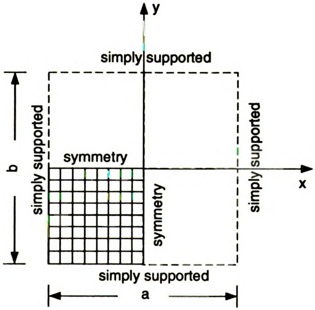

Table 6.3 Normalized, central transverse-deflection of a simply supported, rectangular [0/90/0] laminate under sinusoidal transverse-pressure

S = a / h	U101	ABAQUS/S4R	Palazotto & Dennis	Reddy*	3D Elasticity*
4	2.742	3.164	2.647	2.641	2.82
10	0.912	0.936	0.864	0.862	0.919
20	0.604	0.613	0.595	0.594	0.610
100	0.503	0.509	0.507	0.507	0.508

* theoretical solutions

[0/90/0] laminate
E_{11} = 258.6 GPa = 37.5 x 10^6 psi
E_{22} = 10.3 GPa = 1.5x 10^6 psi
ν_{12} = 0.25
G_{12} = 5.2 GPa = 0.75 x 10^6 psi
G_{13} = 2.1 GPa = 0.3 x 10^6 psi
G_{23} = 2.1 GPa = 0.3 x 10^6 psi
a = 203.2 mm = 8.0 inch
b = 609.6 mm = 24.0 inch
8 x 8 mesh
sinusoidal pressure =
$q_o \sin[\pi(x+a/2)/a] \sin[\pi(y+b/2)/b]$
normalized deflection =
$100 W_c h^3 E_2 / q_o a^4$

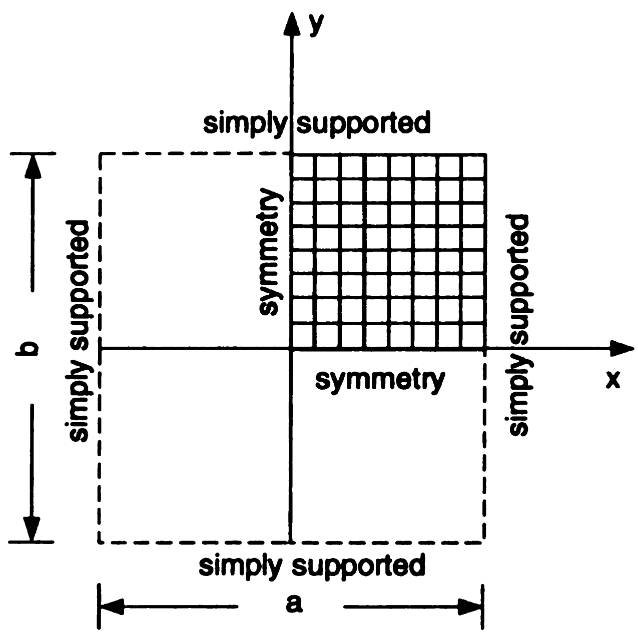

6.4 Shear Locking

Shear locking is a condition in which the element stiffness is immensely overestimated for any reasonable mesh density, thus yielding near-zero solutions [68]. It is observed that some fully integrated, C^0 shell elements that are based on the First-order Shear Deformation Theory are vulnerable to the shear-locking phenomenon [80].

Using a straight beam as an example, the deflection of a thin beam should only be governed by the bending stiffness matrix because the transverse shear deformation is negligible. However, in the case of shear locking as the beam becomes slender, the traverse shear stiffness matrix grows in relation to the bending stiffness matrix as a result of enforcing the constraint of zero transverse shear strain. Accordingly, the traverse shear stiffness matrix acts as a penalty function that yields near-zero transverse-deflection. Even if more elements are used in this case, every additional element usually brings equal amounts of degrees of freedom and constraints when the full integration scheme is used. Therefore, using more elements will not help alleviate the problem. The proceeding arguments can also be expanded to plate problems.

The U101 element does not have a shear-locking problem. The key reason is that the Hermite cubic shape functions are used in the U101 element to describe the transverse deflection w. Using the straight beam case as an example again, the U101 element has Δw, $\Delta w_{,x}$, and Δu_1 as degrees of freedom at each node; hence, the constraint of transverse shear strain is imposed on $\Delta w_{,x}$ and Δu_1 but not directly on the transverse deflection Δw. The aforementioned case presented in Table 6.1 was used again to verify, to some extent, this claim. The new length-to-thickness ratio was chosen as 1000 (S=a/h) for the U101 element via an 8x8 mesh, while the other conditions were kept the same. The result from the U101 element is 98.8% of the theoretical solution by Timonshenko and Woinowsky-Krieger [71].

6.5 Patch Tests

The patch test was first given by Irons [9, 25]. Many authors have emphasized the importance of this test [8, 14, 21, 22, 79]. The consensus is as follows.

1. Passing the patch test is a sufficient condition to convergency but not a necessary condition. Under a convergent situation, the behavior of the real structure can be reproduced as the size of element decreases.

2. It is important to use irregular element shapes in constructing a patch because one finite element formulation may pass the patch test in certain special mesh configuration but not in others.

In the patch test, the elements are assembled in such a way that at least one node is completely surrounded by elements. In performing the test, a displacement field that provides an arbitrary state of constant strain, or a consistent nodal loading, is applied to the boundary nodes. Nodes not on the boundary are neither loaded nor restrained. Solutions for degrees of freedom of all nodes that are not prescribed are sought, and the strains (or stresses) in all elements are computed. The element passes the patch test if the resulting displacements at the internal nodal points correspond with the applied displacement field and the computed strains and stresses at every point in every element agree with analytical values to the limit of computer accuracy [14, 21].

As given in Table 6.4, the U101 element passed the membrane patch test. However, the U101 element did not pass the bending patch test when using the same mesh configuration. The failure in passing the bending patch test is believed to be caused by the mixed approach used in the U101 element [55]. That is, the U101 element uses the nonconforming Hermite cubic shape functions for the variables of Δw, $\Delta w_{,x}$, and $\Delta w_{,y}$ while bilinear shape functions for the variables of Δu, Δv, Δu_1, and Δv_1. The reason for using the mixed approach is because Δw needs C^1 continuity, while Δu, Δv, Δu_1, and Δv_1 need only C^0 continuity. In the bending patch, a pure bending mode is created, either by prescribing rotational degrees of freedom or by applying bending moments. It is impossible to have zero transverse shear strain when for example $\Delta w_{,x}$ and Δu_1 are interpolated differently. One way the problem may be conquered is to reduce the continuity requirement of Δw from C^1 to C^0 by artificially imposing a certain type of constraint on transverse shear strains, e.g. "discrete Kirchhoff" [21]. The consequence of passing the membrane and failing the bending patch tests can be also viewed from the convergency point. The convergency is guaranteed for the U101 element under a membrane loading; however, it may or may not converge under bending. As can seen in the previous cases and later examples, the U101 element has not shown any unconvergency problem under bending conditions.

Table 6.4 Results of membrane patch test

node	coordinates (x , y)	theoretical solutions (U , V) x 10^{-3}	U101 solutions (U , V) x 10^{-3}
1	(0.04, 0.02)	(0.05, 0.04)	(0.05, 0.04)
2	(0.18, 0.03)	(0.195, 0.120)	(0.195, 0.120)
3	(0.16, 0.08)	(0.200, 0.160)	(0.200, 0.160)
4	(0.08, 0.08)	(0.120, 0.120)	(0.120, 0.120)

linear, elastic material
$E_{11} = 1.0 \times 10^6$
$\nu_{12} = 0.25$
$h = 0.001$
at all exterior nodes:
$U = 10^{-3}(x + y/2)$
$V = 10^{-3}(y + x/2)$
at all nodes:
$W = 0$

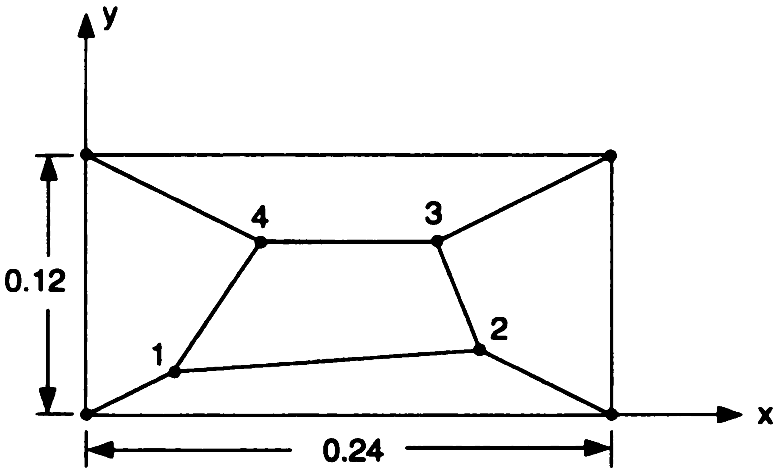

6.6 Large Deflection Effects in Unsymmetric Cross-ply Composite Laminates

Due to the existence of bending-stretching coupling, nonlinear deflection occurred even when an unsymmetric composite laminate is under a small loading. Sun and Chin [70] presented some theoretical solutions for an unsymmetric cross-ply laminate subjected to uniform transverse-pressure. Their analysis was based on the Kirchoff-Love hypothesis, in which the effects of transverse shear deformation were not taken into account. They also used a large deformation theory in von Kármán sense. Accordingly, a special, linear ordinary differential equation with constant coefficients was solved using a plane strain assumption for a laminate under a pin-pin boundary condition.

The relation between the uniform pressure and the normalized, maximal transverse-deflection is shown in Figure 6.9 for a length-to-thickness ratio S of 225. The uniform pressure ranges from 0 to 68.95 kPa (10 psi). The theoretical solution of Sun and Chin is illustrated as a solid line. The solutions from U101, ISSCT (Interlaminar Shear Stress Continuity Theory [32]), and ABAQUS/S4R are all based on the finite element analysis of a 10x1 mesh. It is observed in the figure that the results are consistent with one another because the effect of transverse shear deformation can be neglected in the thin laminate. It is also noticed that the solutions from a positive loading and a negative loading are different. In addition, the in-plane total reaction force at the pinned end is calculated and shown in Figure 6.10. Again, because a large S of 225 is used, good agreements are found among all solutions.

The same structure was subjected to higher pressure of up to 6.89 MPa (1000 psi). The relations between the uniform pressure and the normalized transverse-deflection are shown in Figure 6.11. It is noted that the results split into two groups when the pressure is higher than 2.76 MPa(400 psi). The results from U101 and ABAQUS/S4R are in one group, while the rest are in the other. The largest difference in transverse deflection between the two groups is about 2.6% when the pressure is 6.89 MPa (1000 psi). This result may be due to the use of different large deformation theories. It is noted that U101 and ABAQUS/S4R use an updated Lagrangian approach, while both ISSCT and Sun and Chin use a total Lagrangian approach with von *Kármán* nonlinear strains, which is a simplied version of the full-term Green strains. The difference among the curves from the negative loading is not noticeable.

The next study investigates a similar structure with a smaller length-to-thickness ratio S, i.e. 11.25. The uniform transverse-pressure ranges also from 0 to 6.89 MPa (1000 psi). This loading is in fact small because the laminate is "thicker" now. The purpose of this study is to examine the effect of transverse shear deformation. It can be seen from Figure 6.12 that the transverse deflection from Sun and Chin is smaller than the rest of the theories that consider transverse shear deformation. The difference can be as much as 27.5% at a positive loading of 6.89 MPa (1000 psi). Some interesting observations can be found from the same case for the in-plane, total reaction force shown in Figure 6.13. When the loading is positive, the reaction force remains negative. Until the the loading reaches 3.45 MPa (500 psi), the reaction force starts to increase positively. It eventually becomes positive. A negative reaction force in this study actually indicates that the laminate pushes the end supports instead of pulling them.

The last set of curves are given in Figure 6.14 in which a positive transverse-pressure of 68.95 kPa (10 psi) is applied to the same structure using various length-to-thickness ratios (S=L/h). The largest transverse-deflections from all finite element formulations are normalized by the corresponding theoretical results from Sun and Chin. By doing so, the results of Sun and Chin are actually a horizontal line of 1.0 in Figure 6.14. Again, due to the effect of transverse shear deformation, larger transverse-deflections were found in U101, ISSCT, and ABAQUS/S4R for thicker laminates. However, these results approach Sun and Chin's solution as the laminate becomes thinner.

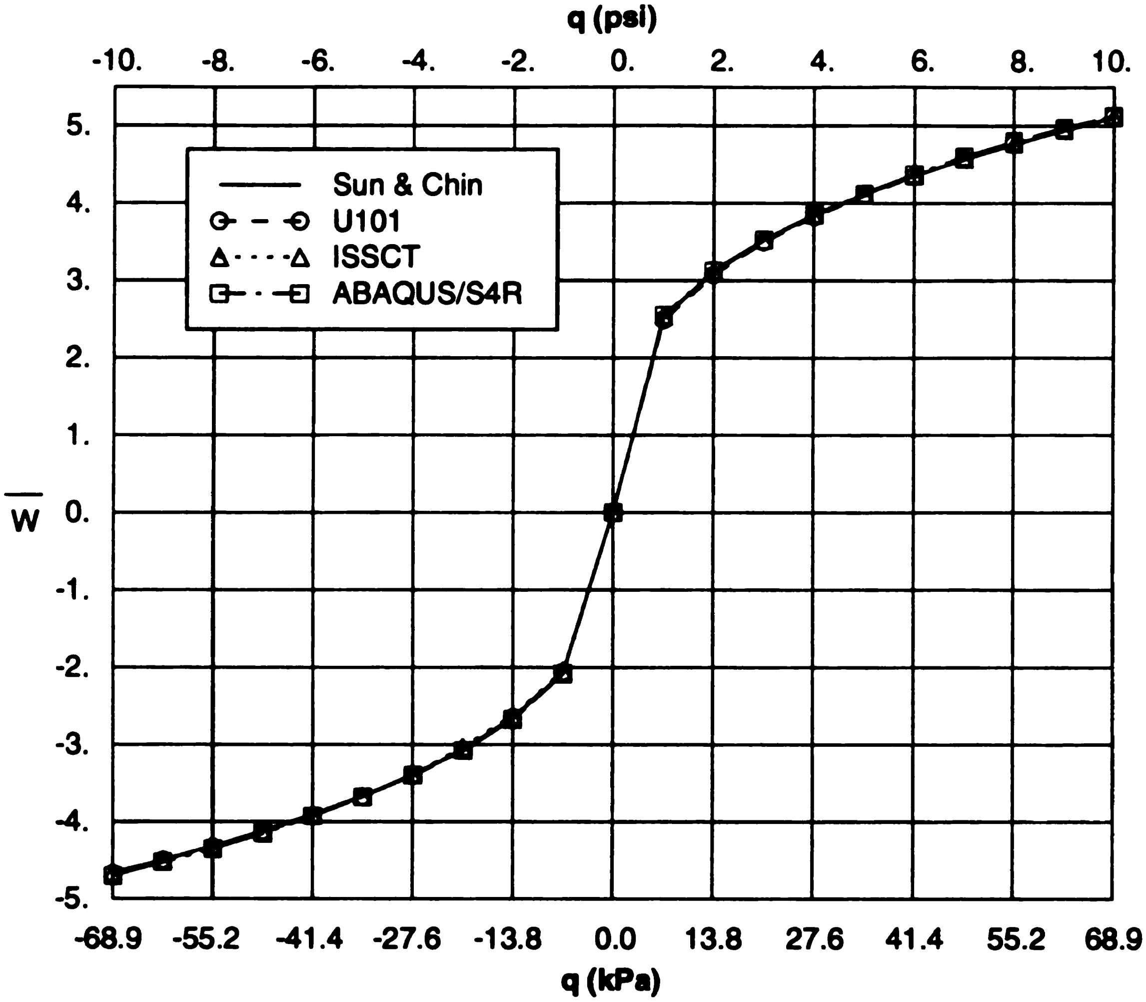

[0/90] cross-ply laminate
E_{11} = 137.9 GPa = 20.0 x 10^6 psi
E_{22} = 9.7 GPa = 1.4 x 10^6 psi
G_{12}=G_{23}=G_{13}= 4.8 GPa = 0.7 x 10^6psi
ν_{12} = 0.3
L = 228.6 mm = 9 inch
h = 1.02 mm = 0.04 inch
S = L / h = 225
mesh = 10 x 1

$\overline{W} = W_{max} / h$

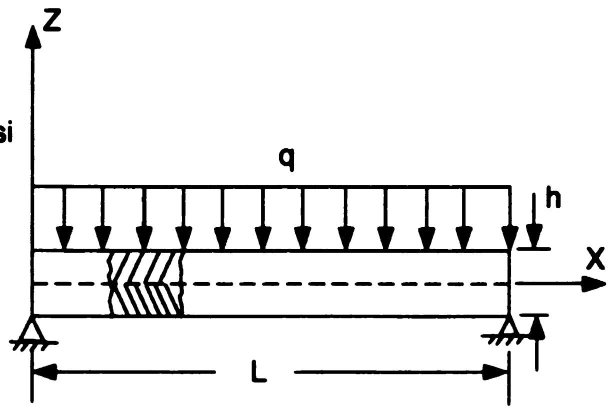

Figure 6.9 Small load vs. transverse deflection curve of a S=225, [0/90] unsymmetric laminate

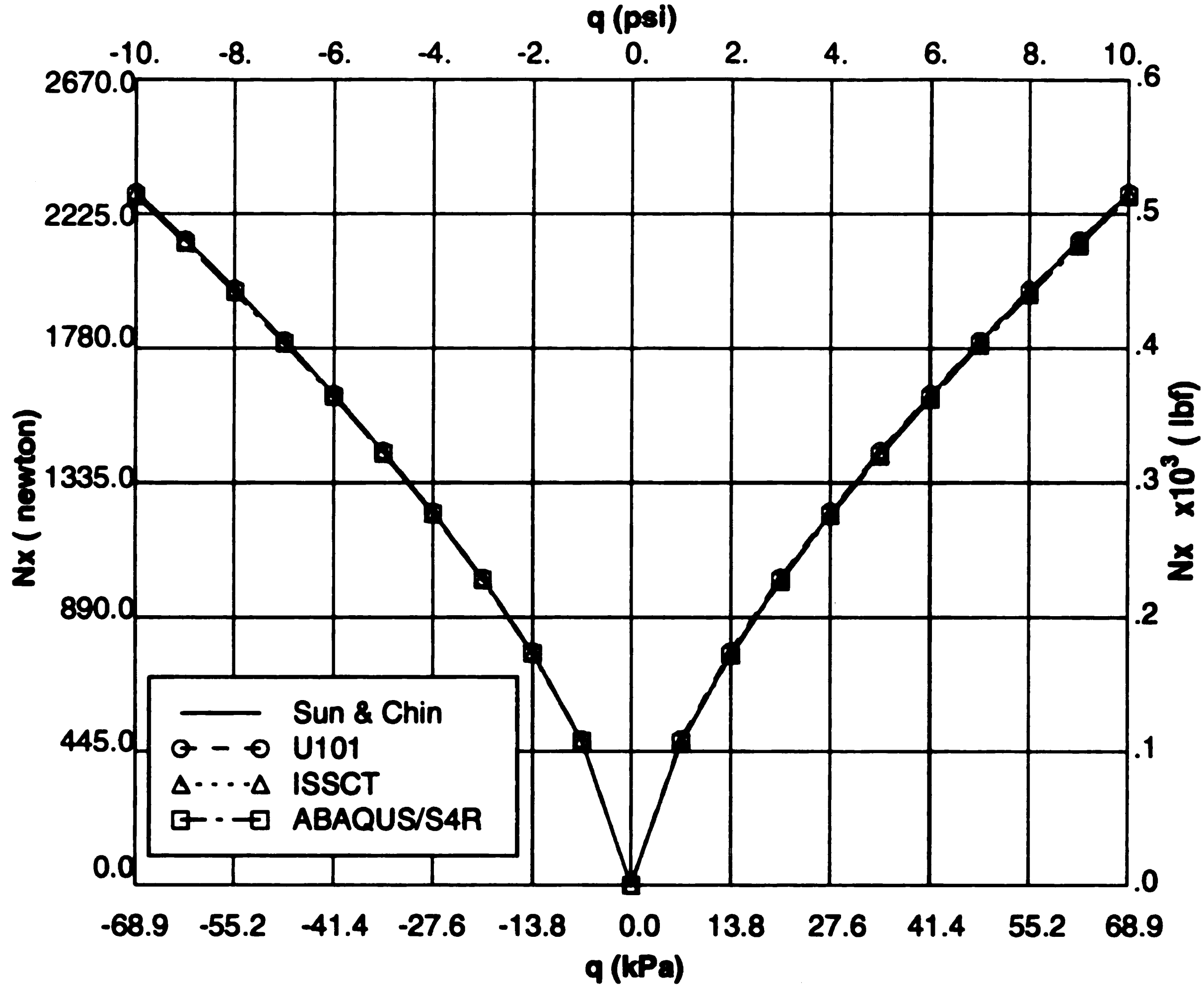

[0/90] cross-ply laminate
E_{11} = 137.9 GPa = 20.0 x 10^6 psi
E_{22} = 9.7 GPa = 1.4 x 10^6 psi
G_{12}=G_{23}=G_{13}= 4.8 GPa = 0.7 x 10^6psi
ν_{12} = 0.3
L = 228.6 mm = 9 inch
h = 1.02 mm = 0.04 inch
S = L / h = 225
mesh = 10 x 1
Nx = total in-plane force at supported end

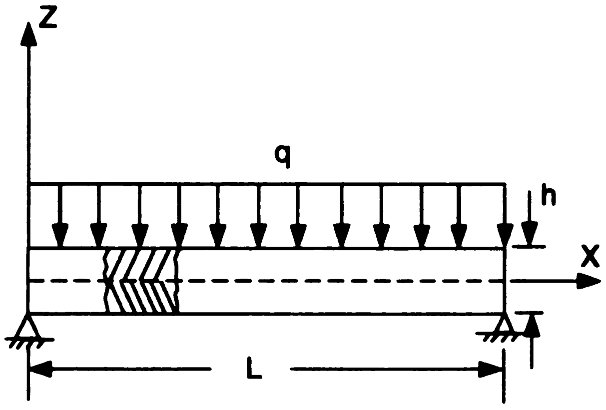

Figure 6.10 Small load vs. in-plane force curve of a S=225, [0/90] unsymmetric laminate

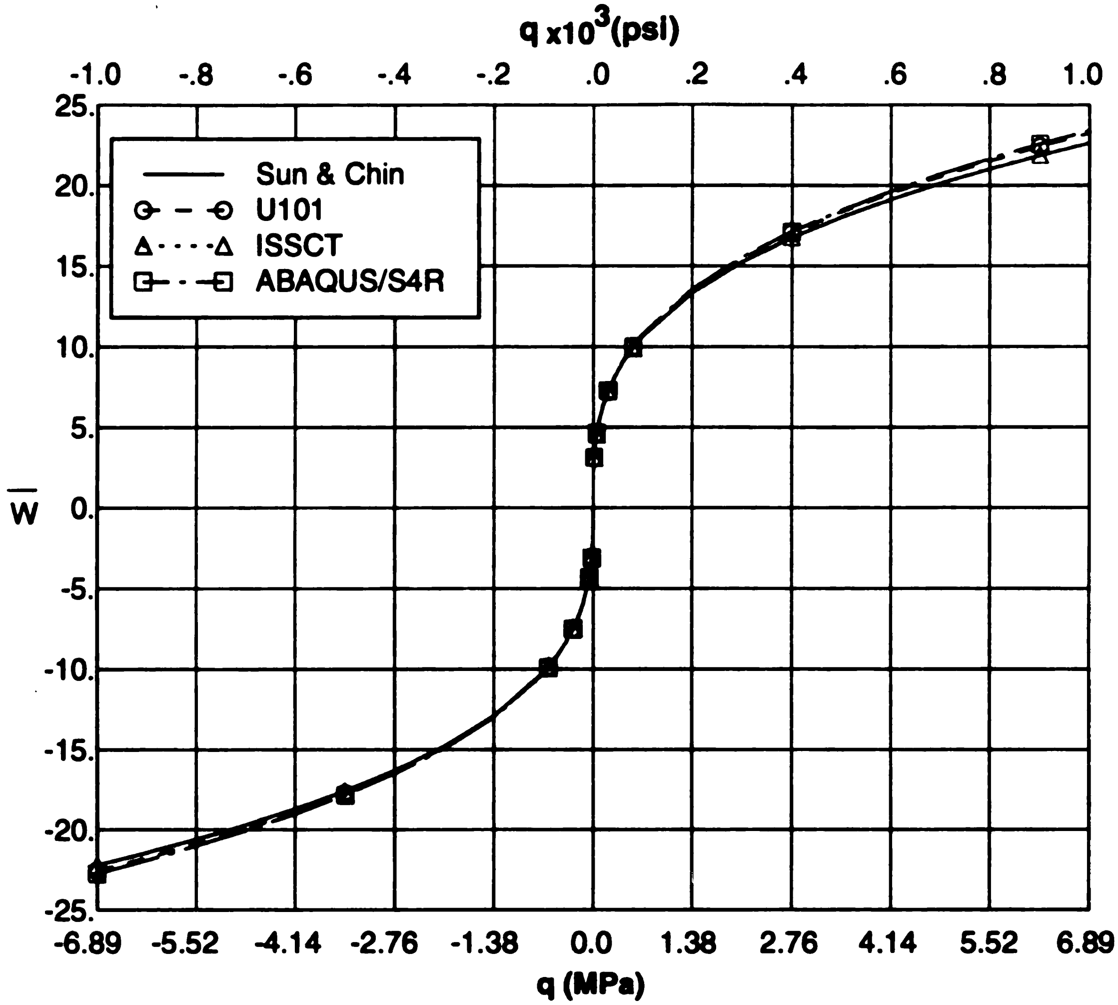

[0/90] cross-ply laminate
E_{11} = 137.9 GPa = 20.0 x 10^6 psi
E_{22} = 9.7 GPa = 1.4 x 10^6 psi
G_{12}=G_{23}=G_{13}= 4.8 GPa = 0.7 x 10^6psi
ν_{12} = 0.3
L = 228.6 mm = 9 inch
h = 1.02 mm = 0.04 inch
S = L / h = 225
mesh = 10 x 1

$\overline{W} = W_{max} / h$

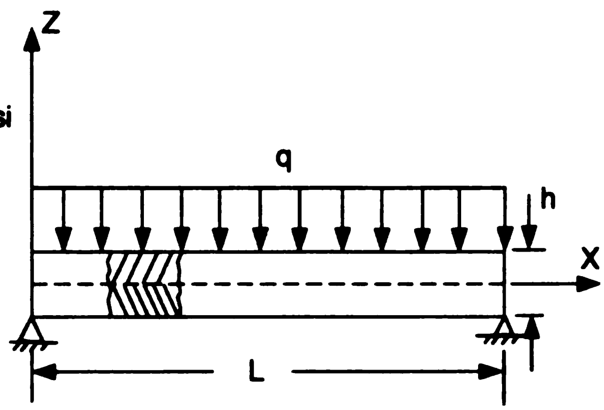

Figure 6.11 Large load vs. transverse deflection curve of a S=225, [0/90] unsymmetric laminate

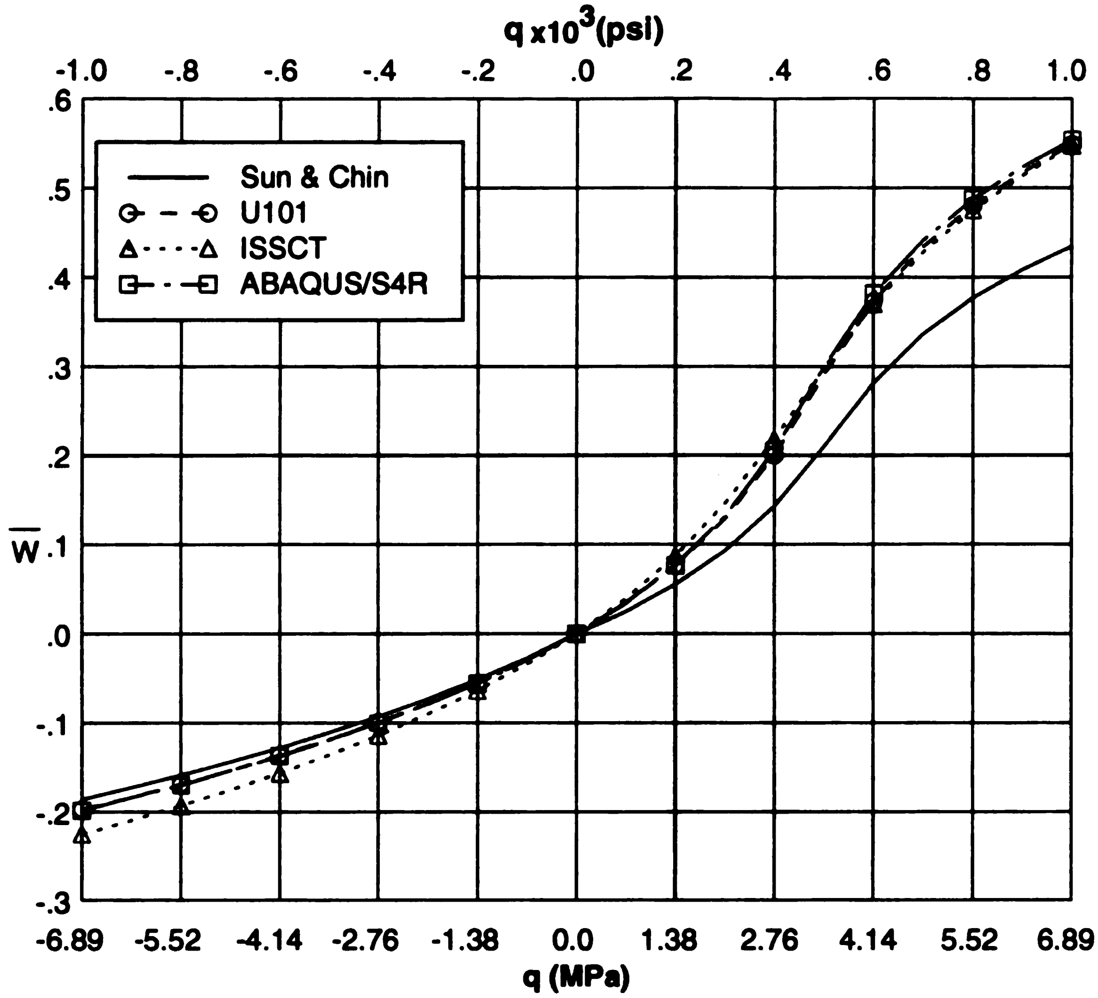

[0/90] cross-ply laminate
E_{11} = 137.9 GPa = 20.0 x 10^6 psi
E_{22} = 9.7 GPa = 1.4 x 10^6 psi
G_{12}=G_{23}=G_{13}= 4.8 GPa = 0.7 x 10^6psi
ν_{12} = 0.3
L = 228.6 mm = 9 inch
h = 20.32 mm = 0.8 inch
S = L / h = 11.25
mesh = 10 x 1

$\overline{W} = W_{max} / h$

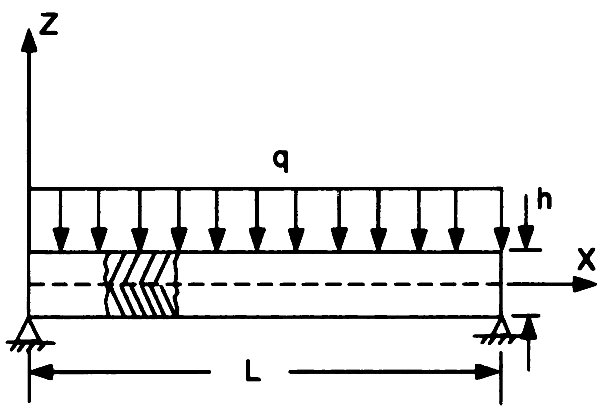

Figure 6.12 Large load vs. transverse deflection curve of a S=11.25, [0/90] unsymmetric laminate

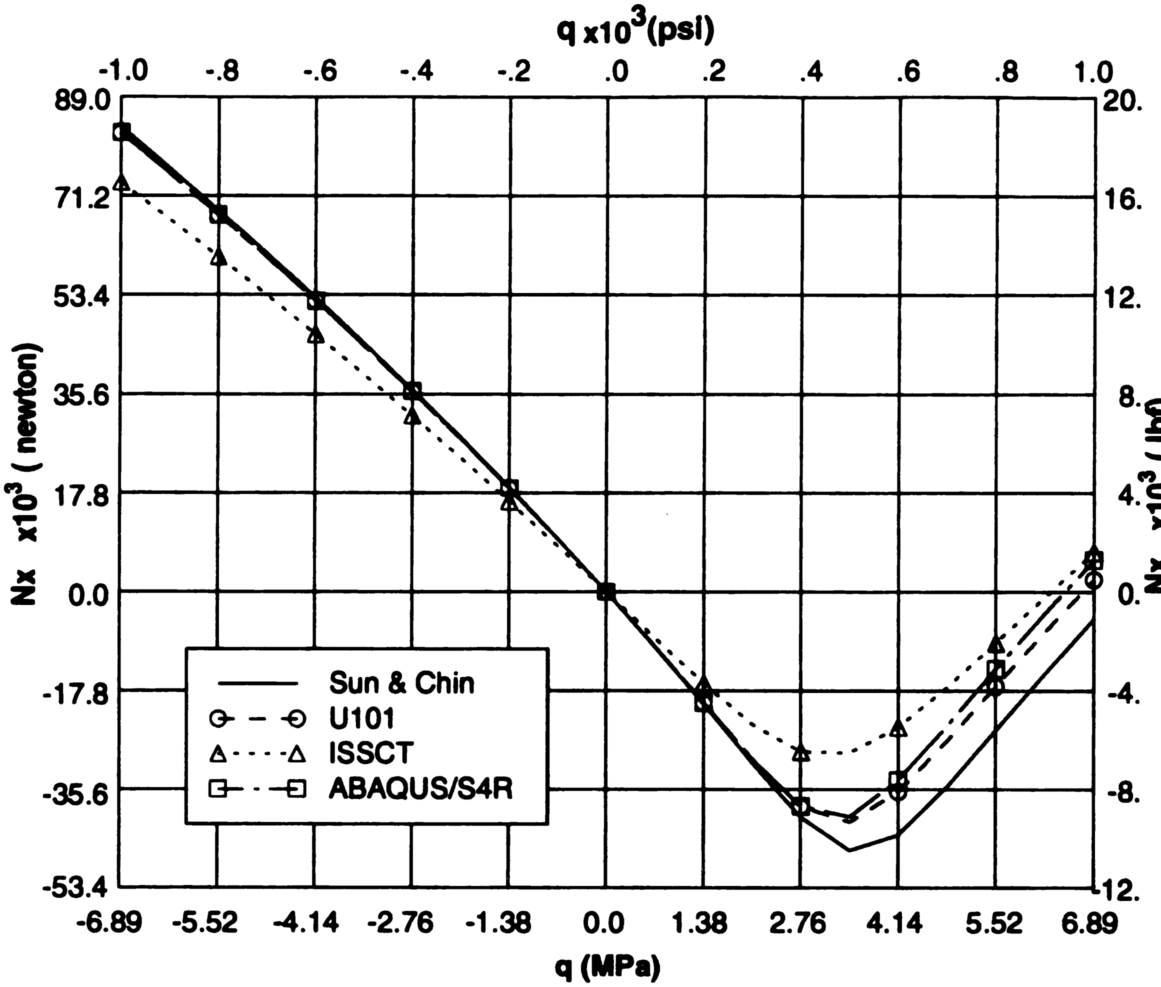

[0/90] cross-ply laminate
E_{11} = 137.9 GPa = 20.0 x 10^6 psi
E_{22} = 9.7 GPa = 1.4 x 10^6 psi
G_{12}=G_{23}=G_{13}= 4.8 GPa = 0.7 x 10^6psi
ν_{12} = 0.3
L = 228.6 mm = 9 inch
h = 20.32 mm = 0.8 inch
S = L / h = 11.25
mesh = 10 x 1
Nx = total in-plane force at
supported end

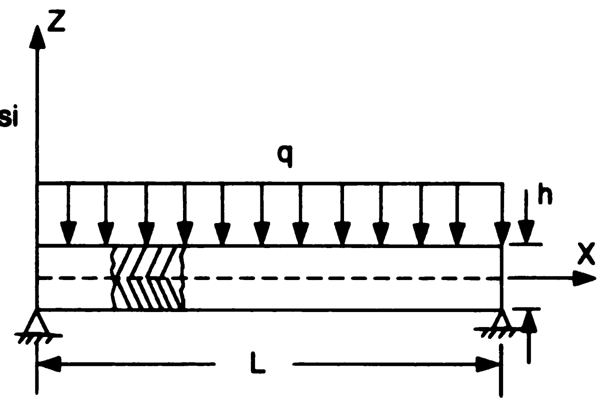

Figure 6.13 Large load vs. in-plane force curve of a S=11.25, [0/90] unsymmetric laminate

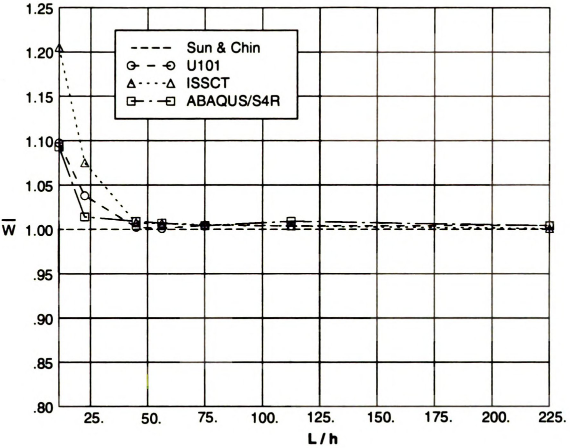

[0/90] cross-ply laminate
E_{11} = 137.9 GPa = 20.0 x 10^6 psi
E_{22} = 9.7 GPa = 1.4 x 10^6 psi
G_{12}=G_{23}=G_{13}= 4.8 GPa = 0.7 x 10^6psi
ν_{12} = 0.3
L = 228.6 mm = 9 inch
S = L / h

$\overline{W}$ = max. deflection normalized by
Sun & Chin's solution

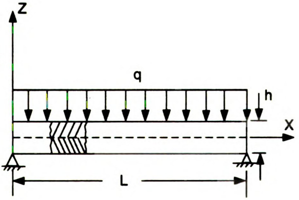

Figure 6.14 Length-to-thickness ratio vs. transverse deflection curve of a small loading, [0/90] unsymmetric laminate

6.7 Comparison of Laminates Under Large Deformation with Experimental Data

There are very few articles in the literature that investigate laminated composites under large bending-deflection using experimental approaches. The tests done by Zaghloul [74] and Kennedy [76, 77] in the early 70s presented some expermental data for symmetric and unsymmetric laminates subjected to large transverse-deflection. The symmetric and unsymmetric laminates were made of an epoxy matrix and unidirectional glass fabrics by a hand-lay-up process. Both clamped and simply-supported boundary conditions were performed in the tests. A uniform, transverse air-pressure was also applied to both square and rectangular laminates placed in an air chamber. The maximal transverse-deflection at the center of the laminate was measured with a mechanical dial-gauge.

In addition to the experimental work, Zaghloul and Kennedy also presented a simple phenomenological method [74, 75] to determine the laminate constants from the properties of fiber and epoxy. The calculated constants were then employed in a set of governing nonlinear equations, which were then solved by a finite difference technique. The governing equations were based on a plain stress condition and also accounted for the Kirchhoff-Love hypothesis and von Kármán nonlinear strains.

Three studies were performed using U101 and ABAQUS/S4R with a 12x12 biaxially symmetric mesh. The first study was for a square $[60]_4$ orthotropic laminate with clamped boundaries. The maximal transverse-deflections (normalized by the laminate thickness) and the setup of the study are shown in Figure 6.15. It is found that the transverse deflection from U101 is about 6% less than the experimental data at 13.8 kPa (2 psi), while ABAQUS/S4R is about 9% less.

The second study is for a square $[0/90]_2$ laminate with simply supported boundaries. The results of the normalized, central deflection are depicted in Figure 6.16. In addition to U101 and ABAQUS/S4R, the numerical results obtained by Zaghloul using the aforementioned finite difference method is also presented. Again, all the numerical results tend to have less deflection than the experimental data. At 7.6 kPa (1.1 psi), the central deflection of ABAQUS/S4R is 6.5% less than that of the experimental data, followed by U101 8.0% less, and Zaghloul's 13.6% less. As mentioned above, Zaghloul's formulation was based on the Kirchhoff-Love hypothesis, which did not consider transverse shear deformation.

The third study is for a square $[-60_4/60_4]$ laminate with clamped boundaries. By following the same setup as used in Figures 6.15 and 6.16, the normalized, central deflections are shown in Figure 6.17, in which ABAQUS/S4R and U101 have 7.2% and 9.5% less deflections than the experimental data, respectively.

In establishing the comparison between the experimental data and the numerical results, the testing setup and specimen fabrication should be carefully examined and their differences should be identified. Although Zaghloul [74] gave quite detailed descriptions regarding the testing setup and specimen fabrication, there were some unclear aspects. For example, there were not enough details to support that the boundary conditions used in the numerical analysis could truly represent those used in the experiments. Besides, the accuracy of air-pressure measurements in the experiment was unknown. With these issues in mind, the numerical results within 90% accuracy of the experimental data should be considered satisfactory.

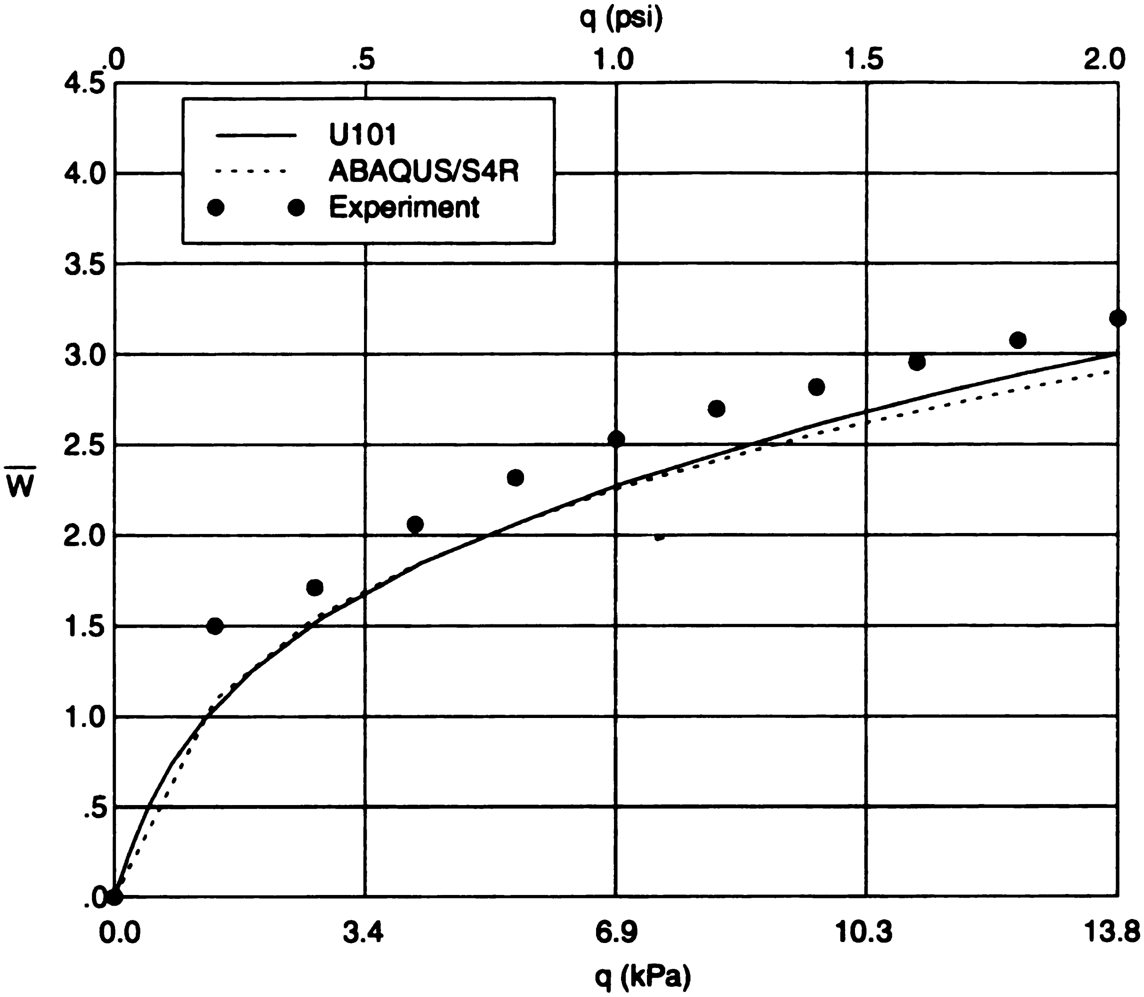

[60/60/60/60] laminate
E_{11} = 20.68 GPa = 3.00 x 10^6 psi
E_{22}= 8.83 GPa = 1.28 x 10^6 psi
G_{12} = 2.55 GPa = 0.37 x 10^6 psi
G_{23} = 1.38 GPa = 0.20 x 10^6 psi
G_{13} = 1.38 GPa = 0.20 x 10^6 psi
ν_{12} = 0.32
a = b = 304.8mm = 12 inch
h = 1.7 mm = 0.066 inch
S = a / h = 182
uniform pressure = q
mesh = 12 x 12

$\overline{W} = W_{max} / h$

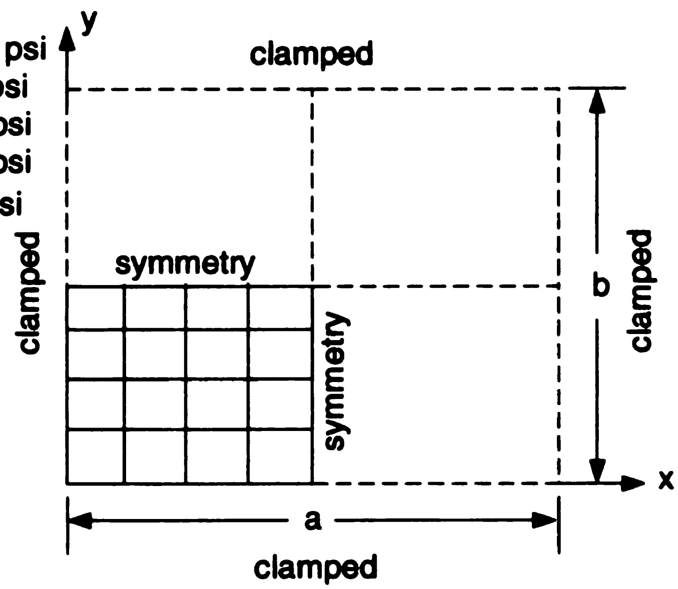

Figure 6.15 Normalized, central transverse-deflection of a [60]$_4$ laminate under uniform pressure

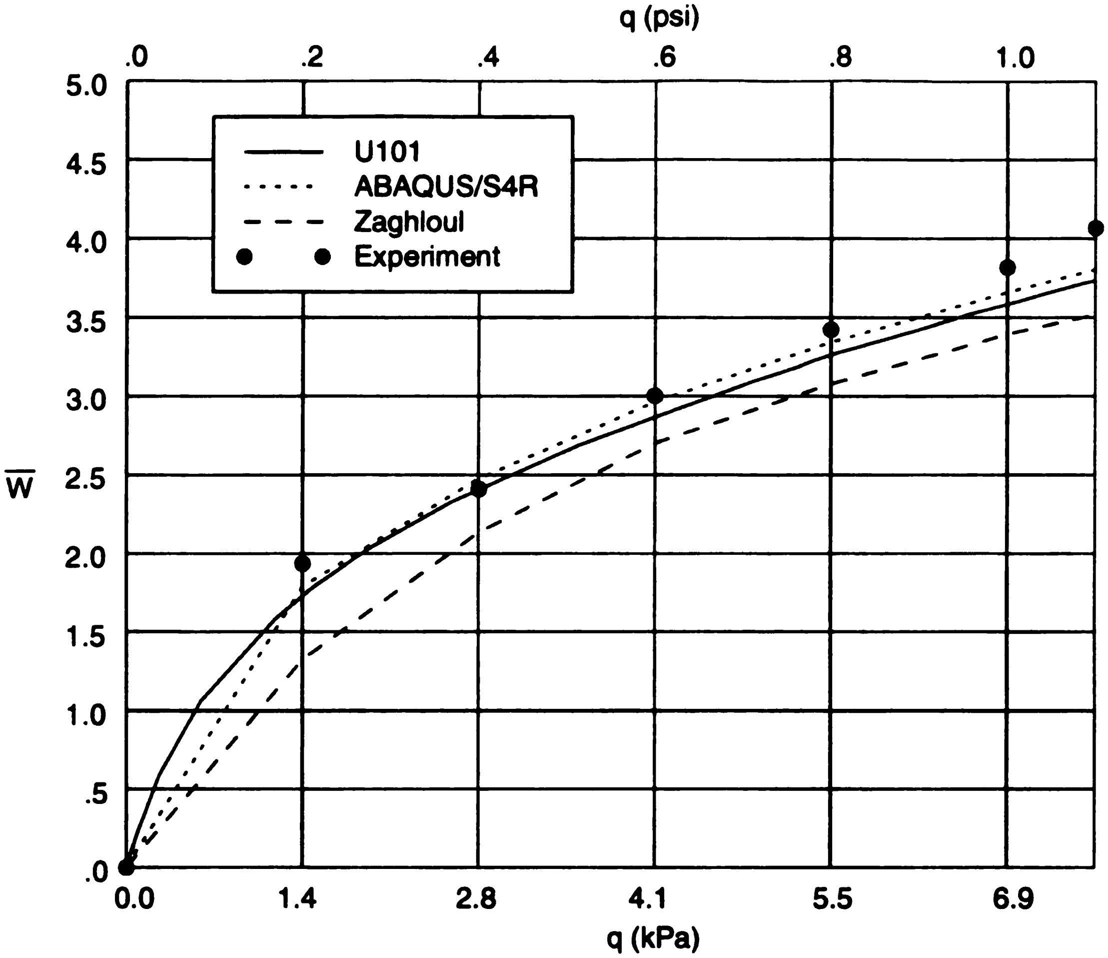

[0/90/0/90] laminate
E_{11} = 20.68 GPa = 3.00 x 10^6 psi
E_{22} = 8.83 GPa = 1.28 x 10^6 psi
G_{12} = 2.55 GPa = 0.37 x 10^6 psi
G_{23} = 1.38 GPa = 0.20 x 10^6 psi
G_{13} = 1.38 GPa = 0.20 x 10^6 psi
ν_{12} = 0.32
a = b = 304.8mm = 12 inch
h = 1.9 mm = 0.076 inch
S = a / h = 158
uniform pressure = q
mesh = 12 x 12
$\overline{W} = W_{max} / h$

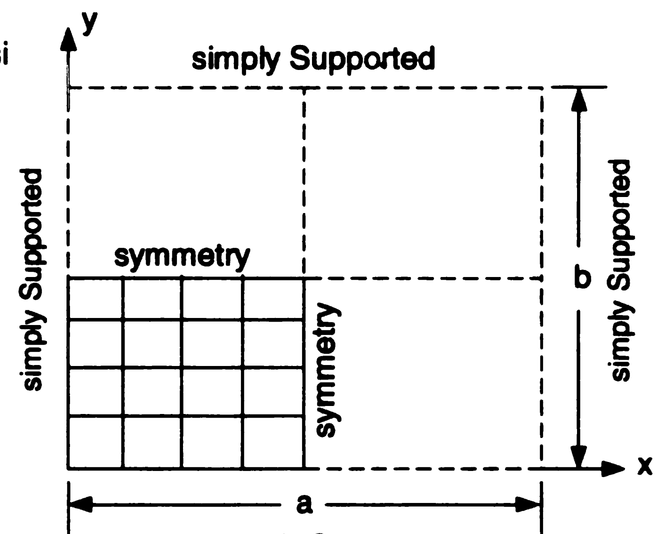

Figure 6.16 Normalized, central transverse-deflection of a [0/90]2 laminate under uniform pressure

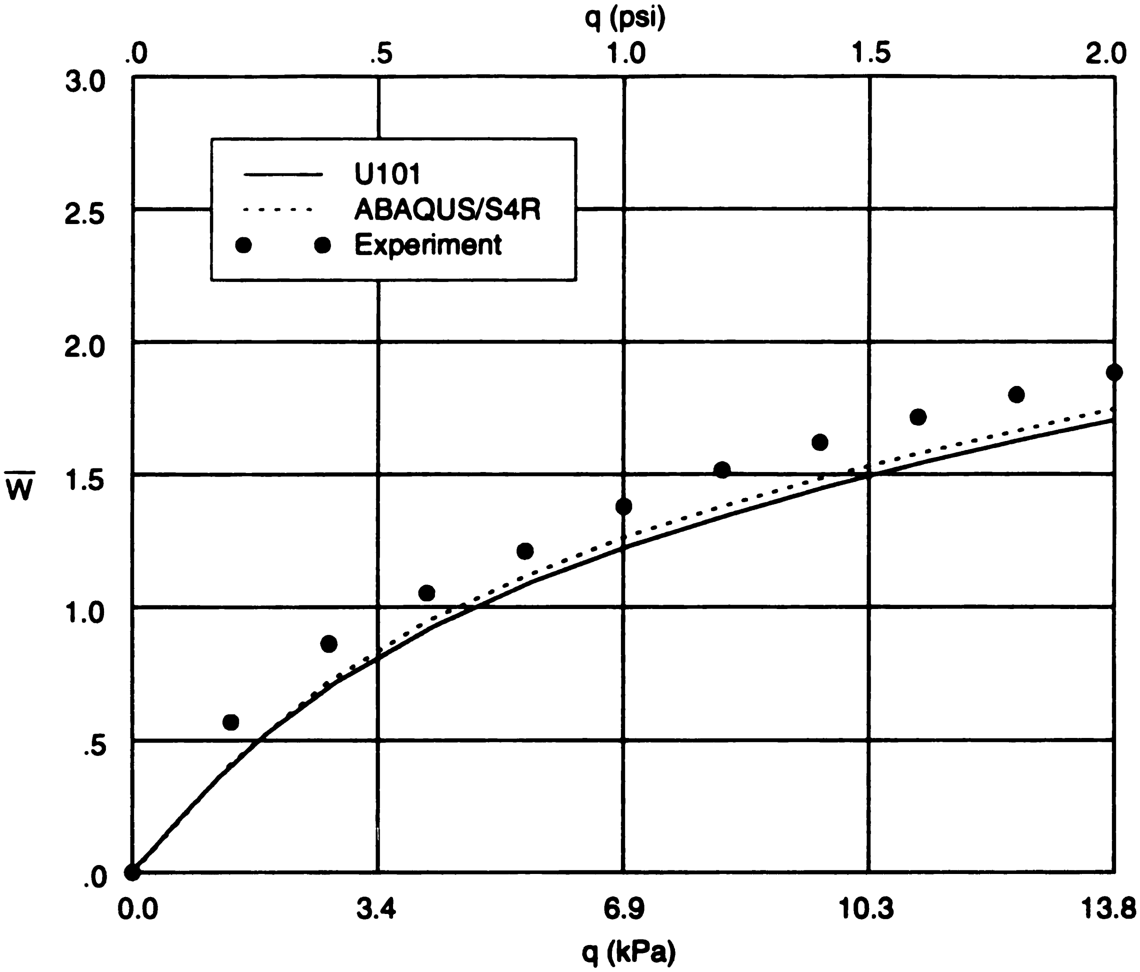

$[-60_4/60_4]$ laminate
E_{11} = 20.68 GPa = 3.00 x 10^6 psi
E_{22} = 8.83 GPa = 1.28 x 10^6 psi
G_{12} = 2.55 GPa = 0.37 x 10^6 psi
G_{23} = 1.38 GPa = 0.20 x 10^6 psi
G_{13} = 1.38 GPa = 0.20 x 10^6 psi
ν_{12} = 0.32
a = b = 304.8mm = 12 inch
h = 2.4 mm = 0.095 inch
S = a / h = 126
uniform pressure = q
mesh = 12 x 12
$\overline{W} = W_{max} / h$

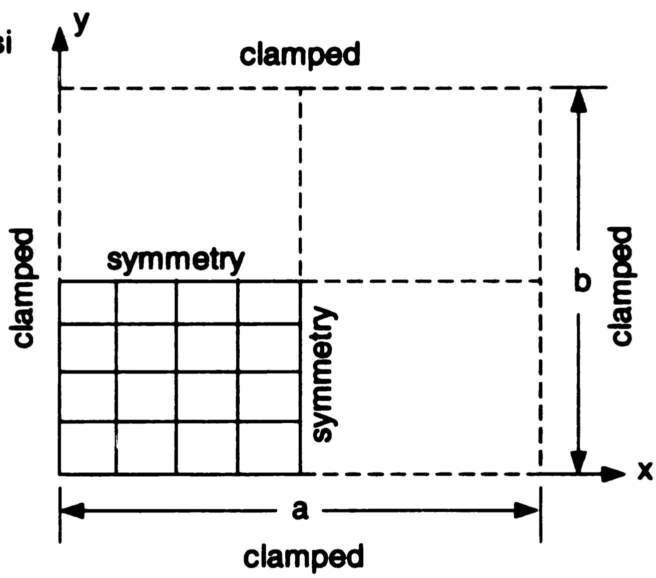

Figure 6.17 Normalized, central transverse-deflection of a $[-60_4/60_4]$ laminate under uniform pressure

Chapter 7

CONCLUSIONS AND RECOMMENDATIONS

7.1 Conclusions

This thesis shows the problem-solving methodology improving the accuracy and efficiency of the finite element simulation of composite laminates under large deformation. An updated Lagrangian approach is employed to analyze structures subjected to large deformation using the rate-of-deformation tensor and the Truesdell rate of Cauchy stress. The Generalized Zigzag Theory (ZIGZAG) presented by Li and Liu [38] is used to account for the laminated composites. Although it can provide excellent linear solutions, ZIGZAG has never been used for finite element formulation. Furthermore, there has never been an attempt to combine the updated Lagrangian approach and any Zigzag Theories for large deformation of laminated composites.

The conclusions of this thesis are listed below:

1. A general procedure of deriving the governing equations for structures undergoing

large deformations (large rotations and large strains) was established. The procedure was an updated Lagrangian approach, which utilized the Truesdell rate of Cauchy stress tensor and the rate-of-deformation tensor. This procedure was general enough that it was not limited to any specific type of displacement fields.

2. A set of incremental displacement components was successfully derived from the Generalized Zigzag Theory (ZIGZAG). Although the theory described the displacements of laminated composites layer by layer, the total number of unknown variables remained constant, i.e. independent of layer number.

3. Based on the ZIGZAG, a four-node shell element (designated as U101) was formulated. It had seven degrees of freedom at each node. The kinky in-plane displacements through the laminate thickness could be naturally displayed. All stress calculations were based on constitutive equations. The transverse shear stresses were continuous through the laminate thickness; no shear correction factor was necessary, and no recovering process through equilibrium equations was required.

4. An innovative method of constructing the Jacobian matrix was demonstrated. The Zigzag Jacobian provided a consistent way of describing both kinematics and geometry within each element.

5. Extensive benchmark problems were presented by using the U101 element. The purpose of the studies was to investigate the performance and to gauge the accuracy of the element. The element gave excellent convergency and accuracy in problems that dealt with isotropic and laminated composites under linear and nonlinear deformations. In addition, the element offered reasonable agreement with some experimental data without any shear locking problem. Although it did not pass a bending patch

test, there was no sign of convergency problems.

7.2 Recommendations

To bring the U101 element presented herein to more complete fruition, the following topics are recommended for future studies:

1. Lower continuity requirement for transverse displacement Δw: Instead of using the C^1 Hermite cubic shape function, one may want to use only the C^0 continuity shape function for Δw. The use of shape functions of the same order for all degrees of freedom seems to be more consistent in logic.

2. Damage models for delamination analysis: Delamination is a primary damage mode in laminated composites. Implementation of a damage model capable of identifying delamination is critically important to laminated composite analysis.

3. Buckling and post-buckling analyses: Improving the buckling resistance is a challenge task in designing shell-type composite structures. A standard set of benchmark problems should be given to evaluate the capability of the U101 element in buckling and post-buckling analysis. The inclusion of a damage model into the U101 element is a prerequisite in this study.

4. A selectively reduced integration scheme: The U101 element uses a four-point Gauss-Legendre integration scheme. If the number of integration points can be reduced while the degree of accuracy is maintained, the computation time can be greatly shortened.

5. Triangular element: For a composite structure with irregular boundaries, triangular elements are better than rectangular elements in describing the boundaries.

6. Dynamic analysis: Impact response is an important concern in laminated composite analysis. Dynamic analysis is necessary when inertia effect has to be considered.

7. Independent finite element program: The U101 element is currently implemented as a subroutine in ABAQUS/Standard. Every time the program is to be executed, the FORTRAN subroutine needs to be compiled and linked to the main code. This process is very time consuming. Besides, the utilization of data storage space is not optimized. If the element is to become more versatile, a stand-alone program would be desired.

APPENDICES

APPENDIX A

CONSISTENT LINEARIZATION

The meaning of consistent linearization here is to use a systematic process to obtain linear approximation of a set of nonlinear equations within a small neighborhood of some known approximate solution to the nonlinear problem.

Let us consider the motion of a material(in this case, it is also equal to the mesh motion) is given by

$$x_i^v = X_i + u_i^v, \tag{A.1}$$

and the new motion is

$$\begin{aligned} x_i^{v+1} &= x_i^v + \Delta u_i \\ &= X_i + u_i^v + \Delta u_i, \end{aligned} \tag{A.2}$$

in which the superscript v is interpreted as the increment "counter".

Now consider an abstract nonlinear function, $\mathcal{F}$, of components of a vector field x_i^{v+1}, that satisfies the following nonlinear equation

$$\mathcal{F}(x_i^{v+1}) = 0 \tag{A.3}$$

Assuming that $\mathcal{F}(x_i^{v+1})$ is sufficiently smooth (i.e. differentiable) in the neighborhood of a given (known) "point", x_i^v, it may be expanded in a Taylor series about x_i^v to obtain

$$\mathcal{F}(x_i^{v+1}) = \mathcal{F}(x_i^v) + \frac{d}{d\epsilon}\mathcal{F}(x_i^v + \epsilon\Delta u_i)\Big|_{\epsilon=0} + R(x_i^v) \tag{A.4}$$

in which the sum of first two terms of the right hand side of Eq.(A.4) is the linearized part of $\mathcal{F}$ and it is a measure of the rate of change of $\mathcal{F}$ in the direction of Δu_i at the point x_i^v. And R is the remaining higher order term, which by Taylor's theorem vanishes faster than the linearized part as $\Delta u_i \to 0$. ϵ is a scale parameter. Denoting the second right-hand-side term by

$$\mathcal{L}[\mathcal{F}]_{x_i^v} \stackrel{def}{=} \frac{d}{d\epsilon}\mathcal{F}(x_i^v + \epsilon\Delta u_i)\Big|_{\epsilon=0} \tag{A.5}$$

By neglecting the R term and employing Eqs.(A.3), (A.4) and (A.5), we obtain the following linear approximation (locally) to the original nonlinear problem - Eq.(A.3)

$$-\mathcal{L}[\mathcal{F}]_{x_i^v} = \mathcal{F}(x_i^v) \tag{A.6}$$

where the only unknown is Δu_i, all other quantities being evaluated at the known reference point x_i^v.

Iterative use of Eqs.(A.6) and (A.2) may be identified with the Newton-Raphson solution algorithm, where Eq.(A.6) is used to computer the iterative change (Δu_i) and Eq.(A.2) updates the solution between increments. To simplify subsequent writing, the subscript x_i^v is dropped with an understanding that

$$\mathcal{L}[\mathcal{F}] = \mathcal{L}[\mathcal{F}]_{x_i^v} \tag{A.7}$$

The following few examples of $\mathcal{L}[\mathcal{F}]$ will be helpful for the later derivation.

1. the deformation gradient, $F_{ij} = \partial x_i/\partial X_j$,

$$\mathcal{L}[F_{ij}] = \frac{d}{d\epsilon}\left\{\frac{\partial(x_i^v + \epsilon\Delta u_i)}{\partial X_j}\right\}\Big|_{\epsilon=0} = \frac{\partial \Delta u_i}{\partial X_j} \tag{A.8}$$

2. the Jacobian, $J = det\ (F_{ij})$,

$$\begin{aligned}
\mathcal{L}[J] &= \frac{d}{d\epsilon}\left\{det\left(\frac{\partial(x_i^v + \epsilon\Delta u_i)}{\partial X_j}\right)\right\}\Bigg|_{\epsilon=0} \\
&= J^v \Delta u_{i,i} \\
&= J^v \frac{\partial \Delta u_i}{\partial x_i}
\end{aligned} \tag{A.9}$$

3. inverse of the deformation gradient, F_{ij}^{-1},

$$\mathbf{F}\mathbf{F}^{-1} = 1$$

$$\mathcal{L}[\mathbf{F}]\mathbf{F}^{-1} + \mathbf{F}\mathcal{L}[\mathbf{F}^{-1}] = \mathbf{0}$$

$$\mathcal{L}[\mathbf{F}^{-1}] = -\mathbf{F}^{-1}\mathcal{L}[\mathbf{F}]\mathbf{F}^{-1} \tag{A.10}$$

Therefore, the components of $\mathcal{L}[\mathbf{F}^{-1}]$ are:

$$\mathcal{L}[F_{ij}^{-1}] = -F_{ik}^{-1}\frac{\partial \Delta u_k}{\partial X_l}F_{lj}^{-1} \tag{A.11}$$

APPENDIX B

SOME SPECIAL MATRICES FOR FINITE ELEMENT FORMULATION

$[XU_0]$ is a 1 by 28 vector and its non-zero components are listed as follows, for $i = 1, 2, 3, 4$:

$$\begin{aligned}
XU_0(1, 7(i-1)+1) &= N_i \\
XU_0(1, 7(i-1)+3) &= S_2^k\,(\partial\mathcal{H}_{i1}/\partial x) \\
XU_0(1, 7(i-1)+4) &= S_1^k N_i \\
XU_0(1, 7(i-1)+6) &= S_2^k\,(\partial\mathcal{H}_{i2}/\partial x) \\
XU_0(1, 7(i-1)+7) &= S_2^k\,(\partial\mathcal{H}_{i3}/\partial x)
\end{aligned}$$

$[XU_1]$ is a 1 by 28 vector and its non-zero components are listed as follows, for $i = 1, 2, 3, 4$:

$$\begin{aligned}
XU_1(1, 7(i-1)+3) &= R_2^k\,(\partial\mathcal{H}_{i1}/\partial x) \\
XU_1(1, 7(i-1)+4) &= R_1^k N_i
\end{aligned}$$

$$
\begin{aligned}
XU_1(1,7(i-1)+6) &= R_2^k\,(\partial\mathcal{H}_{i2}/\partial x) \\
XU_1(1,7(i-1)+7) &= R_2^k\,(\partial\mathcal{H}_{i3}/\partial x)
\end{aligned}
$$

$[XU_2]$ is a 1 by 28 vector and its non-zero components are listed as follows, for $i = 1, 2, 3, 4$:

$$
\begin{aligned}
XU_2(1,7(i-1)+3) &= A_2\,(\partial\mathcal{H}_{i1}/\partial x) \\
XU_2(1,7(i-1)+4) &= A_1 N_i \\
XU_2(1,7(i-1)+6) &= A_2\,(\partial\mathcal{H}_{i2}/\partial x) \\
XU_2(1,7(i-1)+7) &= A_2\,(\partial\mathcal{H}_{i3}/\partial x)
\end{aligned}
$$

$[XU_3]$ is a 1 by 28 vector and its non-zero components are listed as follows, for $i = 1, 2, 3, 4$:

$$
\begin{aligned}
XU_3(1,7(i-1)+3) &= B_2\,(\partial\mathcal{H}_{i1}/\partial x) \\
XU_3(1,7(i-1)+4) &= B_1 N_i \\
XU_3(1,7(i-1)+6) &= B_2\,(\partial\mathcal{H}_{i2}/\partial x) \\
XU_3(1,7(i-1)+7) &= B_2\,(\partial\mathcal{H}_{i3}/\partial x)
\end{aligned}
$$

$[XV_0]$ is a 1 by 28 vector and its non-zero components are listed as follows, for $i = 1, 2, 3, 4$:

$$
\begin{aligned}
XV_0(1,7(i-1)+2) &= N_i \\
XV_0(1,7(i-1)+3) &= P_2^k\,(\partial\mathcal{H}_{i1}/\partial y) \\
XV_0(1,7(i-1)+5) &= P_1^k N_i \\
XV_0(1,7(i-1)+6) &= P_2^k\,(\partial\mathcal{H}_{i2}/\partial y) \\
XV_0(1,7(i-1)+7) &= P_2^k\,(\partial\mathcal{H}_{i3}/\partial y)
\end{aligned}
$$

$[XV_1]$ is a 1 by 28 vector and its non-zero components are listed as follows, for $i = 1, 2, 3, 4$:

$$
XV_1(1,7(i-1)+3) = O_2^k\,(\partial\mathcal{H}_{i1}/\partial y)
$$

$$XV_1(1,7(i-1)+5) = O_1^k N_i$$

$$XV_1(1,7(i-1)+6) = O_2^k\left(\partial\mathcal{H}_{i2}/\partial y\right)$$

$$XV_1(1,7(i-1)+7) = O_2^k\left(\partial\mathcal{H}_{i3}/\partial y\right)$$

$[XV_2]$ is a 1 by 28 vector and its non-zero components are listed as follows, for $i = 1,2,3,4$:

$$XV_2(1,7(i-1)+3) = C_2\left(\partial\mathcal{H}_{i1}/\partial y\right)$$

$$XV_2(1,7(i-1)+5) = C_1 N_i$$

$$XV_2(1,7(i-1)+6) = C_2\left(\partial\mathcal{H}_{i2}/\partial y\right)$$

$$XV_2(1,7(i-1)+7) = C_2\left(\partial\mathcal{H}_{i3}/\partial y\right)$$

$[XV_3]$ is a 1 by 28 vector and its non-zero components are listed as follows, for $i = 1,2,3,4$:

$$XV_3(1,7(i-1)+3) = D_2\left(\partial\mathcal{H}_{i1}/\partial y\right)$$

$$XV_3(1,7(i-1)+5) = D_1 N_i$$

$$XV_3(1,7(i-1)+6) = D_2\left(\partial\mathcal{H}_{i2}/\partial y\right)$$

$$XV_3(1,7(i-1)+7) = D_2\left(\partial\mathcal{H}_{i3}/\partial y\right)$$

$[XW_0]$ is a 1 by 28 vector and its non-zero components are listed as follows, for $i = 1,2,3,4$:

$$XW_0(1,7(i-1)+3) = \mathcal{H}_{i1}$$

$$XW_0(1,7(i-1)+6) = \mathcal{H}_{i2}$$

$$XW_0(1,7(i-1)+7) = \mathcal{H}_{i3}$$

$[MA]$ is a 5 by 28 matrix and its non-zero components are listed as follows, for $i = 1,2,3,4$:

$$MA(1,7(i-1)+1) = \partial N_i/\partial x$$

$$MA(1,7(i-1)+3) = S_2^k\left(\partial^2\mathcal{H}_{i1}/\partial x^2\right)$$

$$
\begin{aligned}
MA(1,7(i-1)+4) &= S_1^k\,(\partial N_i/\partial x) \\
MA(1,7(i-1)+6) &= S_2^k\left(\partial^2\mathcal{H}_{i2}/\partial x^2\right) \\
MA(1,7(i-1)+7) &= S_2^k\left(\partial^2\mathcal{H}_{i3}/\partial x^2\right) \\
MA(2,7(i-1)+2) &= \partial N_i/\partial y \\
MA(2,7(i-1)+3) &= P_2^k\left(\partial^2\mathcal{H}_{i1}/\partial y^2\right) \\
MA(2,7(i-1)+5) &= P_1^k\,(\partial N_i/\partial y) \\
MA(2,7(i-1)+6) &= P_2^k\left(\partial^2\mathcal{H}_{i2}/\partial y^2\right) \\
MA(2,7(i-1)+7) &= P_2^k\left(\partial^2\mathcal{H}_{i3}/\partial y^2\right) \\
MA(3,7(i-1)+1) &= \partial N_i/\partial y \\
MA(3,7(i-1)+2) &= \partial N_i/\partial x \\
MA(3,7(i-1)+3) &= S_2^k\left(\partial^2\mathcal{H}_{i1}/\partial x\partial y\right)+P_2^k\left(\partial^2\mathcal{H}_{i1}/\partial x\partial y\right) \\
MA(3,7(i-1)+4) &= S_1^k\,(\partial N_i/\partial y) \\
MA(3,7(i-1)+5) &= P_1^k\,(\partial N_i/\partial x) \\
MA(3,7(i-1)+6) &= S_2^k\left(\partial^2\mathcal{H}_{i2}/\partial x\partial y\right)+P_2^k\left(\partial^2\mathcal{H}_{i2}/\partial x\partial y\right) \\
MA(3,7(i-1)+7) &= S_2^k\left(\partial^2\mathcal{H}_{i3}/\partial x\partial y\right)+P_2^k\left(\partial^2\mathcal{H}_{i3}/\partial x\partial y\right)
\end{aligned}
$$

$[MB]$ is a 5 by 28 matrix and its non-zero components are listed as follows, for $i = 1,2,3,4$:

$$
\begin{aligned}
MB(4,7(i-1)+3) &= \left(O_2^k+1\right)(\partial\mathcal{H}_{i1}/\partial y) \\
MB(4,7(i-1)+5) &= O_1^k N_i \\
MB(4,7(i-1)+6) &= \left(O_2^k+1\right)(\partial\mathcal{H}_{i2}/\partial y) \\
MB(4,7(i-1)+7) &= \left(O_2^k+1\right)(\partial\mathcal{H}_{i3}/\partial y) \\
MB(5,7(i-1)+3) &= \left(R_2^k+1\right)(\partial\mathcal{H}_{i1}/\partial x) \\
MB(5,7(i-1)+4) &= R_1^k N_i
\end{aligned}
$$

$$MB(5,7(i-1)+6) = \left(R_2^k+1\right)(\partial\mathcal{H}_{i2}/\partial x)$$

$$MB(5,7(i-1)+7) = \left(R_2^k+1\right)(\partial\mathcal{H}_{i3}/\partial x)$$

$[MD_1]$ is a 5 by 28 matrix and its non-zero components are listed as follows, for $i = 1, 2, 3, 4$:

$$MD_1(1,7(i-1)+3) = R_2^k\left(\partial^2\mathcal{H}_{i1}/\partial x^2\right)$$

$$MD_1(1,7(i-1)+4) = R_1^k(\partial N_i/\partial x)$$

$$MD_1(1,7(i-1)+6) = R_2^k\left(\partial^2\mathcal{H}_{i2}/\partial x^2\right)$$

$$MD_1(1,7(i-1)+7) = R_2^k\left(\partial^2\mathcal{H}_{i3}/\partial x^2\right)$$

$$MD_1(2,7(i-1)+3) = O_2^k\left(\partial^2\mathcal{H}_{i1}/\partial y^2\right)$$

$$MD_1(2,7(i-1)+5) = O_1^k(\partial N_i/\partial y)$$

$$MD_1(2,7(i-1)+6) = O_2^k\left(\partial^2\mathcal{H}_{i2}/\partial y^2\right)$$

$$MD_1(2,7(i-1)+7) = O_2^k\left(\partial^2\mathcal{H}_{i3}/\partial y^2\right)$$

$$MD_1(3,7(i-1)+3) = (R_2+O_2)\left(\partial^2\mathcal{H}_{i1}/\partial x\partial y\right)$$

$$MD_1(3,7(i-1)+4) = R_1(\partial N_i/\partial y)$$

$$MD_1(3,7(i-1)+5) = O_1(\partial N_i/\partial x)$$

$$MD_1(3,7(i-1)+6) = (R_2+O_2)\left(\partial^2\mathcal{H}_{i2}/\partial x\partial y\right)$$

$$MD_1(3,7(i-1)+7) = (R_2+O_2)\left(\partial^2\mathcal{H}_{i3}/\partial x\partial y\right)$$

$$MD_1(4,7(i-1)+3) = 2C_2(\partial\mathcal{H}_{i1}/\partial y)$$

$$MD_1(4,7(i-1)+5) = 2C_1N_i$$

$$MD_1(4,7(i-1)+6) = 2C_2(\partial\mathcal{H}_{i2}/\partial y)$$

$$MD_1(4,7(i-1)+7) = 2C_2(\partial\mathcal{H}_{i3}/\partial y)$$

$$MD_1(5,7(i-1)+3) = 2A_2(\partial\mathcal{H}_{i1}/\partial x)$$

$$MD_1(5,7(i-1)+4) = 2A_1N_i$$

$$MD_1(5,7(i-1)+6) = 2A_2\,(\partial\mathcal{H}_{i2}/\partial x)$$

$$MD_1(5,7(i-1)+7) = 2A_2\,(\partial\mathcal{H}_{i3}/\partial x)$$

$[MD_2]$ is a 5 by 28 matrix and its non-zero components are listed as follows, for $i = 1,2,3,4$:

$$\begin{aligned}
MD_2(1,7(i-1)+3) &= A_2\left(\partial^2\mathcal{H}_{i1}/\partial x^2\right) \\
MD_2(1,7(i-1)+4) &= A_1\,(\partial N_i/\partial x) \\
MD_2(1,7(i-1)+6) &= A_2\left(\partial^2\mathcal{H}_{i2}/\partial x^2\right) \\
MD_2(1,7(i-1)+7) &= A_2\left(\partial^2\mathcal{H}_{i3}/\partial x^2\right) \\
MD_2(2,7(i-1)+3) &= C_2\left(\partial^2\mathcal{H}_{i1}/\partial y^2\right) \\
MD_2(2,7(i-1)+5) &= C_1\,(\partial N_i/\partial y) \\
MD_2(2,7(i-1)+6) &= C_2\left(\partial^2\mathcal{H}_{i2}/\partial y^2\right) \\
MD_2(2,7(i-1)+7) &= C_2\left(\partial^2\mathcal{H}_{i3}/\partial y^2\right) \\
MD_2(3,7(i-1)+3) &= (A_2+C_2)\left(\partial^2\mathcal{H}_{i1}/\partial x\partial y\right) \\
MD_2(3,7(i-1)+4) &= A_1\,(\partial N_i/\partial y) \\
MD_2(3,7(i-1)+5) &= C_1\,(\partial N_i/\partial x) \\
MD_2(3,7(i-1)+6) &= (A_2+C_2)\left(\partial^2\mathcal{H}_{i2}/\partial x\partial y\right) \\
MD_2(3,7(i-1)+7) &= (A_2+C_2)\left(\partial^2\mathcal{H}_{i3}/\partial x\partial y\right) \\
MD_2(4,7(i-1)+3) &= 3D_2\,(\partial\mathcal{H}_{i1}/\partial y) \\
MD_2(4,7(i-1)+5) &= 3D_1 N_i \\
MD_2(4,7(i-1)+6) &= 3D_2\,(\partial\mathcal{H}_{i2}/\partial y) \\
MD_2(4,7(i-1)+7) &= 3D_2\,(\partial\mathcal{H}_{i3}/\partial y) \\
MD_2(5,7(i-1)+3) &= 3B_2\,(\partial\mathcal{H}_{i1}/\partial x) \\
MD_2(5,7(i-1)+4) &= 3B_1 N_i
\end{aligned}$$

$$MD_2(5,7(i-1)+6) = 3B_2\,(\partial\mathcal{H}_{i2}/\partial x)$$

$$MD_2(5,7(i-1)+7) = 3B_2\,(\partial\mathcal{H}_{i3}/\partial x)$$

$[MD_3]$ is a 5 by 28 matrix and its non-zero components are listed as follows, for $i = 1,2,3,4$:

$$MD_3(1,7(i-1)+3) = B_2\left(\partial^2\mathcal{H}_{i1}/\partial x^2\right)$$

$$MD_3(1,7(i-1)+4) = B_1\,(\partial N_i/\partial x)$$

$$MD_3(1,7(i-1)+6) = B_2\left(\partial^2\mathcal{H}_{i2}/\partial x^2\right)$$

$$MD_3(1,7(i-1)+7) = B_2\left(\partial^2\mathcal{H}_{i3}/\partial x^2\right)$$

$$MD_3(2,7(i-1)+3) = D_2\left(\partial^2\mathcal{H}_{i1}/\partial y^2\right)$$

$$MD_3(2,7(i-1)+5) = D_1\,(\partial N_i/\partial y)$$

$$MD_3(2,7(i-1)+6) = D_2\left(\partial^2\mathcal{H}_{i2}/\partial y^2\right)$$

$$MD_3(2,7(i-1)+7) = D_2\left(\partial^2\mathcal{H}_{i3}/\partial y^2\right)$$

$$MD_3(3,7(i-1)+3) = (B_2+D_2)\left(\partial^2\mathcal{H}_{i1}/\partial x\partial y\right)$$

$$MD_3(3,7(i-1)+4) = B_1\,(\partial N_i/\partial y)$$

$$MD_3(3,7(i-1)+5) = D_1\,(\partial N_i/\partial x)$$

$$MD_3(3,7(i-1)+6) = (B_2+D_2)\left(\partial^2\mathcal{H}_{i2}/\partial x\partial y\right)$$

$$MD_3(3,7(i-1)+7) = (B_2+D_2)\left(\partial^2\mathcal{H}_{i3}/\partial x\partial y\right)$$

$[GU_0]$ is a 3 by 28 matrix and its non-zero components are listed as follows, for $i = 1,2,3,4$:

$$GU_0(1,7(i-1)+1) = \partial N_i/\partial x$$

$$GU_0(1,7(i-1)+3) = S_2^k\left(\partial^2\mathcal{H}_{i1}/\partial x^2\right)$$

$$GU_0(1,7(i-1)+4) = S_1^k\,(\partial N_i/\partial x)$$

$$GU_0(1,7(i-1)+6) = S_2^k\left(\partial^2\mathcal{H}_{i2}/\partial x^2\right)$$

$$GU_0(1, 7(i-1)+7) = S_2^k \left(\partial^2 \mathcal{H}_{i3}/\partial x^2\right)$$

$$GU_0(2, 7(i-1)+1) = \partial N_i/\partial y$$

$$GU_0(2, 7(i-1)+3) = S_2^k \left(\partial^2 \mathcal{H}_{i1}/\partial x \partial y\right)$$

$$GU_0(2, 7(i-1)+4) = S_1^k \left(\partial N_i/\partial y\right)$$

$$GU_0(2, 7(i-1)+6) = S_2^k \left(\partial^2 \mathcal{H}_{i2}/\partial x \partial y\right)$$

$$GU_0(2, 7(i-1)+7) = S_2^k \left(\partial^2 \mathcal{H}_{i3}/\partial x \partial y\right)$$

$$GU_0(3, 7(i-1)+3) = R_2^k \left(\partial \mathcal{H}_{i1}/\partial x\right)$$

$$GU_0(3, 7(i-1)+4) = R_1^k N_i$$

$$GU_0(3, 7(i-1)+6) = R_2^k \left(\partial \mathcal{H}_{i2}/\partial x\right)$$

$$GU_0(3, 7(i-1)+7) = R_2^k \left(\partial \mathcal{H}_{i3}/\partial x\right)$$

$[GU_1]$ is a 3 by 28 matrix and its non-zero components are listed as follows, for $i = 1, 2, 3, 4$:

$$GU_1(1, 7(i-1)+3) = R_2^k \left(\partial^2 \mathcal{H}_{i1}/\partial x^2\right)$$

$$GU_1(1, 7(i-1)+4) = R_1^k \left(\partial N_i/\partial x\right)$$

$$GU_1(1, 7(i-1)+6) = R_2^k \left(\partial^2 \mathcal{H}_{i2}/\partial x^2\right)$$

$$GU_1(1, 7(i-1)+7) = R_2^k \left(\partial^2 \mathcal{H}_{i3}/\partial x^2\right)$$

$$GU_1(2, 7(i-1)+3) = R_2^k \left(\partial^2 \mathcal{H}_{i1}/\partial x \partial y\right)$$

$$GU_1(2, 7(i-1)+4) = R_1^k \left(\partial N_i/\partial y\right)$$

$$GU_1(2, 7(i-1)+6) = R_2^k \left(\partial^2 \mathcal{H}_{i2}/\partial x \partial y\right)$$

$$GU_1(2, 7(i-1)+7) = R_2^k \left(\partial^2 \mathcal{H}_{i3}/\partial x \partial y\right)$$

$$GU_1(3, 7(i-1)+3) = 2A_2 \left(\partial \mathcal{H}_{i1}/\partial x\right)$$

$$GU_1(3, 7(i-1)+4) = 2A_1 N_i$$

$$GU_1(3, 7(i-1)+6) = 2A_2 \left(\partial \mathcal{H}_{i2}/\partial x\right)$$

$$GU_1(3,7(i-1)+7) = 2A_2\,(\partial\mathcal{H}_{i3}/\partial x)$$

$[GU_2]$ is a 3 by 28 matrix and its non-zero components are listed as follows, for $i = 1,2,3,4$:

$$GU_2(1,7(i-1)+3) = A_2\left(\partial^2\mathcal{H}_{i1}/\partial x^2\right)$$

$$GU_2(1,7(i-1)+4) = A_1\,(\partial N_i/\partial x)$$

$$GU_2(1,7(i-1)+6) = A_2\left(\partial^2\mathcal{H}_{i2}/\partial x^2\right)$$

$$GU_2(1,7(i-1)+7) = A_2\left(\partial^2\mathcal{H}_{i3}/\partial x^2\right)$$

$$GU_2(2,7(i-1)+3) = A_2\left(\partial^2\mathcal{H}_{i1}/\partial x\partial y\right)$$

$$GU_2(2,7(i-1)+4) = A_1\,(\partial N_i/\partial y)$$

$$GU_2(2,7(i-1)+6) = A_2\left(\partial^2\mathcal{H}_{i2}/\partial x\partial y\right)$$

$$GU_2(2,7(i-1)+7) = A_2\left(\partial^2\mathcal{H}_{i3}/\partial x\partial y\right)$$

$$GU_2(3,7(i-1)+3) = 3B_2\,(\partial\mathcal{H}_{i1}/\partial x)$$

$$GU_2(3,7(i-1)+4) = 3B_1 N_i$$

$$GU_2(3,7(i-1)+6) = 3B_2\,(\partial\mathcal{H}_{i2}/\partial x)$$

$$GU_2(3,7(i-1)+7) = 3B_2\,(\partial\mathcal{H}_{i3}/\partial x)$$

$[GU_3]$ is a 3 by 28 matrix and its non-zero components are listed as follows, for $i = 1,2,3,4$:

$$GU_3(1,7(i-1)+3) = B_2\left(\partial^2\mathcal{H}_{i1}/\partial x^2\right)$$

$$GU_3(1,7(i-1)+4) = B_1\,(\partial N_i/\partial x)$$

$$GU_3(1,7(i-1)+6) = B_2\left(\partial^2\mathcal{H}_{i2}/\partial x^2\right)$$

$$GU_3(1,7(i-1)+7) = B_2\left(\partial^2\mathcal{H}_{i3}/\partial x^2\right)$$

$$GU_3(2,7(i-1)+3) = B_2\left(\partial^2\mathcal{H}_{i1}/\partial x\partial y\right)$$

$$GU_3(2,7(i-1)+4) = B_1\,(\partial N_i/\partial y)$$

$$GU_3(2,7(i-1)+6) = B_2\left(\partial^2\mathcal{H}_{i2}/\partial x\partial y\right)$$

$$GU_3(2,7(i-1)+7) = B_2\left(\partial^2\mathcal{H}_{i3}/\partial x\partial y\right)$$

$[GV_0]$ is a 3 by 28 matrix and its non-zero components are listed as follows, for $i = 1,2,3,4$:

$$\begin{aligned}
GV_0(1,7(i-1)+2) &= \partial N_i/\partial x \\
GV_0(1,7(i-1)+3) &= P_2^k\left(\partial^2\mathcal{H}_{i1}/\partial x\partial y\right) \\
GV_0(1,7(i-1)+5) &= P_1^k\left(\partial N_i/\partial x\right) \\
GV_0(1,7(i-1)+6) &= P_2^k\left(\partial^2\mathcal{H}_{i2}/\partial x\partial y\right) \\
GV_0(1,7(i-1)+7) &= P_2^k\left(\partial^2\mathcal{H}_{i3}/\partial x\partial y\right) \\
GV_0(2,7(i-1)+2) &= \partial N_i/\partial y \\
GV_0(2,7(i-1)+3) &= P_2^k\left(\partial^2\mathcal{H}_{i1}/\partial y^2\right) \\
GV_0(2,7(i-1)+5) &= P_1^k\left(\partial N_i/\partial y\right) \\
GV_0(2,7(i-1)+6) &= P_2^k\left(\partial^2\mathcal{H}_{i2}/\partial y^2\right) \\
GV_0(2,7(i-1)+7) &= P_2^k\left(\partial^2\mathcal{H}_{i3}/\partial y^2\right) \\
GV_0(3,7(i-1)+3) &= O_2^k\left(\partial\mathcal{H}_{i1}/\partial y\right) \\
GV_0(3,7(i-1)+5) &= O_1^k N_i \\
GV_0(3,7(i-1)+6) &= O_2^k\left(\partial\mathcal{H}_{i2}/\partial y\right) \\
GV_0(3,7(i-1)+7) &= O_2^k\left(\partial\mathcal{H}_{i3}/\partial y\right)
\end{aligned}$$

$[GV_1]$ is a 3 by 28 matrix and its non-zero components are listed as follows, for $i = 1,2,3,4$:

$$\begin{aligned}
GV_1(1,7(i-1)+3) &= O_2^k\left(\partial^2\mathcal{H}_{i1}/\partial x^2\right) \\
GV_1(1,7(i-1)+5) &= O_1^k\left(\partial N_i/\partial x\right)
\end{aligned}$$

$$GV_1(1,7(i-1)+6) = O_2^k\left(\partial^2\mathcal{H}_{i2}/\partial x^2\right)$$

$$GV_1(1,7(i-1)+7) = O_2^k\left(\partial^2\mathcal{H}_{i3}/\partial x^2\right)$$

$$GV_1(2,7(i-1)+3) = O_2^k\left(\partial^2\mathcal{H}_{i1}/\partial y^2\right)$$

$$GV_1(2,7(i-1)+5) = O_1^k\left(\partial N_i/\partial y\right)$$

$$GV_1(2,7(i-1)+6) = O_2^k\left(\partial^2\mathcal{H}_{i2}/\partial y^2\right)$$

$$GV_1(2,7(i-1)+7) = O_2^k\left(\partial^2\mathcal{H}_{i3}/\partial y^2\right)$$

$$GV_1(3,7(i-1)+3) = 2C_2\left(\partial\mathcal{H}_{i1}/\partial y\right)$$

$$GV_1(3,7(i-1)+5) = 2C_1N_i$$

$$GV_1(3,7(i-1)+6) = 2C_2\left(\partial\mathcal{H}_{i2}/\partial y\right)$$

$$GV_1(3,7(i-1)+7) = 2C_2\left(\partial\mathcal{H}_{i3}/\partial y\right)$$

$[GV_2]$ is a 3 by 28 matrix and its non-zero components are listed as follows, for $i = 1,2,3,4$:

$$GV_2(1,7(i-1)+3) = C_2\left(\partial^2\mathcal{H}_{i1}/\partial x\partial y\right)$$

$$GV_2(1,7(i-1)+5) = C_1\left(\partial N_i/\partial x\right)$$

$$GV_2(1,7(i-1)+6) = C_2\left(\partial^2\mathcal{H}_{i2}/\partial x\partial y\right)$$

$$GV_2(1,7(i-1)+7) = C_2\left(\partial^2\mathcal{H}_{i3}/\partial x\partial y\right)$$

$$GV_2(2,7(i-1)+3) = C_2\left(\partial^2\mathcal{H}_{i1}/\partial y^2\right)$$

$$GV_2(2,7(i-1)+5) = C_1\left(\partial N_i/\partial y\right)$$

$$GV_2(2,7(i-1)+6) = C_2\left(\partial^2\mathcal{H}_{i2}/\partial y^2\right)$$

$$GV_2(2,7(i-1)+7) = C_2\left(\partial^2\mathcal{H}_{i3}/\partial y^2\right)$$

$$GV_2(3,7(i-1)+3) = 3D_2\left(\partial\mathcal{H}_{i1}/\partial y\right)$$

$$GV_2(3,7(i-1)+5) = 3D_1N_i$$

$$GV_2(3,7(i-1)+6) = 3D_2\left(\partial\mathcal{H}_{i2}/\partial y\right)$$

$$GV_2(3,7(i-1)+7) = 3D_2\,(\partial\mathcal{H}_{i3}/\partial y)$$

$[GV_3]$ is a 3 by 28 matrix and its non-zero components are listed as follows, for $i = 1,2,3,4$:

$$
\begin{aligned}
GV_3(1,7(i-1)+3) &= D_2\left(\partial^2\mathcal{H}_{i1}/\partial x\partial y\right)\\
GV_3(1,7(i-1)+5) &= D_1\,(\partial N_i/\partial x)\\
GV_3(1,7(i-1)+6) &= D_2\left(\partial^2\mathcal{H}_{i2}/\partial x\partial y\right)\\
GV_3(1,7(i-1)+7) &= D_2\left(\partial^2\mathcal{H}_{i3}/\partial x\partial y\right)\\
GV_3(2,7(i-1)+3) &= D_2\left(\partial^2\mathcal{H}_{i1}/\partial y^2\right)\\
GV_3(2,7(i-1)+5) &= D_1\,(\partial N_i/\partial y)\\
GV_3(2,7(i-1)+6) &= D_2\left(\partial^2\mathcal{H}_{i2}/\partial y^2\right)\\
GV_3(2,7(i-1)+7) &= D_2\left(\partial^2\mathcal{H}_{i3}/\partial y^2\right)
\end{aligned}
$$

$[GW_0]$ is a 3 by 28 matrix and its non-zero components are listed as follows, for $i = 1,2,3,4$:

$$
\begin{aligned}
GW_0(1,7(i-1)+3) &= \partial\mathcal{H}_{i1}/\partial x\\
GW_0(1,7(i-1)+6) &= \partial\mathcal{H}_{i2}/\partial x\\
GW_0(1,7(i-1)+7) &= \partial\mathcal{H}_{i3}/\partial x\\
GW_0(2,7(i-1)+3) &= \partial\mathcal{H}_{i1}/\partial y\\
GW_0(2,7(i-1)+6) &= \partial\mathcal{H}_{i2}/\partial y\\
GW_0(2,7(i-1)+7) &= \partial\mathcal{H}_{i3}/\partial y
\end{aligned}
$$

APPENDIX C

TRUESDELL INCREMENTAL CONSTITUTIVE EQUATION

Combining Eqs.(2.16) and (2.23), we obtain

$$\begin{aligned} \nabla\sigma^t_{ij} &= \sigma^{\nabla}_{ij} + \sigma^v_{ij}\Delta u_{k,k} - \sigma^v_{il}\Delta u_{j,l} \\ &+ \Delta u_{i,l}\sigma^v_{lj} + W_{ik}\sigma^v_{kj} - \sigma^v_{ik}W_{kj} \end{aligned} \tag{C.1}$$

Using Eqs.(3.28) and (4.8), Eq.(C.1) can be expressed as

$$\begin{aligned} C^t_{ijkl}\Delta u_{(k,l)} &= C_{ijkl}\Delta u_{(k,l)} + \sigma^v_{ij}\Delta u_{k,k} - \sigma^v_{il}\Delta u_{j,l} \\ &- \sigma^v_{jl}\Delta u_{i,l} + \Delta u_{[i,k]}\sigma^v_{kj} + \sigma^v_{ik}\Delta u_{[k,j]} \\ &= C_{ijkl}\Delta u_{(k,l)} + \sigma^v_{ij}\Delta u_{k,k} - \sigma^v_{il}\Delta u_{j,l} - \sigma^v_{jl}\Delta u_{i,l} \\ &+ \frac{1}{2}\left(\sigma^v_{ik}\Delta u_{[j,k]} + \sigma^v_{ik}\delta_{lk}\Delta u_{[j,l]}\right) + \frac{1}{2}\left(\sigma^v_{jk}\Delta u_{[i,k]} + \sigma^v_{jk}\delta_{kl}\Delta u_{[i,l]}\right) \\ &= C_{ijkl}\Delta u_{(k,l)} + \sigma^v_{ij}\Delta u_{k,k} - \sigma^v_{il}\Delta u_{j,l} - \sigma^v_{jl}\Delta u_{i,l} \\ &+ \frac{1}{2}\left(\sigma^v_{il}\Delta u_{[j,l]} + \sigma^v_{jl}\Delta u_{[i,l]} + \sigma^v_{ik}\Delta u_{[j,k]} + \sigma^v_{jk}\Delta u_{[i,k]}\right) \\ &= C_{ijkl}\Delta u_{(k,l)} + \sigma^v_{ij}\Delta u_{k,k} - \sigma^v_{il}\Delta u_{j,l} - \sigma^v_{jl}\Delta u_{i,l} \end{aligned}$$

$$
\begin{aligned}
&+ \quad \frac{1}{4}(\sigma^v_{il}\Delta u_{j,l} - \sigma^v_{il}\Delta u_{l,j} + \sigma^v_{jl}\Delta u_{i,l} - \sigma^v_{jl}\Delta u_{l,i} \\
&+ \quad \sigma^v_{ik}\Delta u_{j,k} - \sigma^v_{ik}\Delta u_{k,j} + \sigma^v_{jk}\Delta u_{i,k} - \sigma^v_{jk}\Delta u_{k,i}) \\
&= \quad C_{ijkl}\Delta u_{(k,l)} + \sigma^v_{ij}\Delta u_{k,k} + \frac{1}{2}(-\sigma^v_{il}\Delta u_{j,l} - \sigma^v_{jl}\Delta u_{j,l} \\
&- \quad \sigma^v_{ik}\Delta u_{j,k} - \sigma^v_{jk}\Delta u_{i,k}) + \frac{1}{4}(\sigma^v_{il}\Delta u_{j,l} - \sigma^v_{il}\Delta u_{l,j} \\
&+ \quad \sigma^v_{jl}\Delta u_{i,l} - \sigma^v_{jl}\Delta u_{l,i} + \sigma^v_{ik}\Delta u_{j,k} - \sigma^v_{ik}\Delta u_{k,j} \\
&+ \quad \sigma^v_{jk}\Delta u_{i,k} - \sigma^v_{jk}\Delta u_{k,i}) \\
&= \quad C_{ijkl}\Delta u_{(k,l)} + \frac{1}{2}\sigma^v_{ij}\delta_{kl}\left(\Delta u_{k,l} + \Delta u_{l,k}\right) \\
&- \quad \frac{1}{4}\left(\sigma^v_{ik}\Delta u_{j,k} + \sigma^v_{il}\Delta u_{l,j} + \sigma^v_{jk}\Delta u_{i,k} + \sigma^v_{jl}\Delta u_{l,i}\right) \\
&- \quad \frac{1}{4}\left(\sigma^v_{ik}\Delta u_{k,j} + \sigma^v_{il}\Delta u_{j,l} + \sigma^v_{jk}\Delta u_{k,i} + \sigma^v_{jl}\Delta u_{i,l}\right) \\
&= \quad C_{ijkl}\Delta u_{(k,l)} + \sigma^v_{ij}\delta_{kl}\Delta u_{(k,l)} \\
&- \quad \frac{1}{4}\left(\sigma^v_{ik}\delta_{jl} + \sigma^v_{il}\delta_{jk} + \sigma^v_{jk}\delta_{il} + \sigma^v_{jl}\delta_{ik}\right)\left(\Delta u_{k,l} + \Delta u_{l,k}\right) \\
&= \quad C_{ijkl}\Delta u_{(k,l)} + \sigma^v_{ij}\delta_{kl}\Delta u_{(k,l)} \\
&- \quad \frac{1}{2}\left(\sigma^v_{ik}\delta_{jl} + \sigma^v_{il}\delta_{jk} + \sigma^v_{jk}\delta_{il} + \sigma^v_{jl}\delta_{ik}\right)\Delta u_{(k,l)} \qquad \text{(C.2)}
\end{aligned}
$$

Therefore, we obtain

$$
\begin{aligned}
C^t_{ijkl} &= C_{ijkl} + \sigma^v_{ij}\delta_{kl} \\
&- \frac{1}{2}\left(\sigma^v_{ik}\delta_{jl} + \sigma^v_{il}\delta_{jk} + \sigma^v_{jk}\delta_{il} + \sigma^v_{jl}\delta_{ik}\right) \qquad \text{(C.3)}
\end{aligned}
$$

APPENDIX D

ABAQUS/Standard CONVERGENCY CRITERIA

D.1 The Solution of Nonlinear Problems

While the commercial program ABAQUS/Standard is still evolving, the objective of this chapter is to document the convergency criteria used in the current thesis. The description of convergency criteria is reproduced from ABAQUS/Standard User's Manual [2] Sec.8.2.1. ABAQUS/Standard (ABAQUS in subsequent writing) uses a direct, Gauss elimination method to solve a system of simultaneous linear algebraic equations. Usually, many sets of simultaneous linear algebraic equations must be solved to obtain nonlinear solutions.

The nonlinear load-displacement curve for a structure is shown in Figure D.1. The objective of the analysis is to determine this response. In a nonlinear analysis the solution cannot be calculated by solving a single system of nonlinear equations, as would be done in a linear problem. Instead, the solution is found by specifying the loading as a function of time and incrementing time to obtain the nonlinear response. Therefore, ABAQUS breaks the simulation into a number of *load increments* and finds the approximate equilibrium configuration at the end of each load increment. Using the Newton-Raphson method, it often takes ABAQUS several iterations to determine an acceptable solution to each load increment.

D.2 Steps, Increments, and Iterations

1. The time history for a simulation consists of one or more *steps*. The user defines the steps, which generally consist of an analysis procedure option, loading options, and output request options. Different loads, boundary conditions, analysis procedure options, and output requests can be used in each step.

2. An *increment* is part of a step. In nonlinear analyses each step is broken into increments so that the nonlinear solution path can be followed. The user suggests the size of the first increment, and ABAQUS automatically choose the size of the subsequent increments. At the end of each increment the structure is in (approximate) equilibrium and results are available for writing to the restart, data, or results files.

3. An *iteration* is an attempt at finding an equilibrium solution in an increment. If the model is not in equilibrium at the end of the iteration, ABAQUS tries another iteration. With every iteration the solution that ABAQUS obtains should be closer to equilibrium; however, sometimes the iteration process may diverge - subsequent iterations may move away form the equilibrium state. In that case ABAQUS may terminate the iteration process and attempt to find a solution with a smaller increment size.

D.3 Convergency

Consider the internal (nodal) forces, I, and the external force, P, acting on a body. The internal load acting on a node are caused by the stresses in the elements that are attached to that node. For the body in equilibrium, the net force acting at every node must be zero. Therefore, the basic statement of equilibrium is that the internal force I, and the external force, P, must balance each other:

$$P - I = 0 \tag{D.1}$$

The nonlinear response of a structure to a small load increment, ΔP, is shown in Figure D.1. ABAQUS uses the structure's tangent stiffness, K_0, which is based on its configuration at u_0, and ΔP to calculate a displacement correction, u_a^c, for the structure. Using u_a^c, the structure's configuration is updated to u_a. ABAQUS then calculates the structure's internal force, I_a, in this updated configuration. The difference between the total applied load, P, and I_a can now be calculated as

$$R_a = P - I_a \tag{D.2}$$

where R_a is the *force residual* for the iteration.

If R_a is zero at every degree of freedom in the model, point a in Figure D.1 would lie on the load deflection curve and the structure would be in equilibrium. In a nonlinear problem R_a will never be exactly zero, so ABAQUS compares it to a tolerance value. If R_a is less than this force residual tolerance at all nodes, ABAQUS accepts the solution as being in equilibrium. By default, this tolerance value is set to 0.5% of an average force in the structure, averaged over time. ABAQUS automatically calculates this spatially and time-averaged force throughout the simulation.

If R_a is less than the current tolerance value, P and I_a are considered to be in equilibrium and u_a is a valid equilibrium configuration for the structure under applied load. However, before ABAQUS accepts the solution, it also checks that the largest displacement correction, u_a^c, is small relative to the total incremental displacement, $\Delta u_a = u_a - u_0$. If u_a^c is greater than a fraction (1% by default) of the incremental displacement, ABAQUS performances another iteration. Both convergence checks must be satisfied before a solution is said to have converged for that load increment.

If the solution from an iteration is not converged, ABAQUS performs another iteration to try to bring the internal and external forces into balance. First, ABAQUS forms the new stiffness, K_a, for the structure based on the updated configuration, u_a. This stiffness, together with the residual R_a, determines another displacement correction, u_b^c, that bring the system closer to equilibrium (point b in Figure D.1). ABAQUS calculates a new force residual, R_b, using internal forces from the structure's new configuration, u_b. Again, the largest force residual at any degree of freedom, R_b, is compared against the force residual tolerance, and the displacement correction for the second iteration, u_b^c, is compared to the increment of displacement, Δu_b. If necessary, ABAQUS performs further iteration.

D.4 Automatic Incrementation Control

By default, ABAQUS automatically adjusts the size of the time increments to solve non-linear problems efficiently. The user needs to suggest only the size of the first increment in each step of the simulation, after which ABAQUS automatically adjusts the size of the increments. If the user does not provide a suggested initial increment size, ABAQUS will attempt to apply all of the load defined in the step in a single increment. For highly non-linear problems, ABAQUS will have to reduce the increment size repeatedly to obtain a solution.

The number of iterations needed to find a converged solution for a time increment will vary depending on the degree of nonlinearity in the system. With the default incrementation control, the procedure works as follows. If the solution has not converged within 16 iterations or it the solution appears to diverge, ABAQUS abandons the increment and starts again with the increment size set to 25% of its previous value. It then attempts to find a converged solution with this smaller load increment. If the solution still fails to converge, ABAQUS reduces the increment size again. This process is continued until a solution is found. If the time increment becomes smaller than the minimum defined by the user or more than five attempts are needed, ABAQUS stops the analysis.

If the increment converges in fewer that than iterations, this indicates that the solution is being found fairly easily. Therefore, ABAQUS automatically increases the increment size by 50% if two consecutive increments require fewer that 5 iterations to obtain a converged solution.

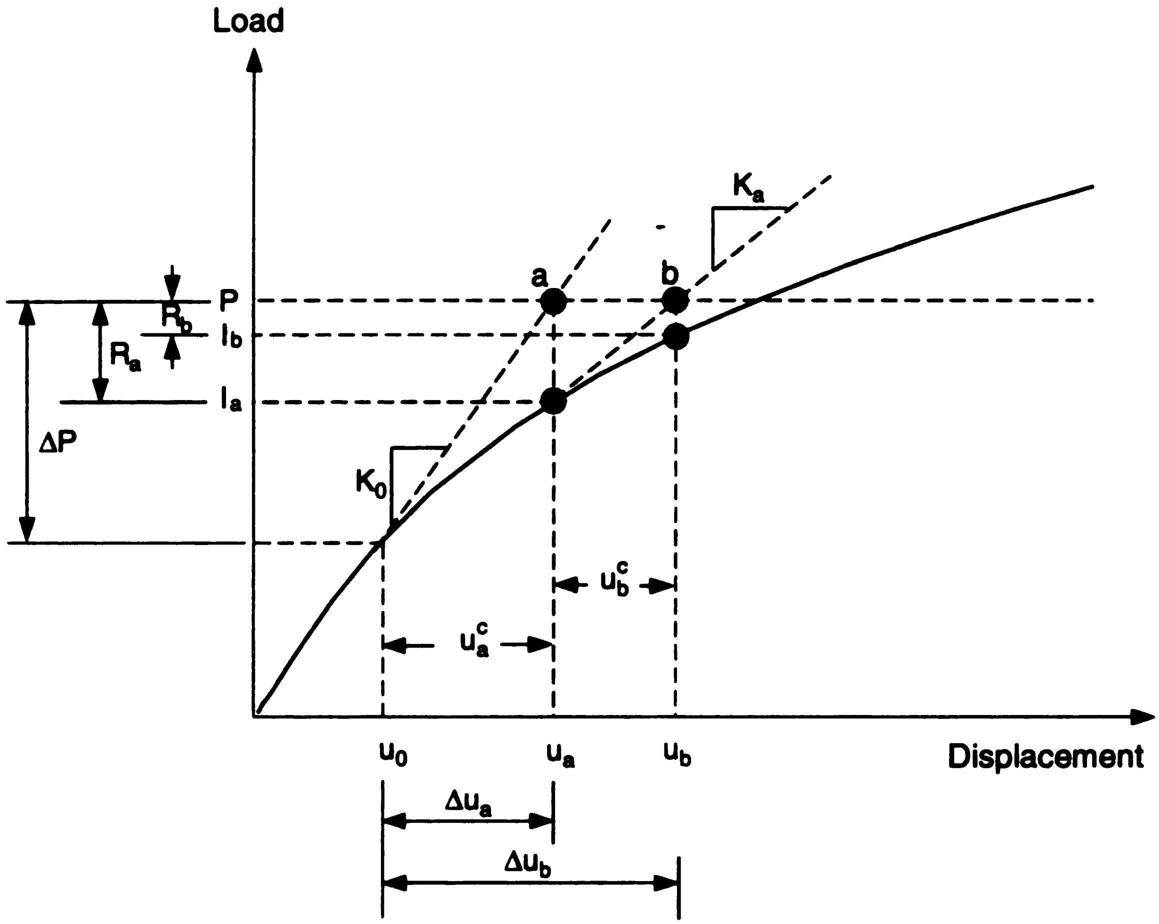

Figure D.1 First and second iteration of an increment

BIBLIOGRAPHY

BIBLIOGRAPHY

[1] *ABAQUS/Standard Example Problems Manual* (1996), Volume I & II, version 5.6, Hibbitt, Karlsson & Sorensen, Inc., Pawtucket, RI.

[2] *ABAQUS/Standard User's Manual* (1996), Volume I, II & II, version 5.6, Hibbitt, Karlson & Sorensen, Inc., Pawtucket, RI.

[3] *ABAQUS Theory Manual* (1995), version 5.5, Hibbitt, Karlsson & Sorensen, Inc., Pawtucket, RI.

[4] *ABAQUS/Standard Verification Manual* (1995), version 5.5, Hibbitt, Karlsson & Sorensen, Inc., Pawtucket, RI.

[5] Altiero, N. (1987), *Finite Element Method*, Course Notes, Michigan State University, East Lansing, Michigan.

[6] Barbero, E.J. and Reddy, J.N. (1990), "An Accurate Determination of Stresses in Thick Laminates Using a Generalized Plate Theory," *International Journal for Numerical Methods in Engineering*, **29**, 1-14.

[7] Barbero, E.J. and Reddy, J.N. (1990), "Nonlinear Analysis of Composite Laminates Using a Generalized Laminated Plate Theory," *AIAA Journal*, **28**, 1987-1994.

[8] Bathe, K.-J. (1996), *Finite Element Procedures*, Prentice-Hall, Englewood Cliffs, New Jersey.

[9] Bazeley, G.P., Cheung, Y.K., Irons, B.M., and Zienkiewicz, O.C. (1966), "Triangular Elements in Bending - Conforming and Non-conforming Solutions," *Proc. 1st Conf. Matrix in Structural Mechanics*, AFFDLTR-CC-80, Air Force Inst. Tech., Wright-Patterson AF Base, Ohio, 547-576.

[10] Belytschko, T. and Hughes, T.J.R. ed. (1983), *Computational Methods in Mechanics - Volume 1: Computational Methods in Transient Analysis*, Chapter 1, North-Holland Publisher, New York, New York.

[11] Belytschko, T., Lin, J.I. and Tsay, C.-S. (1984), "Explicit Algorithms for the Nonlinear Dynamics of Shells," *Computer Methods in Applied Mechanics and Engineering*, **42**, 225-251.

[12] Chia, C.Y. (1972), "Large Deflection of Rectangular Orthotropic Plates," *Journal of Engineering Mechanics Division, Proceeding, ASCE*, **98**, 1285-1298.

[13] Chia, C.Y. (1980), *Nonlinear Analysis of Plates*, McGraw-Hill, Inc., New York, New York.

[14] Cook, R.D. (1989), *Concepts and Application of Finite Element Analysis*, 3rd ed., Wiley, New York.

[15] Crisfield M.A. (1991), *Non-linear Finite Element Analysis of Solids and Structures - Volume 1: Essentials*, John Wiley & Sons, New York.

[16] Dienes, J.K. (1979), "On the Analysis of Rotation and Stress Rate in Deforming Bodies," *Acta Mechanica*, **32**, 217-232.

[17] Di Sciuva, M. (1992), "Multilayered Anisotropic Plate Models with Continuous Interlaminar Stress," *Composite Structures*, **22**, 149-167.

[18] Flanagan, D.P. and Taylor, L.M. (1987), "An Accurate Numerical Algorithm for Stress Integration with Finite Rotations," *Computer Methods in Applied Mechanics and Engineering*, **62**, 305-320.

[19] Fung, Y.C. (1965), *Foundations of Solid Mechanics*, Prentice-Hall, Englewood Cliffs, New Jersey.

[20] Halleux, J.P. and Donea, J. (1985), "A Discussion of Cauchy Stress Formulations for Large Strain Analysis," *Finite Element Methods for Nonlinear Problems: Europe-US Symposium*, Bergan, Bathe and Wunderlich ed., Trondheim, Norway, 61-74.

[21] Hinton, E. and Owen, D.R.J. (1979), *An Introduction to Finite Element Computations*, Pineridge Press Limited, Swansea, UK.

[22] Hughes, T.J.R. (1987), *The Finite Element Method - Linear Static and Dynamic Finite Element Analysis*, Prentice-Hall, Englewood Cliffs, New Jersey.

[23] Hughes, T.J.R. and Belytschko, T. (1995), *Nonlinear Finite Element Analysis*, notes of a short course, Palo Alto, California.

[24] Hughes, T.J.R. and Liu, W.K. (1981), "Nonlinear Finite Element Analysis of Shells: Part I. Three-dimensional Shells," *Computer Methods in Applied Mechanics and Engineering*, **26**, 331-362.

[25] Irons, B.M. (1974), "The Patch Test for Engineers," *Proc. Finite Symp. Atlas Computer Lab.*, Chilton, Didcot, England, 171-192.

[26] Kapania, R.K. and Raciti, S. (1989), "Nonlinear Vibration of Unsymmetrically Laminated Beams," /em AIAA Journal, **27**, 201-210.

[27] Kapania, R.K. and Raciti, S. (1989), "Recent Advances in Analysis of Laminated Beams and Plates, Part I: Shear Effects and Buckling," *AIAA Journal*, **v27n7**, 923-934.

[28] Kardestuncer, H. (1989), Editor in Chief, *Finite Element Handbook*, Part 2, Chapter 6, McGraw-Hill, New York.

[29] Knight, N.F. Jr. and Starnes, J.H. Jr. (1985), "Postbuckling Behavior of Axially Compressed Graphite-Epoxy Cylindrical Panels with Circular Holes," *Transactions of the ASME*, **107**, 394-402.

[30] Kweon, J.H. and Hong, C.S. (1993), "Postbuckling Analysis of Composite Laminated Cylindrical Panels Under Axial Compression," *AIAA Journal*, **v31n8**, 1535-1537.

[31] Kweon, J.H., Hong, C.S. and Lee, I.C. (1995), "Postbuckling Compressive Strength of Graphite/Epoxy Laminated Cylindrical Panels Loaded in Compression," *AIAA Journal*, **v33n2**, 217-222.

[32] Lee, C.Y. (1991), *A Study of the Interlaminar Stress Continuity Theories for Composite Analysis*, Ph.D. Dissertation, Dept. of Materials Science and Mechanics, Michigan State University, East Lansing, Michigan.

[33] Lee, C.Y. and Liu, D. (1992), "An Interlaminar Stress Continuity Theory for Laminated Composite Analysis," *Computers and Structures*, **v42n1**, 69-78.

[34] Lee, C.Y. and Liu, D. (1993), "Nonlinear Analysis of Composite Plates Using Interlaminar Shear Stress Continuity Theory," *Composite Engineering*, **v3n2**, 151-168.

[35] Lee, L.J., Huang, K.Y., Hwang, D.G. and Pai, C.K. (1993), "Geometrical Nonlinear Analysis of Composite Cylindrical Shell Panels Subjected to Impact," *Finite Elements in Analysis and Design*, **15**, 135-149.

[36] Lee, Y.K. (1992), "Shear Banding and Material Instability in Finite Deformed Compressible Materials: An Example in Thin Sheets," *International Journal of Plasticity*, **v8**, 543-565.

[37] Li, X. (1994), *Investigation on Laminated Plate Theories*, Ph.D. Dissertation, Dept. of Materials Science and Mechanics, Michigan State University, East Lansing, Michigan.

[38] Li, X. and Liu, D. (1995), "Zigzag Theory for Composite Laminates," *AIAA Journal*, **v33n6**, 1163-1165.

[39] Li, X. and Liu, D. (1997), "Generalized Laminated Theories Based on Double Superposition Hypothesis," *International Journal for Numerical Methods in Engineering*, **v40n8**, 1197-1212.

[40] Liao, C.L. and Reddy, J.N. (1989), "Continuum-Based Stiffened Composite Shell Element for Geometrically Nonlinear Analysis," *AIAA Journal*, **v27n1**, 95-101.

[41] Liu, D. (1988), "Impact-induced Delamination - A View of Bending Stiffness Mismatching," *Journal of Composite Materials*, **22**, 674-691.

[42] Liu, D. and Li, X. (1996), "An Overall View of Laminate Theories Based on Displacement Hypothesis," *Journal of Composite Materials*, **30**, 1539-1561.

[43] Liu, W.K. (1988), *Advanced Finite Element Methods*, Course Notes, Northwestern University, Evanston, Illinois.

[44] Lo, K.H., Christensen, R.M., and Wu, E.M. (1977), "A High-order Theory of Plate Deformation - Part 1: Homogeneous Plates," *Journal of Applied Mechanics*, **v44**, 663-668.

[45] Lo, K.H., Christensen, R.M., and Wu, E.M. (1978), "Stress Solution Determination for High Order Plate Theory," *International Journal of Solids and Structures*, **v14**, 655-662.

[46] Lu, X. and Liu, D. (1992), "An Interlaminar Shear Stress Continuity Theory for Both Thin and Thick Composite Laminates," *Journal of Applied Mechanics*, **59**, 502-509.

[47] MacNeal, R.H. and Harder, R.L. (1985), "A proposed Standard Set of Problems to Test Finite Element Accuracy," *Finite Elements in Analysis and Design*, **1**, 3-20.

[48] Malvern, L.E. (1969), *Introduction to the Mechanics of a Continuous Medium*, Prentice Hall, Englewood Cliffs, New Jersey.

[49] Mase, G.E. and Mase, G.T. (1992), *Continuum Mechanics for Engineering*, CRC Press, Boca Raton, Florida.

[50] Mattiasson, K., Bengtsson, A. and Samuelsson, A. (1985), "On the Accuracy and Efficiency of Numerical Algorithms for Geometrically Nonlinear Structural Analysis," *Finite Element Methods for Nonlinear Problems: Europe-US Symposium*, Bergan, Bathe and Wunderlich ed., Trondheim, Norway, 3-23.

[51] Mindlin, R.D. (1951), "Influence of Rotatory Inertia and Shear on Flexural Motions of Isotropic Elastic Plates," *Journal of Applied Mechanics*, **v18**, 31-38.

[52] Osias, J.R. and Swedlow, J.L. (1973), "Finite Elasto-Plastic Deformation-I: Theory and Numerical Examples," *International Journal of Solids Structures*, **v10**, 321-339.

[53] Pagano, N.J. (1969), "Exact Solutions for Composite Laminates in Cylindrical Bending," *Journal of Composite Materials*, **v3**, 398-411.

[54] Pagano, N.J. (1970), "Exact Solutions for Rectangular Bidirectional Composites and Sandwich Plates," *Journal of Composite Materials*, **v3**, 20-35.

[55] Palazotto, A.N. and Dennis, S.T. (1992), *Nonlinear Analysis of Shell Structures*, AIAA Education Series.

[56] Pipes, R.B. and Pagano, N.J. (1974), "Interlaminar Stress in Composite Laminates - An Approximate Elasticity Solution," *Journal of Applied Mechanics*, **41**, 668-672.

[57] Prager, W. (1961), "An Elementary Discussion of Definitions of Stress Rate," *Quart. Appl. Math.*, **v18n4**, 403-407.

[58] Prager, W. (1962), "On Higher Rates of Stress and Deformation," *Mech. Phys. Solids*, **10**, 133-138.

[59] Reddy, J.N. (1982), "Analysis of Layered Composite Plates Accounting for Large Deflections and Transverse Shear Strains," *Recent Advances in Non-linear Computational Mechanics*, Chapter 6, 155-203, Pineridge Press Limited, Swansea, U.K.

[60] Reddy, J.N. (1984), "A Refined Nonlinear Theory of Plates with Transverse Shear Deformation," *International Journal of Solids and Structures*, **20**, 881-896.

[61] Reddy, J.N. (1984), "A Simple Higher-order Theory for Laminated Composite Plates," *Journal of Applied Mechanics*, **51**, 745-752.

[62] Reddy, J.N. (1984), *Energy and Variational Methods in Applied Mechanics*, Wiley, New York.

[63] Reddy, J.N. (1990), "A General Non-linear Third-order Theory of Plates with Moderate Thickness," *International Journal of Non-linear Mechanics*, **25**, 677-686.

[64] Reddy, J.N. and Chandrashekhara, K. (1985), "Nonlinear Analysis of Laminated Shells Including Transverse Shear Strains," *AIAA Journal*, **v23n3**, 440-441.

[65] Reissner, E. (1945), "The effect of Transverse Shear Deformation on the Bending of Elastic Plates," *Journal of Applied Mechanics*, **v12**, A69-A77.

[66] Singh, G. and Sadasiva Rao, Y.V.K. (1987), "Nonlinear Vibration of thick Composite Plates," *Journal of Sound and Vibration*, **115**, 367-371.

[67] Srinivas, S. and Rao, A.K. (1970), "Bending, Vibration, and Buckling of Simply Supported Thick Orthotropic Rectangular Plates and Laminates," *International Journal of Solids and Structures*, **6**, 1463-1481.

[68] Stanley, G. M. (1985), *Continuum-Based Shell Elements*, Ph.D. Dissertation, Dept. of Applied Mechanics, Stanford University, Palo Alto, California.

[69] Sun, C.T. and Chin, H. (1988), "Analysis of Asymmetric Composite Laminates," *AIAA Journal*, **26**, 714-718.

[70] Sun, C.T. and Chin, H. (1988), "On Large Deflection Effects in Unsymmetric Cross-Ply Composite Laminates," *Journal of Composite Materials*, **22**, 1045-1059.

[71] Timoshenko, S. and Woinowsky-krieger S. (1959), *Theory of Plates and Shells*, 2nd ed., McGraw-Hill, New York.

[72] Toledano, A. and Murakamim, H. (1987), "A High-order Laminated Plate Theory with Improved In-plane Responses," *International Journal of Solids Structures*, **v23n1**, 111-131.

[73] Yip, Y.C. (1996), *A 3-D Laminated Plate Finite Element with Zig-zag Sublaminate Approximations for Composite and Sandwich Panels*, Ph.D. Dissertation, Dept. of Materials Science and Mechanics, Michigan State University, East Lansing, Michigan.

[74] Zaghloul, M.S.A. (1972), *Analytical and Experimental Investigations of Filamentary-Composite Laminated Plates*, Ph.D. Dissertation, Dept. of Civil Engineering, University of Windsor, Windsor, Ontario, Canada.

[75] Zaghloul, M.S.A. and Kennedy, J.B. (1974), "Material Constants of Filamentary-Composite Laminates," *Aeronautical Journal*, **v78n766**, 464-467.

[76] Zaghloul, M.S.A. and Kennedy, J.B. (1975), "Nonlinear Behavior of Symmetrically Laminated Plates," *Journal of Applied Mechanics*, 234-236.

[77] Zaghloul, M.S.A. and Kennedy, J.B. (1975), "Nonlinear Behavior of Unsymmetrically Laminated Plates," *Journal of the Engineering Mechanics Division*, 169-186.

[78] Zhu, Y. and Zacharia, T. (1996), "A New One-point Quadrature, Quadrilateral Shell Element with Drilling Degrees of Freedom," *Computer Methods in Applied Mechanics and Engineering*, **136**, 165-203.

[79] Zienkiewicz, O.C. and Taylor, R.L. (1989), *The Finite Element Methods - Volume 1: Basic Formulation and Linear Problems*, 4th edition, McGraw-Hill International (UK).

[80] Zienkiewicz, O.C. and Taylor, R.L. (1991), *The Finite Element Methods - Volume 2: Solid and Fluid Mechanics, Dynamics and Non-linearity*, 4th edition, McGraw-Hill International (UK).

[81] Zienkiewicz, O.C., Too, J. and Taylor, R.L. (1971), "Reduced Integration Technique in General Analysis of Plates and Shells," *International Journal for Numerical Methods in Engineering*, **3**, 275-290.

[82] Chiang, H.Y., private communication.

[83] Hill, L., private communication.

[84] Lee, Y.K., private communication.

[85] Nagtegaal, J., private communication.